2012

Combustion instability automated acoustic mode detection methodology for a subscale combustion chamber with a single injector

Joel Carpenter

Combustion Instability Automated Acoustic Mode Detection Methodology for a Subscale Combustion Chamber with a Single Injector

by

JOEL CARPENTER

A THESIS

Submitted in partial fulfillment of the requirements
for the degree of Master of Science in Engineering
in
The Department of Mechanical and Aerospace Engineering
to
The School of Graduate Studies
of
The University of Alabama in Huntsville

HUNTSVILLE, ALABAMA

2012

In presenting this thesis in partial fulfillment of the requirements for a master's degree from The University of Alabama in Huntsville, I agree that the Library of this University shall make it freely available for inspection. I further agree that permission for extensive copying for scholarly purposes may be granted by my advisor or, in his/her absence, by the Chair of the Department or the Dean of the School of Graduate Studies. It is also understood that due recognition shall be given to me and to The University of Alabama in Huntsville in any scholarly use which may be made of any material in this thesis.

Joel Carpenter — 7/12/2012

Joel Preston Carpenter — Date

THESIS APPROVAL FORM

Submitted by Joel P. Carpenter in partial fulfillment of the requirements for the degree of Master of Science in Engineering in Aerospace Engineering and accepted on behalf of the Faculty of the School of Graduate Studies by the thesis committee.

We, the undersigned members of the Graduate Faculty of The University of Alabama in Huntsville, certify that we have advised and/or supervised the candidate of the work described in this thesis. We further certify that we have reviewed the thesis manuscript and approve it in partial fulfillment of the requirements for the degree of Master of Science in Engineering in Aerospace Engineering.

5/23/12 Committee Chair
Dr. Robert A. Frederick Jr. (Date)

5/23/12
Dr. David M. Lineberry (Date)

5/24/2012
Dr. James Blackmon (Date)

5/24/2012 Department Chair
Dr. Keith Hollingsworth (Date)

05/24/12
College Dean
Dr. Shankar Mahalingam (Date)

Rhonda Kay Gaede 7/10/12 Graduate Dean
Dr. Rhonda Kay Gaede (Date)

ABSTRACT

School of Graduate Studies
The University of Alabama in Huntsville

Degree Master of Science in Engineering

College/Dept. Engineering/Mechanical and Aerospace Engineering

Name of Candidate Joel P. Carpenter

Title Combustion Instability Automated Acoustic Mode Detection Methodology for a Subscale Combustion Chamber with a Single Injector

A methodology has been developed that automatically analyzes pressure data taken from multiple transducers in a subscale chamber with a single injector. The methodology determines the acoustic mode present during combustion instability, the frequency, the pressure amplitude, and the mode orientation within the chamber. The analysis compares the theoretical phase, amplitude ratios among transducers, and the cut on frequency based on the wave equation to determine modes. The program looks for tangential, radial and combined modes. When analyzing computer generated acoustic test data with Gaussian noise, the program can identify the acoustic mode when the signal-to-noise ratio is as low as two. Previously published data were analyzed and verified the validity of the program developed. An analysis of these test data showed that the program finds matches in up to 61% of tests analyzed. The modes found in the test data were 1-R and 2-T modes.

Abstract Approval:	Committee Chair	Robert A. Frederick Jr. Dr. Robert A. Frederick Jr.
	Department Chair	D. Keith Hollingsworth Dr. Keith Hollingsworth
	Graduate Dean	Rhonda Kay Gaede 7/10/12 Dr. Rhonda Kay Gaede

ACKNOWLEDGEMENTS

This research is a continuation of combustion instability research that has been done at the PRC since 2007. I would like to thank all of those whose work at the PRC preceded mine, as their work made this possible. I would like to thank John Bennewitz for all of his help throughout my time spent working on this. His guidance was essential in the completion of this work. Ben Richman was also of great help and did a large part of the pioneering research in this subject before I began my research.

I would like to thank my committee members who include my advisor, Dr. Robert Frederick Jr., Dr. James Blackmon and Dr. David Lineberry for their support and guidance throughout this research. Dr. Frederick was instrumental in assisting me with this research, and I would like to thank him for providing the necessary direction and inspiring the ideas for this work. Dr. Lineberry was particularly helpful during this research, providing numerous helpful ideas and solutions. The challenging and insightful questions asked by Dr. Blackmon during the research process provided an extra depth to the research that otherwise would not have been considered.

I would also like to thank Tony Hall, the PRC Facility Engineer for making all of this testing possible. Also of special thanks is fellow graduate student Chad Eberhart, who spent a large amount of time teaching me the basics of combustion instability.

TABLE OF CONTENTS

LIST OF FIGURES

LIST OF TABLES

LIST OF SYMBOLS

AR	Amplitude Ratio
ω	Angular Frequency
A	Area
P_c	Chamber Pressure
a	Chamber Radius
ρ	Density
P’	Dynamic Pressure
Φ	Equivalence Ratio
FFT	Fast Fourier Transform
P1	First Pressure Transducer
f	Frequency
inj	Injector
ku	Kurtosis
μ	Mean
$\bar{X}$	Mean Sample Population
MW	Molecular Weight
MR	Momentum Ratio
Ox	Oxidizer
P	Pressure
prop	Propellant
s_X	Sample Population Standard Deviation
P2	Second Pressure Transducer

S/N	Signal to Noise Ratio
sk	Skewness
γ	Specific Heat Ratio
c	Speed of Sound
σ	Standard Deviation
T	Temperature
P3	Third Pressure Transducer
t	Time
$\dot{m}$	Velocity
VR	Velocity Ratio
$\dot{Q}$	Volumetric Flow Rate
QR	Volumetric Flow Rate Ratio

PREFACE

Combustion instability research has been ongoing at the University of Alabama in Huntsville (UAH) Propulsion Research Center (PRC) since 2007. Using full-scale injectors of all types, the test facility has been able to reproduce all commonly encountered combustion instability modes. To this date, the facility has been able to produce vast amounts of combustion instability data, far beyond the processing capabilities of the PRC. This prompted the need for this research, the development of a comprehensive methodology for quickly analyzing the combustion data. Described in this thesis is the method developed, which uses a Matlab program to match the experimental combustion data to theoretically derived acoustic mode shapes based on the wave equation.

Chapter 1 provides a background of combustion instability and the various research that has been done at the PRC. Chapter 2 develops the acoustic wave equation used to formulate the analysis methodology. Chapter 3 describes various statistical parameters that can be used to evaluate the signal to noise ratios of experimental data that has the form of a sinusoid. The development of the mode-matching algorithm and Matlab program is described in Chapter 4. Verification of this program is done on both artificial data generated from theory (Chapter 5) and combustion instability test data collected at the PRC (Chapter 6). Chapter 7 provides a thorough summary of all results and a list of future work.

CHAPTER ONE

INTRODUCTION

Propose of Research

The purpose of this research was to develop an automated methodology capable of quickly analyzing the data taken from the Combustion Instability Test Facility at the UAH PRC. Current methods of analyzing the data, while robust, are very labor intensive. To date only about 10% of the data taken for any given set of experiments has been analyzed. These data points were selected do to a variety of factors such as tests with the highest amplitudes, or ones that contain frequencies under investigation. Using this method, large amounts of data are left unanalyzed and several months could be spent analyzing the selected data points.

The automated analysis method to be developed had to accurately determine the acoustic mode present during combustion instability, the amplitude of the pressure during the instability, the frequency at which it occurred, and the orientation of the acoustic mode within the combustion chamber.

Combustion Instability

Combustion instability results due to the coupling between the fluid mechanics (acoustics) in combination with the combustion chamber and the combustion process. A system must dissipate more oscillatory energy than it is supplied at all frequencies to have a stable design. High Frequency combustion instabilities are most destructive since energy content increases with frequency, capable of destroying an engine in less than 1 second. Smooth rocket combustion occurs when pressure fluctuations do not exceed ±5% of mean chamber pressure. Unstable combustion (combustion instability) has organized oscillations occurring at regular intervals with a peak pressure that is greater than 10% of the mean chamber pressure [1].

All rocket engines must go through stability testing to prove that they are stable. The most famous case of combustion instability occurred when designing the F-1 rocket engine used on the first stage of the Saturn V rocket. Due to the engine's large combustion chamber, instabilities were severe. The injector in the F-1 proved to be the most important component with regard to its stability [2]. Figure 1.1 shows an F-1 Engine. Even modern engines, such as the J2X, which will serve as the engine for the upper stage of the new Space Launch System, must prove that they are stable during flight. A picture of a J2X is shown in Figure 1.2.

Combustion instability is generally split into three categories; low frequency ranging from 10 – 400 Hz; intermediate frequency from 400-1000 Hz; and high frequency over 1000 Hz. Low frequency combustion instability tends to be linked with the propellant feed system and is sometimes called chugging. Intermediate frequency combustion instability, also called buzzing, is less the least dangerous. It is mostly linked with mechanical vibrations of the propulsion systems. High frequency combustion instability, also known as screeching is the most destructive [1], [3]. For this research, only high frequency combustion instabilities were considered. Table 1.1 provides a summary of the three general types of combustion instability.

Table 1.1 The three general types of combustion instability [1].

Type	Frequency Range (Hz)	Cause Relationship
Low Frequency - Chugging, Feed System Instability	10-400	Linked with pressure interactions between propellant feed system, if not the entire vehicle, and combustion chamber.
Intermediate Frequency - Buzzing	400-1000	Linked with mechanical vibrations of propulsion structure, injector manifold, flow eddies, fuel/oxidizer ratio fluctuations, and propellant feed system resonances.
High Frequency - screaming, screeching or squealing	Greater than 1000	Linked with combustion process forces (pressure waves) and chamber acoustical resonance properties.

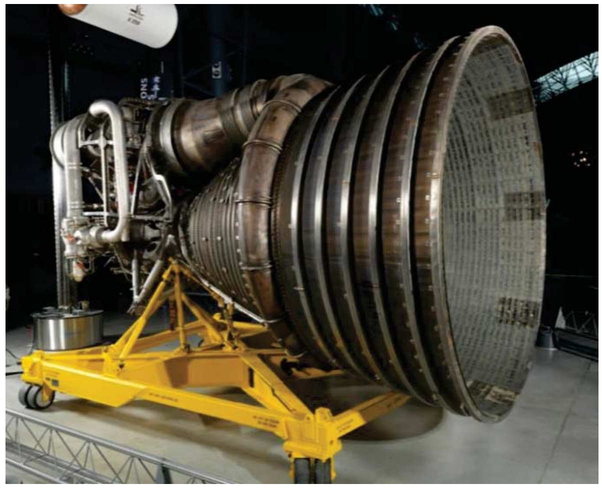

Figure 1.1 F-1 Engine used on the first stage of the Saturn V [4].

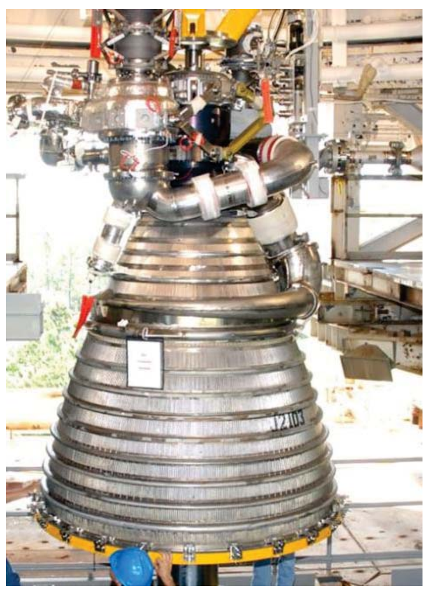

Figure 1.2 J2-X engine, to be used on the upper stage of the Space Launch System [5].

Acoustic Modes

Combustion instability is classified in terms of the acoustic modes that it most resembles. There are three different acoustic modes that can occur. These are longitudinal, tangential and radial. These are shown in Figure 1.3. Modes also occur in different orders. The higher the order, the more node lines the mode has. For example, a first tangential (1-T) mode has one node line, and a second tangential (2-T) mode has two node lines. Node lines are locations where the pressure does not fluctuate. That is to say the dynamic pressure change at the node line location is zero. Figure 1.4 shows a 1-T and a 2-T mode with the node lines labeled. On the right half of Figure 1.4 a 1-R and a 2-R mode are shown. Combined modes can also exist and show an increasingly complex shape. Combined modes for the 1-T, 1-R, the 1-T, 2-R and the 2-T, 1-R are shown in Figure 1.5.

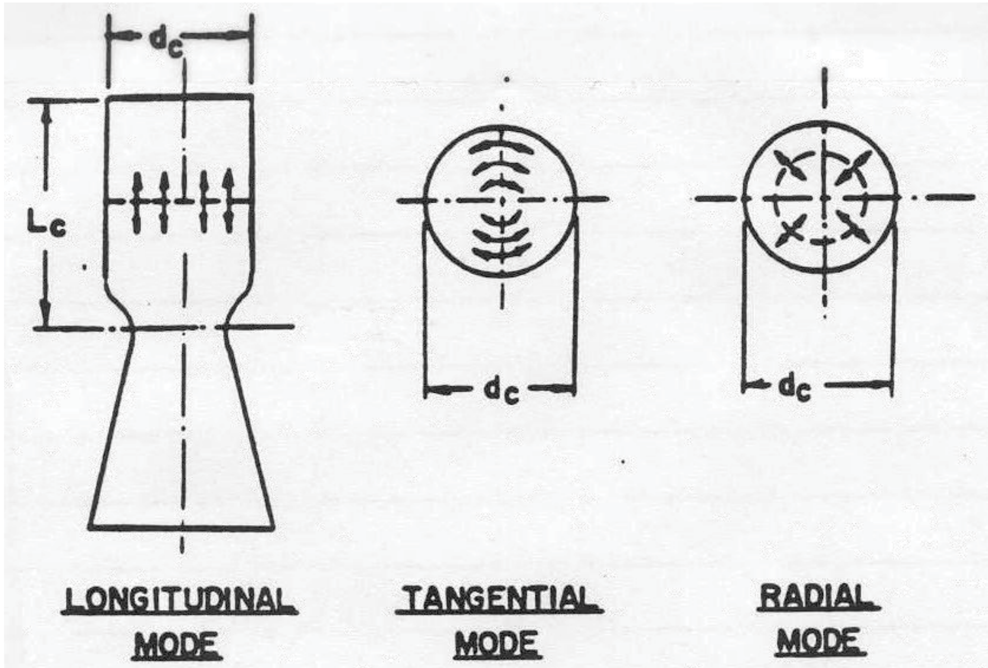

Figure 1.3 Three types of combustion instability acoustic modes [6].

- L_c = Chamber length
- d_c= Chamber diameter

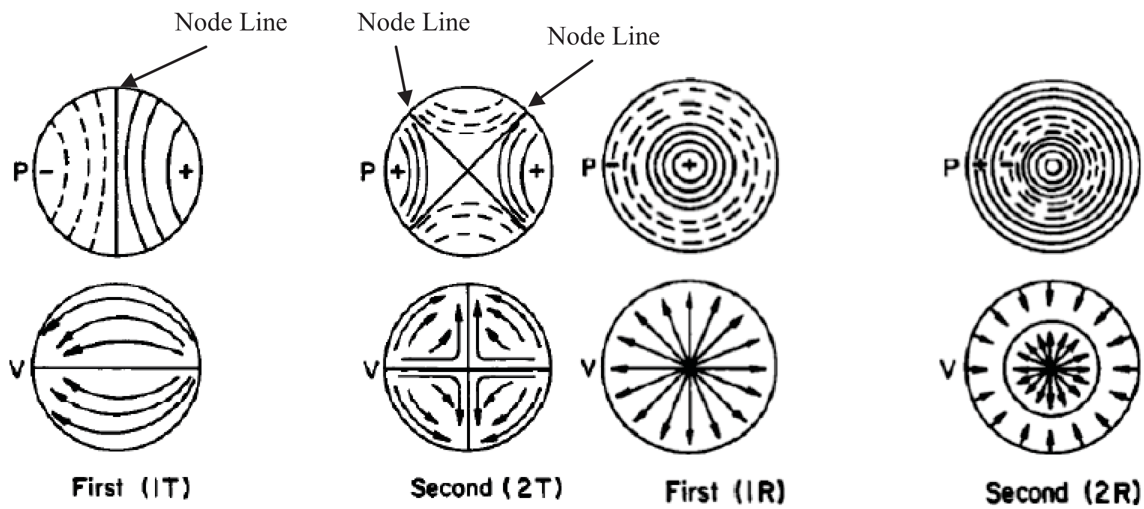

Figure 1.4 The first tangential (1-T), second tangential (2-T), first radial (1-R) and second radial (2-R) modes. Pressure distribution is shown in the top row, and velocity distribution on the bottom [6].

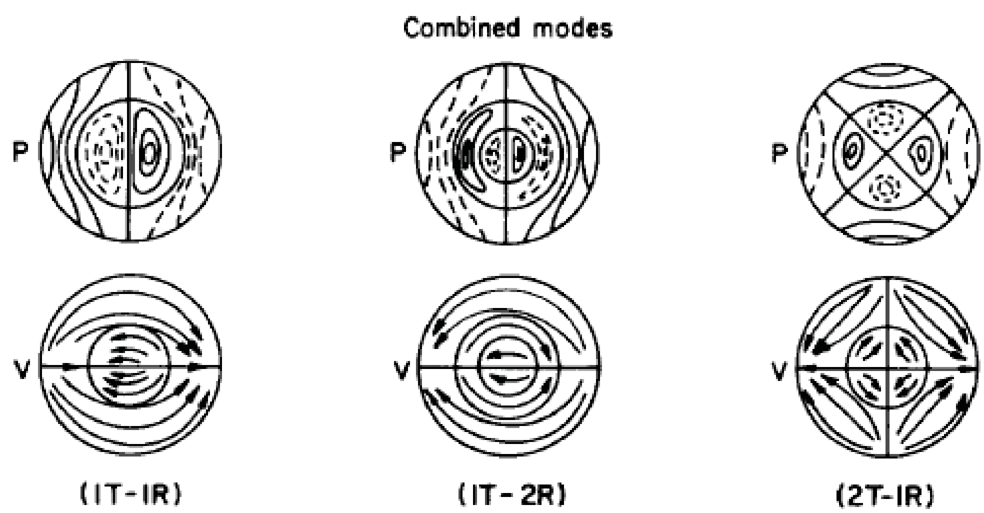

Figure 1.5 Combined modes have increasingly more complex mode shapes [6].

Experimental Methodology

The general processes involved in generating thrust in a liquid rocket combustion chamber are injection, atomization, vaporization, mixing and reaction, and then expansion. It is convenient to think of these sequentially, but these processes may take place simultaneously in a given region of space [3].

The methodology used at the PRC is a partial modeling of the process that focuses on the injector as the main source of high frequency combustion instability. The main idea is that propellant mixing is considered the dominant factor affecting combustion stability [7]. A schematic of a possible setup for using this methodology is shown in Figure 1.6. The gaseous propellants used in this experimental setup are assumed to behave as supercritical liquids. A comparison between the flow characteristics of a subcritical gas and a supercritical liquid is shown in Figure 1.7.

This test methodology has numerous advantages. It allows for the study of the instability behavior of one injector based upon flow rates and injector geometry. This method is very cost effective when compared to full scale testing. There is less hardware and it is generally nondestructive of the tested parts. It is easy to quickly change injectors, allowing for the testing of many different injector geometries and shapes. This method is very useful in generating large amounts of combustion instability data.

There are some disadvantages to this method. Since only one injector is studied at a time, it does not take into consideration coupling between injectors. It is only a component level test, and extrapolating the information gathered to a full-scale engine may be difficult. There are also numerous assumptions for testing which must be taken into consideration when analyzing the data.

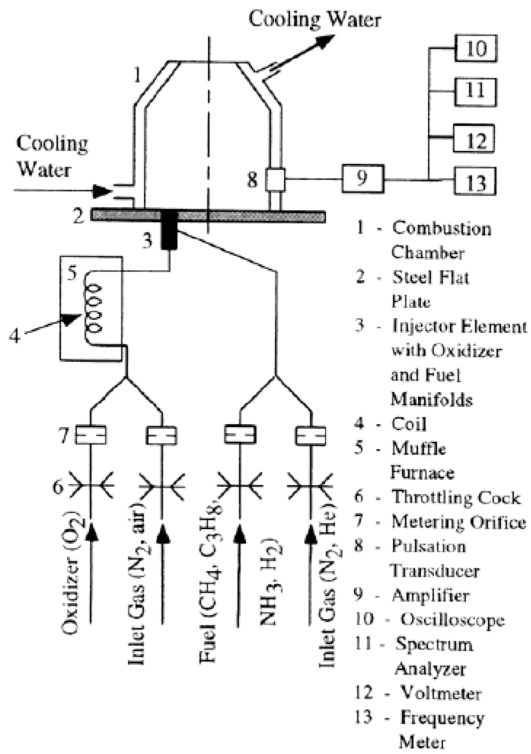

Figure 1.6 Schematic of a single element model setup and instrumentation [7].

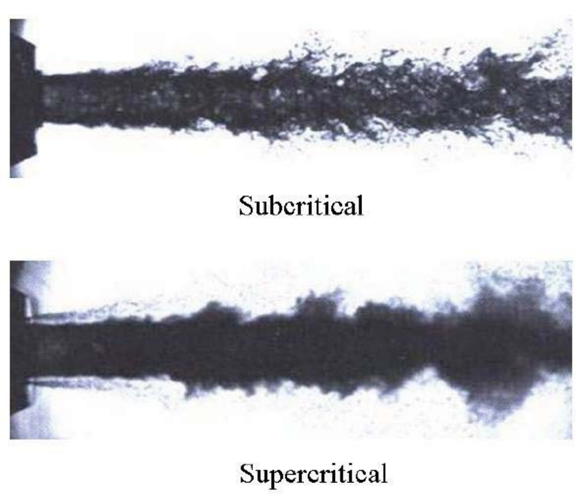

Figure 1.7 Comparison of flows between subcritical gas and supercritical liquid [9].

The following describes the scaling methodology,

1. General principles of approximate partial modeling or simulation of a complex process are employed. This approach permits selecting one or several physical phenomena from the great number that constitutes full-scale combustion processes, which represent the most typical features of the aspect under study. With this approach, satisfying all of the similarity conditions is not mandatory, and success depends on correctly detecting the governing parameters and reproducing them in modeled conditions. In addition, the physical model should not only represent the full-scale processes correctly, but also be much simpler. The comparison of model and full-scale results is the most comprehensive means of verifying the assumptions made in the development of the approximate partial modeling method.

2. Injector elements with full-scale geometry are used in the model. This approach provides for the most convenient comparison between the model and the full scale.

3. The influence of neighboring element sprays on the combustion process in the initial section of the spray (which is mostly sensitive to disturbances) can be neglected, because bipropellant injector elements are assumed to operate, to a substantial extent, independently.

4. Selection of boundary conditions and governing criteria are based on physical concepts of the process being studied.

5. The boundaries of regions of spontaneous excitation and damping in the mode tests are determined by propellant mass flow rate variation. Changes of the boundary positions are indicative of the increased or decreased combustion stability to soft (spontaneous) or hard (dynamic) excitation.

6. Combustion chamber mean pressure p exerts no principal influence on chamber acoustic field spatial parameters, which are defined by the relative value of acoustic pressure oscillations p'/p.

7. The phases of the combustion chamber acoustics and the combustion process in the model should be identical to that of the full-scale chamber, i.e.,

$$\Omega = (\tau f)_m^{-1} = (\tau f)_{fs}^{-1}.$$

Here f = 1/Tp is the acoustic oscillation frequency specified by oscillation period Tp and τ is the characteristic delay time, i.e., the duration of the propellant conversion to combustion gases. A set of design and operating parameters, proportional to τ, is determined by analyses of the physical features of the processes and the known analytical or experimental relations for typical atomization and mixing patterns. The processes, as far as the amplitude criterion $N_A = |\delta_{gen}|/\delta_{ac}$ is concerned, are assumed to be self-similar in most cases; therefore, the dimensionless phase criterion Ω is the only stability parametric criterion to be determined.

8. The phases of the injector manifolding acoustics and the injection processes in the model should be identical to that of the full-scale injector, i.e.,

$$\Omega = (\tau_{inj} f)_m^{-1} = (\tau_{inj} f)_{fs}^{-1}.$$

This identity represents the time delay τ_{inj} of propagation of acoustic disturbances along an injector passage of length L_{inj} at a sound velocity c_{inj} , where $\tau_{inj} \sim L_{inj}/c_{inj} \sim L/f_{inj}$, and f_{inj} is the natural frequency of the injector being investigated. This identity is satisfied by selecting proper geometry of the model feed manifolds and by setting such gaseous propellant temperature at which the sound velocity in model and full-scale tests would be the same, $c_{inj,m} = c_{inj,fs}$.

9. “The combustion chamber transverse oscillation frequencies in the model should be the same as in the full-scale chamber,

$$f_{c,m} = f_{c,fs}.$$

This condition is satisfied by a proper selection of model chamber diameter d_m, accounting for effective chamber combustion sound velocity c_m

$$d_m = \frac{d_{fs} c_m}{c_{fs}}.”$$

10. Injector elements to be investigated in a single-element setup should be placed close to the combustion wall, where tangential mode oscillation amplitudes are highest. High frequency combustion instability is most often encountered during the development of combustion chambers and gas generators for liquid rocket engines, and instabilities in transverse tangential modes are most likely to occur.

11. Mixing is the governing factor in the whole complex of physical and chemical processes in combustion chambers and gas generators. This is because in high pressure liquid rocket engines, especially with staged combustion cycles, atomization and vaporization are not rate-limiting factors in the entire complex of physical and chemical processes involved in combustion, as they are either completed very quickly or are actually absent. Also, at these high pressures and high temperatures, chemical kinetic processes proceed very quickly and have little part in the total combustion duration in the combustion zone. Thus, because atomization, vaporization, and kinetics process times are relatively unimportant under actual conditions of rocket engine combustion, mixing should be the rate controlling stage of the entire combustion process. The response times of the combustion zone processes should be mainly defined by the mixing time τ_{mix}.

12. Propellants, actual or simulated, are in the gas form. In high-pressure liquid rocket engines, combustion occurs at pressures above the critical pressures of the propellants used, and propellant temperatures at the injector inlet are close to the critical temperature. Under these conditions, the physical properties of the oxidizer and the fuel being injected approach the properties of the dense gas. Thus, when the conditions leading to high-frequency instability in full-scale engines are modeled at low pressure, the modeled conditions will be closer to the actual ones if gaseous propellants are used instead of liquid. For closed cycle (staged combustion) engines, in which one or both propellants are fed to injectors in the gas phase, this approach using gaseous propellants seems even more justified.

13. A special expedient for simulating mixing is assumed: reactive propellants (oxidizer and fuel) are diluted with inert gases (such as nitrogen and helium). This technique permits the volume flow rates and thus the discharge

velocities of the fuel or oxidizer to change without changing reactive component mass flow rate. Consequently, various ratios of the propellant velocities and densities could be provided at the injector element exit with constant values of the reciprocal of the equivalence ratio $\emptyset = (\dot{m}_0/\dot{m}_f)(1/r_{st})$.

14. Reversing the propellant feeds, i.e., feeding the fuel through the oxidizer passage and feeding the oxidizer through the fuel passage, is allowed. Under some conditions, this may provide a better approximation of the model conditions to the full scale. [7]

Similarity Parameters

The important combustion similarity parameters for liquid propellant rocket combustion flows can be obtained from the conservation equations for mass, momentum and energy in nondimensional form. The nondimensional parameters that multiply the dimensionalless differential equations can then be identified [7], [8]. Some of these similarity parameters are given below. For the various experiments discussed in this paper, refer to the reference for that experiment for further discussion of the similarity parameters and how they were determined for that particular experiment. Also considered when designing the experiments was Reynolds Number for both the fuel and oxidizer.

The velocity of the propellant is determined by

$$V = \frac{V\dot{m}_{prop}}{\rho_{prop}A_{inj}}.$$

Volumetric flow rate is

$$\dot{Q} = \frac{\dot{m}_{prop}}{\rho_{prop}}.$$

Velocity ratio is

$$VR = \frac{V_{fuel}}{V_{0x}}.$$

Volumetric flow rate ratio is

$$QR = \frac{\dot{Q}_{fuel}}{\dot{Q}_{ox}}.$$

Momentum Ratio is

$$MR = \frac{\dot{m}_{fuel} V_{fuel}}{\dot{m} v_{0x}}.$$

Equivalence ratio is

$$\Phi = \frac{\left(A/F\right)_{stoic}}{\left(A/F\right)}$$

Instability mode frequency relations between the model and the full-scale chamber are considered equal, as stated in assumption 9 above,

$$f_{c,m} = f_{c,fs}.$$

Experimental Setup at the Propulsion Research Center

The University of Alabama in Huntsville Propulsion Research Center has a sophisticated combustion instability test facility. The test stand has one full-scale injector and uses gaseous methane and oxygen for propellants and nitrogen for diluents. The instrumentation consists of up to nine high frequency pressure transducers with a sample rate of 60,000 Hz, six in chamber thermocouples, fuel and oxygen feed line thermocouples, an ambient air thermocouple, chamber static pressure transducers and the ability to read in frequency and amplitude on a real-time Fast Fourier Transform (FFT).

The high frequency pressure transducers are connected to a 10,000 Hz low pass Butterworth filter. The pressure transducers are located around the circumference of the combustion chamber at angular positions recommended by NASA to get the optimimum resolution of tangential instabilities. The recommended locations along with the actual configuration are shown in Figure 1.8.

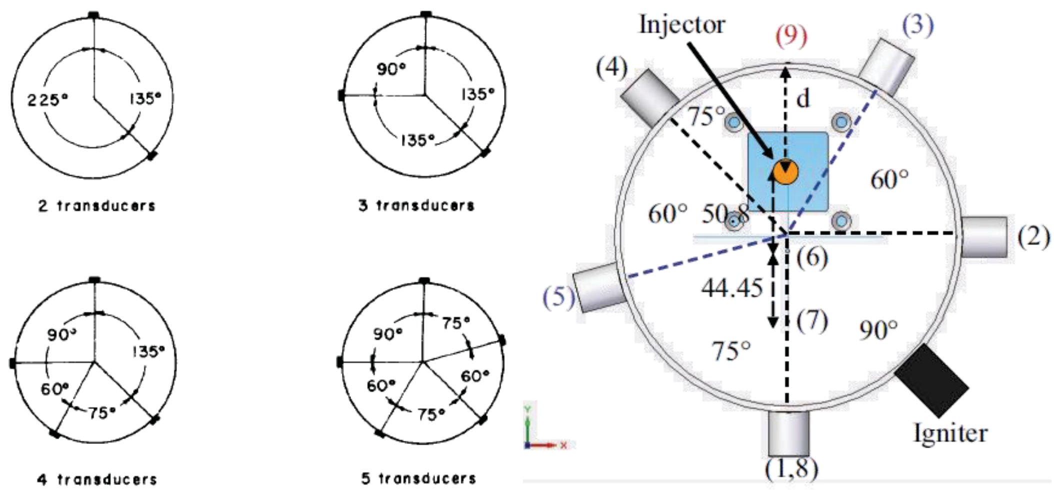

Figure 1.8 NASA recommended pressure transducer locations (left) [6] and the location of the pressure transducers in the experimental combustion chamber at the UAH PRC (right) [10].

The dimensions of the combustion chamber are shown in Figure 1.9, while a typical test configuration of the test area is shown in Figure 1.10. Tests are recorded using high speed video using the mirror shown in Figure 1.10 to avoid heat damage to the camera. Figure 1.11 shows a general schematic of the test facility.

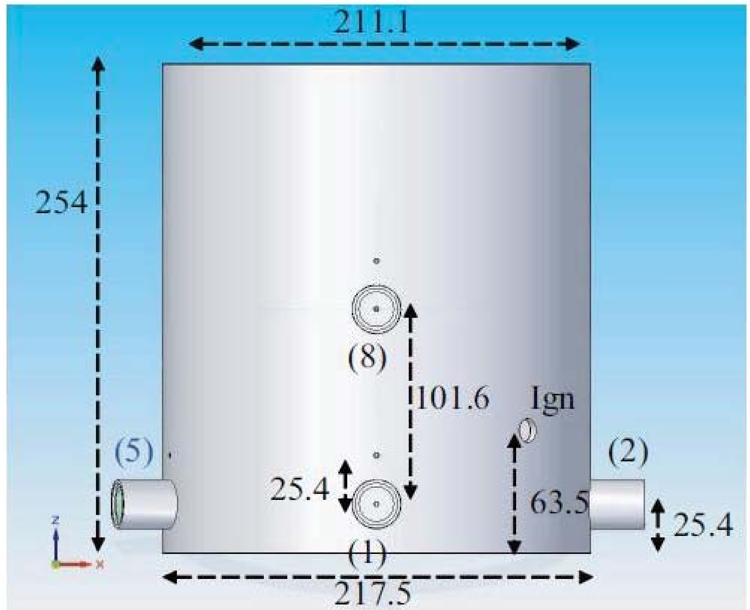

Figure 1.9 Dimensions of the scaled combustion chamber, units are in mm [10].

Figure 1.10 Combustion Instability Test Facility setup.

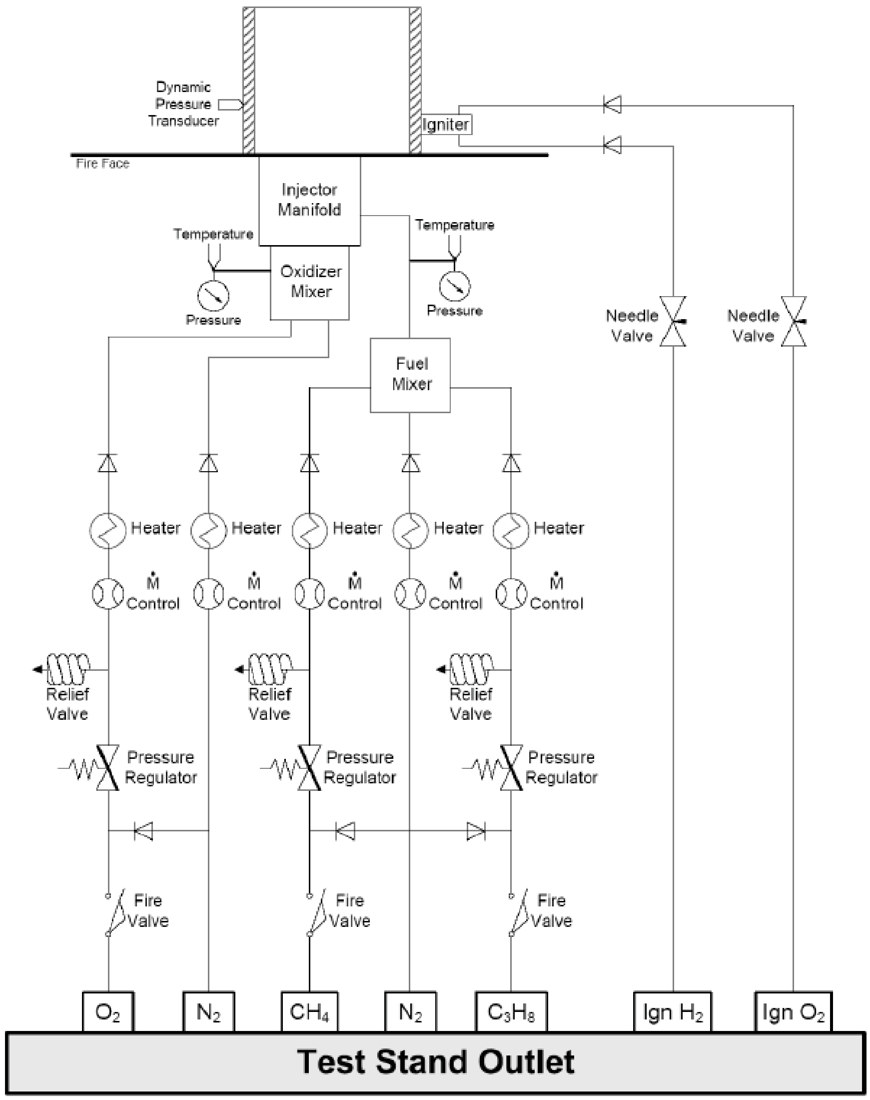

Figure 1.11 Schematic of the Combustion Instability Test Facility [11].

Research that has been done at the Propulsion Research Center

Research on combustion instability at the University of Alabama in Huntsville PRC began in 2007. Ryan Cavitt designed, built and tested the combustion instabillity test facility based on the scaling methodology described in the previous section. His primary objective was to determine if the methodology could recreate high frequency combustion instabilily. Gaseous oxygen and methane were used as propellants. The maximum pressure fluctuations achieved in his tests were 17% peak to peak of the mean chamber pressure. Pentad impinging jet injectors with angels of 30°, 45°, and 60° were tested and each showed different combustion instability characteristics. Mode determination was done by the use of a single pressure transducer and found based upon the frequency of the pressure oscillation. The first radial mode (1-R) and second tangential (2-T) modes were excited in these tests [12], [13] , [14], [15].

Robert Byrd was the next graduate student to work on combustion instability using the same method in 2008. He tested the same impinging pentad injectors that Ryan Cavitt did. Flow rates for his tests varied from 0.11 g/s to 0.55g/s for methane and 0.22 g/s to 4.36 g/s for oxgyen. Three different injector locations were tested; the center of the chamber, 39.8% of the chamber radius and 75.9% of the chamber radius. Peak to peak pressure flucstuations for these tests got up to 17%. Six high frequency pressure transducers were used and both the phase of the pressure oscillation and the frequency were used for mode deteremination. First tangential, second tangential and first radial modes were all found in these tests [10], [16].

Huy Huynh used a similar testing method in 2009 to test a shear coaxial injector. In these tests the injector location was varied from 0% to 88% of the chamber radius. The total gaseous propellant flow rates varied from 1.0 g/s to 3.8 g/s. Six high frequency pressure transducers and phase were used to determine modes. First radial modes occurred at injector locations less than 50% of the chamber radius and tangential modes occurred at chamber locations greater than 50% of the chamber radius. The modes detected had pressure fluctuations amplitudes up to 4.5% of the mean chamber pressure [9].

Shawn Ikard evaluated the stability characteristics of a swirl-coaxial injector in 2009. The testing matched specific scaling parameters of a full scale engine. The scaling parameters were mixture ratio, velocity ratio, momentum ratio and momentum flux ratio. The maximum amplitude of the pressure fluctuations was measured to be 3.52% of the mean chamber pressure. Modes were determined by analyzing the phase, frequency and amplitude of the six high frequency pressure transducers. Chemiluminecence imaging techniques were used and showed that during unstable combustion the combustion zone appear to lift off the injector, this is shown in Figure 1.12 [17].

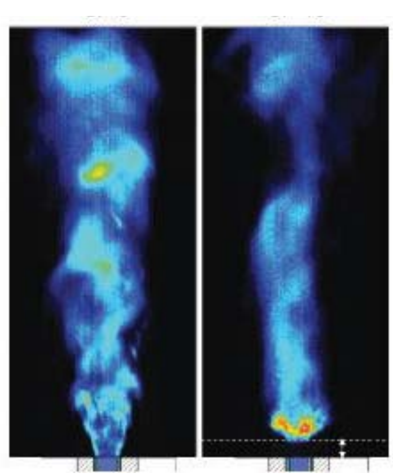

Figure 1.12 Comparison between attached (left) and lifted (right) combustion zone [17].

In 2010 heaters to the propellant feed lines were added to increase the ability to match specific scaling parameters. This work was done by John Brooks. Again the swirl-coaxial injector was tested and the momentum ratio, velocity ratio and equivalence ratio were all simultaneously matched. A 1-T, 1-R mode was matched that had a 2950 Hz signal and varied in amplitude from 0.09% to 0.41% of the mean chambrer pressure. The other dominant mode detected was either a 1-R or 3-T mode at 2350 Hz with an amplitude that varied from 0.084% to 1.19% of the mean chamber pressure [18].

More research, done by Brian Sweeney, attempted to replicate the combustion instability modes and frequences of a well document, full-scale liquid rocket engine that had been built and tested by Rocketdyne using the same experimental setup. This research used a shear-coaxial injector with the same dimensions as those used in the Rocketdyne testing. First this research three different chamber sizes were tested, each with a length of 5 in. and diamters of 2.5 in., 3 in., and 4 in. This allowed for the determination of a chamber size that would theoretically have acoustic characteristics similar to the full scale Rocketdyne engine. The three chambers tested are shown in Figure 1.13. Air entrainment into the chamber and heat loss through the chamber walls was found to be problematic. A 1-T mode pressure oscillation was generated at approximately 4,000 Hz at an amplitude of 0.01% of the mean chamber pressure. This amplitude is very low and did not cause the flame to go unstable [11].

Figure 1.13 The three different scaled combustion chambers used by Brian Sweeney [11].

The air entrainment problem was addressed by Ben Richman in 2011. He attempted to prevent air entrainment by placing plates with various sized orifices ontop of the combustion chamber. He then analyzed the effects this had on the combustion instability properties. The focus was on determining the frequency, amplitude and mode of the pressure oscillations within the combustion chamber. Numerous signal processing and Fourier analysis techniques were employed to analyze the data and compare it to solutions of the wave equation. The results showed that when an orifice plate was used 1-T, 3-T and 5-T modes occurred with 3-T modes being the most common [19].

Anthoney Hotaling in 2011 began research to determine the effect oxygen post length of an injector had on the frequencies that occur within a combustion chamber using this same methodology. He tested two different oxygen post lengths. The first one was the same shear-coaxial injector that Brian Sweeney used and the second one had a reduced oxygen post length. These results are still processing and will be published as a

University of Alabama in Huntsville thesis in 2012. The data collected for these tests is also analyzed in the data analysis section of this paper to verify the analysis methodology that has been developed.

The Korea Areospace Research Insitute also uses an experimental setup similar to the one at UAH to study combustion instability. Their facility also uses gaseous oxygen and methane as propellants. In one experiment they designed several double swirl coaxial injector to compare the first tangential frequency of the scaled chamber to that of a full scale thrust chamber. The results showed that “the coupling between the combustion phenomena and the 1T frequency in the model combustion chamber becomes strenghtened according to the increase of a recess ratio” of the injector [20].

At Georgia Institute of Technology’s Aerospace Combustion Laboratory they have a similar setup which uses heptane and air for propellants. The research focus is on using “smart” fuel injectors that can vary their spray characteristics. The results showed that these “smart” injectors could be used to improve combustion stability and minimize the amplitude of instabilities [21].

CHAPTER TWO

ANALYSIS METHODOLOGY

Acoustic Wave Equation

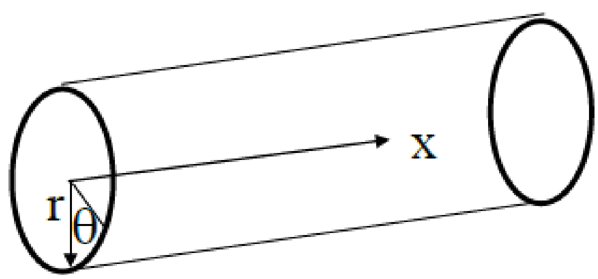

Figure 2.1 Cylindrical coordinates used for this derivation.

The literature recommends using Equation (2.1) to model the high frequencies acoustic modes within a combustion chamber [3][22][23][24]. Figure 2.1 shows the coordinate system used in this analysis. To simplify the analysis, several assumptions have been made in the following derivation:

- There is no mean flow through the combustion chamber.
- The medium is homogenous, that is there are no thermal gradients.
- The analysis is based on a linear model, with small disturbances.

- The flow is isentropic.
- There are no longitudinal modes due to the top of the chamber being open.
- The modes are standing (the pressure node lines are stationary).

Starting from the wave equation

$$\frac{\partial^2 P}{\partial t^2} = c^2 \nabla^2 P \tag{2.1}$$

Where P = Pressure,

c = speed of sound,

∇^2= the Laplacian.

Expanding in cylindrical coordinates

$$\frac{\partial^2 P}{\partial t^2} - c^2 \left[\frac{\partial^2 P}{\partial x^2} + \frac{1}{r}\frac{\partial P}{\partial r} + \frac{\partial^2 P}{\partial r^2} + \frac{1}{r^2}\frac{\partial^2 P}{\partial \theta^2}\right] = 0.$$

Assumed solution form from separation of variables

$$P(x, r, \theta, t) == X(x)R(r)\Theta(\theta)e^{i\omega t},$$

ω = 2π* f,

f = frequency of wave.

Substituting these equations into each other results in

$$-\left(\frac{\omega}{c}\right)^2 = \frac{1}{X(x)}\frac{\partial^2 X(x)}{\partial x^2} + \frac{1}{R(r)}\frac{\partial^2 R(r)}{\partial r^2} + \frac{1}{rR(r)}\frac{\partial R(r)}{\partial r} + \frac{1}{r^2}\frac{\partial^2 \Theta(\theta)}{\partial \Theta^2}.$$

Solving for $\Theta(\theta)$

$$\frac{r^2}{X(x)}\frac{\partial^2 X(x)}{\partial x^2} + \frac{r^2}{R(r)}\frac{\partial^2 R(r)}{\partial r^2} + \frac{r}{R(r)}\frac{\partial R(r)}{\partial r} + \left(\frac{\omega}{c}\right)^2 = \frac{-1}{\Theta(\theta)}\frac{\partial^2 \Theta(\theta)}{\partial \Theta^2} = m^2,$$

$$\frac{\partial^2 \Theta(\theta)}{\partial \Theta^2} + m^2\Theta(\theta) = 0.$$

Solution for $\Theta(\theta)$

$$\Theta(\theta) = Be^{\pm im\theta}.$$

m = an integer, each time it increases by 1 the pattern is repeated.

Solving for X(x)

$$-\frac{1}{X(x)}\frac{\partial^2 X(x)}{\partial x^2} = \frac{1}{R(r)}\frac{\partial^2 R(r)}{\partial r^2} + \frac{1}{rR(r)}\frac{\partial R(r)}{\partial r} + \left(\frac{\omega}{c}\right)^2 - \left(\frac{m}{r}\right)^2 = k_x^2,$$

$$\frac{\partial^2 X(x)}{\partial x^2} + k_x^2 X(x) = 0.$$

Solution for X(x)

$$X(x) = Ce^{\pm ik_x x}.$$

Solving for R(r)

$$\frac{\partial^2 R(r)}{\partial r^2} + \frac{1}{r}\frac{\partial R(r)}{\partial r} + \left[\left(\frac{\omega}{c}\right)^2 - \left(\frac{m}{r}\right)^2 - k_x^2\right] R(r) = 0,$$

$$k_r^2 = \left(\frac{\omega}{c}\right)^2 - k_x^2.$$

$$\frac{\partial^2 R(r)}{\partial r^2} + \frac{1}{r}\frac{\partial R(r)}{\partial r} + \left[k_r^2 - \left(\frac{m}{r}\right)^2\right] R(r) = 0,$$

$$y = k_r r,$$

$$k_r^2 \frac{\partial^2 R(y)}{\partial y^2} + \frac{k_r^2}{y}\frac{\partial R(y)}{\partial y} + k_r^2\left[1 - \left(\frac{m}{r}\right)^2\right] R(y) = 0.$$

Divide by k_r^2

$$\frac{\partial^2 R(r)}{\partial y^2} + \frac{1}{y}\frac{\partial R(r)}{\partial y} + \left[1 - \left(\frac{m}{r}\right)^2\right] R(r) = 0.$$

Solution for R(y) is

$$R(y) = EJ_m(y) + FY_m(y).$$

Where J_m = Bessel function of the first kind and Y_m = Bessel function of the second kind.

Solution for $R(k_r r)$ is

$$R(k_r r) = EJ_m(k_r r) + FY_m(k_r r).$$

The Bessel functions for the first and second kind are shown in the next two figures. Since the Bessel functions of the second kind all diverge as r approaches 0 (the center of the cylinder), this does not provide a physically meaningful result. It would mean that the sound pressure in the center of the duct is infinite. Therefore, only Bessel functions of the first kind provide physical solutions. The solution becomes:

$$\mathrm{R}(\mathrm{k_r r}) = AJ_m(\mathrm{k_r r}).$$

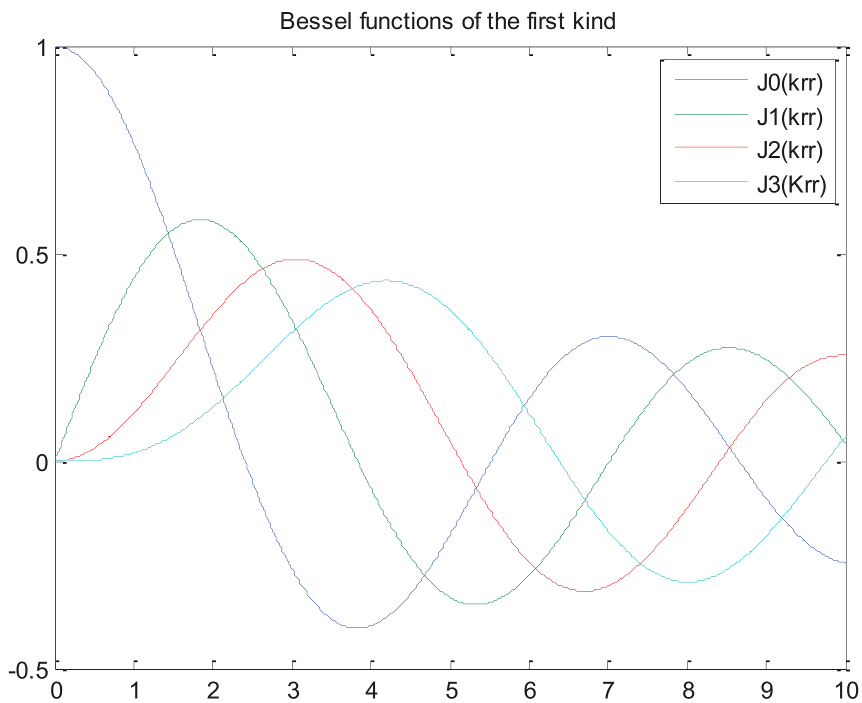

Figure 2.2 Graph of the Bessel Functions of the first kind.

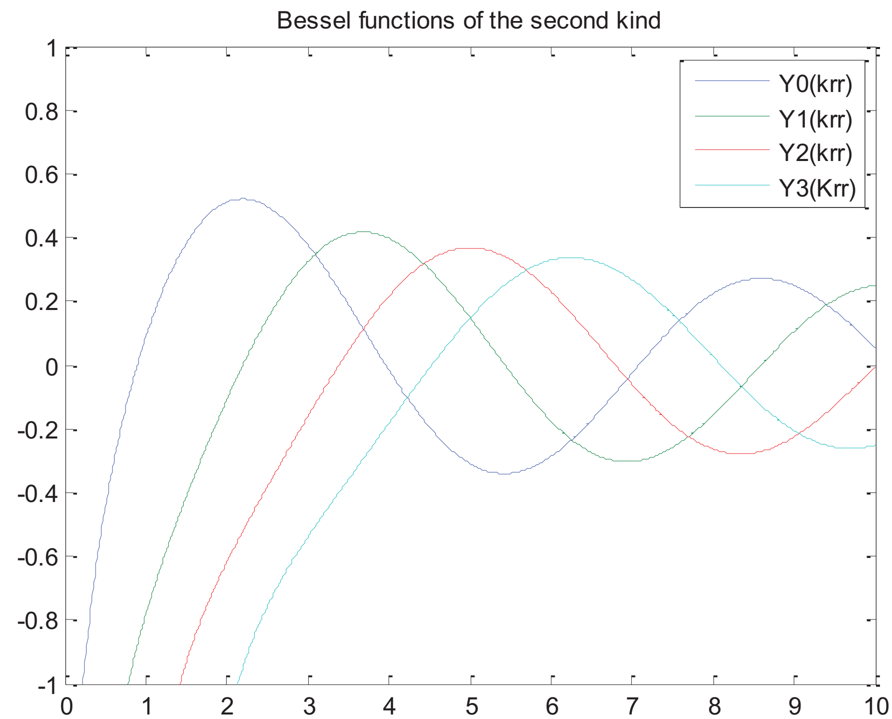

Figure 2.3 Bessel functions of the second kind, all of which diverge as $r \to 0$.

Final Solutions

$$P(x, r, \theta, t) = X(x)R(r)\Theta(\theta)e^{i\omega t},$$

$$X(x) = Ce^{\pm ik_x x},$$

$$\mathrm{R}(\mathrm{k_r r}) = AJ_m(\mathrm{k_r r}),$$

$$\Theta(\theta) = \mathrm{B}e^{\pm \mathrm{im}\theta},$$

$$P(x, r, \theta, t) = AJ_m(\mathrm{k_r r})e^{\pm ik_x x}\mathrm{e}^{\pm \mathrm{im}\theta}e^{i\omega t}.$$

- First term represents wave amplitudes as a function of radial coordinate.
- Second term is the positive or negative longitudinal motion of the wave.

- Third term describes waves going in both circumferential directions.
- The physically measureable sound field is the real part of equation #.

$AJ_m(\mathrm{k_r r})$ is termed the "radial parameter". It is found because the boundary condition for a wave moving down the cylinder (a forward moving wave), the particle velocity at the wall r = a is zero.

$$\frac{\partial p}{dr} = 0 \; at \; r = a.$$

Therefore,

$$\frac{\partial J_m(k_r r)}{\partial(k_r r)} = 0,$$

$$J'_m(k_r a) = 0.$$

There are an infinite number of solutions that satisfy this equation, so it is necessary to split it into the subscripts $\mathrm{k_{mn}}$ to define the different modes. Rewriting $P(x, r, \theta, t)$ with this term:

$$P(x, r, \theta, t) = A_{mn} J_m(\mathrm{k_{mn} r}) e^{\pm i k_x x} \mathrm{e}^{\pm \mathrm{i m \theta}} e^{i\omega t}$$

becomes

$$P(x, r, \theta, t) = A_{mn} J_m(\mathrm{k_{mn} r}) e^{i(\omega t - \mathrm{m\theta} - \mathrm{k_x} x)}.$$

Where k_{mn} is found from the nth root of

$$J'_m(k_{mn}r) = 0,$$

And r is nondimensionalized so that

$$r = \frac{r}{a}.$$

A graph of the derivatives of the Bessel functions of the first kind is shown in the figure below.

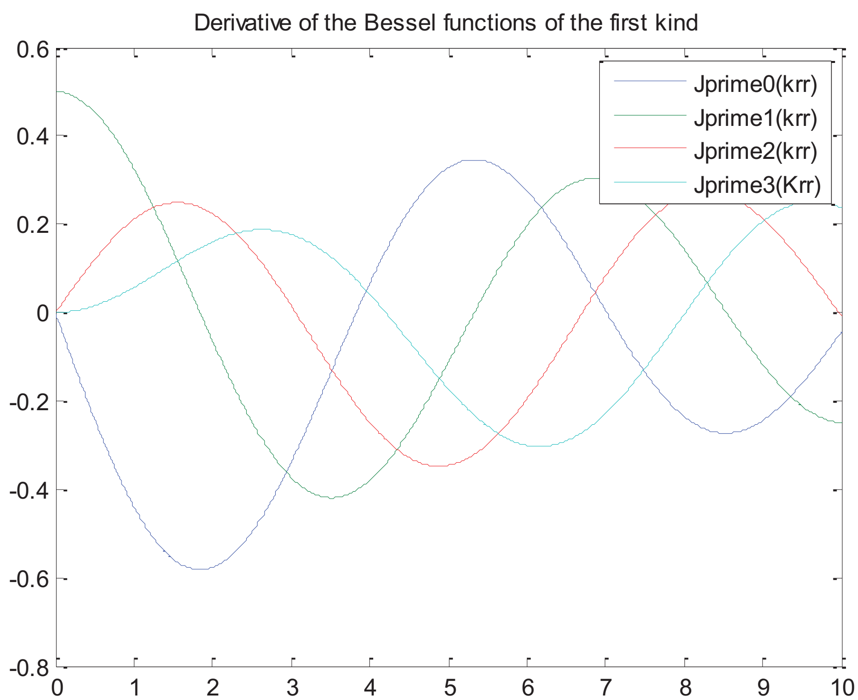

Figure 2.4 Graph of the derivative of the Bessel functions of the first kind.

The solution found so far is for a spinning wave. In order to determine the pressure distribution for a standing wave, a wave going in the opposite direction is added to the original equation,

$$P(x, r, \theta, t) = \frac{1}{2} A_{mn} J_m(\mathrm{k_{mn}r}) e^{i(\omega t - \mathrm{m\theta} - \mathrm{k_x} x)} + \frac{1}{2} A_{mn} J_m(\mathrm{k_{mn}r}) e^{i(\omega t + \mathrm{m\theta} - \mathrm{k_x} x)}. \qquad (2.2)$$

For this experiment, the chamber is a closed-open system. Therefore, longitudinal modes will not be considered in this analysis. Therefore $k_x = 0$,

$$X(x) = e^0 = 1.$$

Then (2.2) reduces to

$$P(x, r, \theta, t) = \frac{1}{2} A_{mn} J_m(\mathrm{k_{mn}r}) e^{i(\omega t - \mathrm{m\theta})} + \frac{1}{2} A_{mn} J_m(\mathrm{k_{mn}r}) e^{i(\omega t + \mathrm{m\theta})}. \qquad (2.3)$$

Equation 2.3 can be simplified further. From Euler's Formula $e^{ix} = \cos(x) + i\sin(x)$, (2.3) can then be rewritten

$$P(x, r, \theta, t) = \frac{1}{2} A_{mn} J_m(\mathrm{k_{mn}r})[\cos(\omega t - \mathrm{m\theta}) + i\sin(\omega t - \mathrm{m\theta})]$$

$$+ \frac{1}{2} A_{mn} J_m(\mathrm{k_{mn}r})[\cos(\omega t + \mathrm{m\theta}) + i\sin(\omega t + \mathrm{m\theta})].$$

Considering only the real part,

$$P(r, \theta, t) = \frac{1}{2} A_{mn} J_m(k_{mn} r) \cos(\omega t - m\theta)$$

$$+ \frac{1}{2} A_{mn} J_m(k_{mn} r) \cos(\omega t + m\theta). \qquad (2.4)$$

Equation (2.4) is the final form of the equation used for this analysis. The order of the m in the k_{mn} term represents the order of the tangential wave. The n in the k_{mn} term represents the order of radial wave. k_{01} = plane wave because the solution to $J'_0(k_{01}r) = 0$ provides only the trivial solution, the solution with no sound in the duct. Therefore, k_{01} is relabeled to be the first order radial mode. Table 2.1 has a summary of all the modes and the k_{mn} term.

As a verification of the use of Equation (2.4), the equation was solved for the entire chamber for a 2-T mode. The results as well as well as the theoretically predicted pressure distribution are shown in Figure 2.5. They match almost exactly.

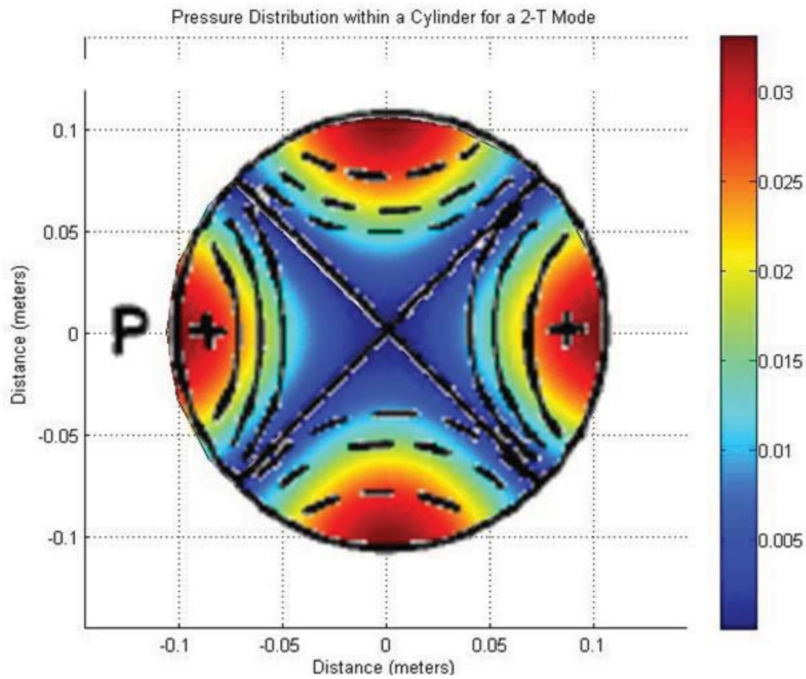

Figure 2.5 A 2-T mode pressure distribution viewed from the top, calculated using the above equation. For comparison, the expected pressure distribution from the literature as shown in Chapter 1 is place on top.

Cut on Frequency

For any mode (m,n combination), there is a minimum frequency below which the mode will not propagate, this is called the cut on frequency.

The cut on frequency is

$$k_{mn}^2 = \left(\frac{\omega}{c}\right)^2 - k_x^2 \text{ [24].}$$

Since for this case $k_x = 0$

$$k_{mn}^2 = \left(\frac{\omega}{c}\right)^2.$$

Cut on frequency at r = a

$$k_{mn} = \left(\frac{\omega}{c}\right) a = \left(\frac{2\pi f}{c}\right) a\,,$$

$$f = \frac{k_{mn} * c}{2\pi * a}. \tag{2.5}$$

That is to say for propagation of the wave $\left(\frac{2\pi f}{c}\right) a > k_{mn}$, and

$$c = \sqrt{\gamma \left(\frac{\bar{R}}{MW}\right) T}.$$

$$R = 8314.3 \frac{J}{kg * mol * K}$$

MW = 28 kg/Kmol,

γ = 1.34,

T = 600K.

The speed of sound then becomes

$$c = \sqrt{1.34 \left(\frac{8314.3 \frac{J}{kg * mol * K}}{28 \text{ kg/Kmol}}\right) 600K}.$$

$$c = 488.61 \text{ m/s}.$$

These are only approximations and may not be appropriate for every experimental setup. These parameters should be based on data taken for any given experiment. Large temperature gradients can exist because of the closed-open chamber design with a single element in the center. Also, mixture with the air and flame combustion products means that the gas properties in the chamber are not constant. The cut on frequencies for each mode has been calculated using these parameters and are shown in Table 2.1.

Table 2.1 The Cut On frequency for each mode.

Mode	m, n	Roots of $J'_m(k_{mn}r) = 0$	Cut On Frequency, (Hz)
Plane Wave	0,0	0	0.00
1-T	1,0	1.8412	1027
2-T	2,0	3.0542	1704
3-T	3,0	4.2012	2344
4-T	4,0	5.3176	2966
5-T	5,0	6.4156	3579
6-T	6,0	7.5013	4185
1-R	0,1	3.8317	2138
2-R	0,2	7.0156	3914
3-R	0,3	10.1735	5675
1-R, 1-T	1, 1	5.3314	2974
1-R, 2-T	2, 1	6.7061	3741
1-R, 3-T	3, 1	8.0152	4471
1-R, 4-T	4, 1	9.2824	5178
2-R, 1-T	1,2	8.5363	4762
2-R, 2-T	2, 2	9.9695	5562

CHAPTER THREE

STATISTICAL PROPERTIES

Many of the signals detected by the high frequencies pressure transducers in the combustion instability experiments have a high level of noise. A preliminary attempt to quantify the noise level in the experiments is described in the theory in this section. There are many methods to do this described in McDonough and Whalen's text "Detection of Signals in Noise" [25].

Central Limit Theorem

This theorem states that if you have a measured value X and that "if X is not dominated by a single error source but instead is affected by multiple, independent error sources, then the resulting distribution for X will be approximately normal." In other words, any completely random event should have a Gaussian distribution [26].

Gaussian Distributions

The Probability Density Function (PDF) of a Gaussian distribution is given by the formula

$$p(x) = \frac{1}{\sigma\sqrt{2\pi}} e^{\left({-(X-\mu)^2}/{2\sigma^2} \right)}.$$

For an infinite number of samples the distribution mean is

$$\mu = \lim_{n\to\infty} \frac{1}{N} \sum_{i=1}^{N} X_i.$$

For an infinite number of samples the standard deviation of the distribution is

$$\sigma = \lim_{n\to\infty} [\frac{1}{N} \sum_{i=1}^{N} (X_i - \mu)^2]^{1/2}.$$

Since it is impractical to consider an infinite number of samples, statistical properties for sample populations that consist of a finite number of measurements must be considered.

The mean of a sample population is

$$\bar{X} = \frac{1}{N} \sum_{i}^{N} X_i.$$

Standard deviation of the sample population is

$$s_X = [\frac{1}{N-1}\sum_{i=1}^{N}(X_i - \bar{X})^2]^{1/2}.$$

A graphical example of a probability density function for a Gaussian distribution with σ= 0.25 and μ = 0 is shown in Figure 3.1. A histogram of experimental data that matches a Gaussian distribution is shown in Figure 3.2. A Gaussian probability density function curve fit shown in red for comparison.

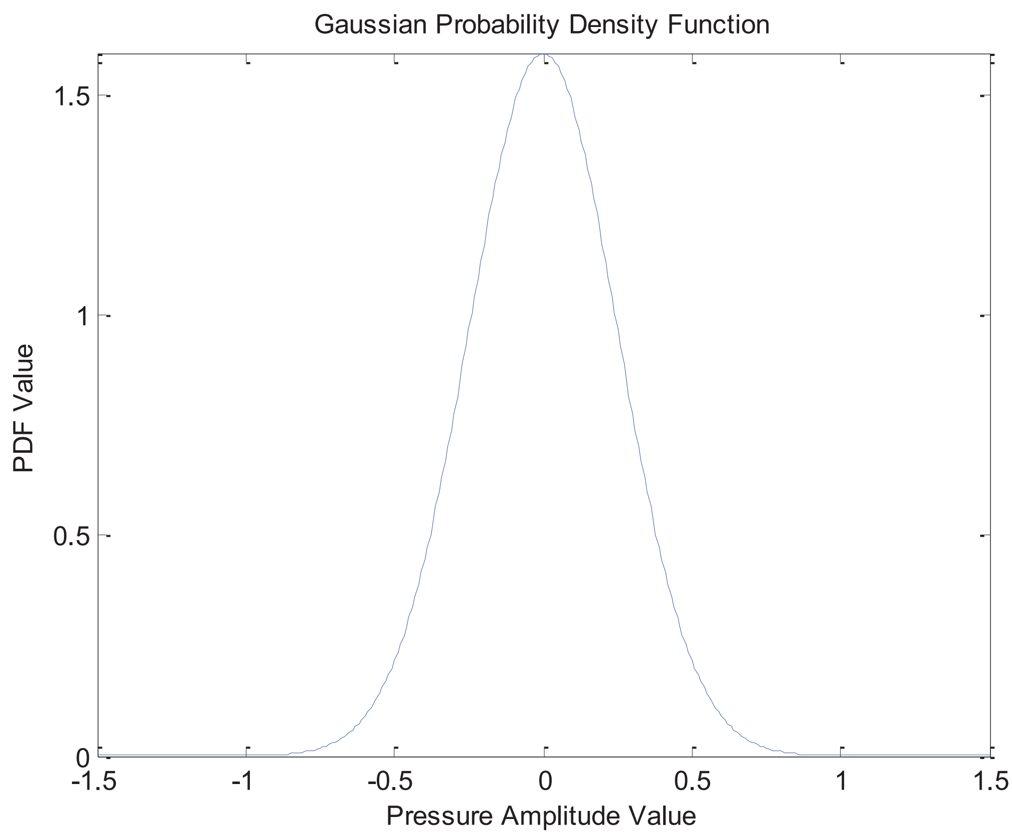

Figure 3.1 The probability density function for a Gaussian distribution with σ= 0.25 and μ = 0.

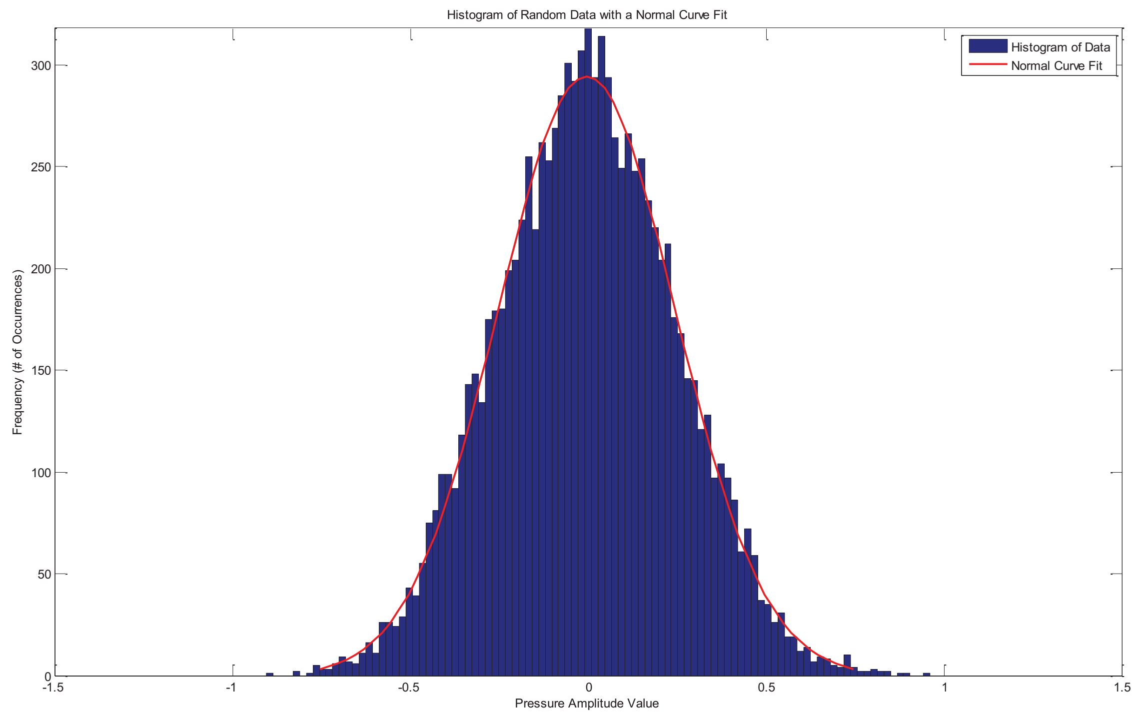

Figure 3.2 A histogram of a random distribution of 10,000 points with σ= 0.25 and μ = 0. The red curve shows a normal (Gaussian) distribution fitted to the data.

Skewness

The skewness provides a measure of how much the sample distribution is centered on the mean [27]. For a Gaussian distribution sk = 0. Skewness is given by

$$sk = \frac{\frac{1}{N}\sum_{i=1}^{N}(X_i - \bar{X})^3}{s_x^{\frac{3}{2}}}.$$

Kurtosis

The kurtosis represents the degree of "peakedness" of a distribution [27]. For a Gaussian distribution ku = 3, and for a sine wave ku = 1.5. The kurtosis is given by

$$ku = \frac{\frac{1}{N}\sum_{i=1}^{N}(X_i - \bar{X})^4}{s_x^2}.$$

Probability Density Function for a Sine Wave

The Probability Density Function (PDF) of a sine wave is given by the formula

$$p(x) = \begin{cases} \dfrac{1}{\pi\sqrt{2\sigma^2 - x^2}} & |x| < \sqrt{2}\sigma \\ 0 & |x| \geq \sqrt{2}\sigma \end{cases} \text{ [28].}$$

The probability density function for a sine wave is characterized by a distinct bimodal shape. A graph of a probability density function for a sine wave is shown in Figure 3.3. Histogram of a sine wave with A = 0.354, σ= 0.25, μ = 0 and Ku = 1.5 is shown in Figure 3.4.

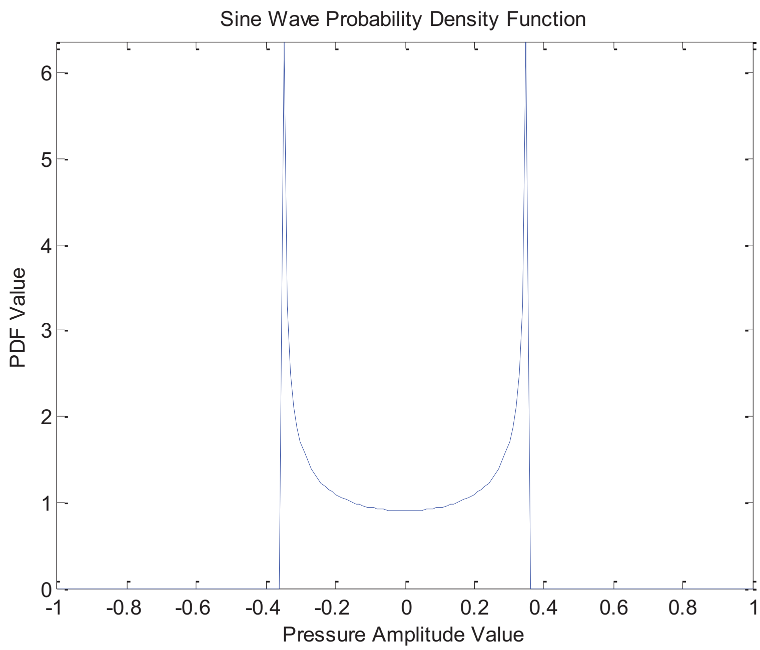

Figure 3.3 The probability density function for a sine wave with σ= 0.25, μ = 0 and Ku = 1.5.

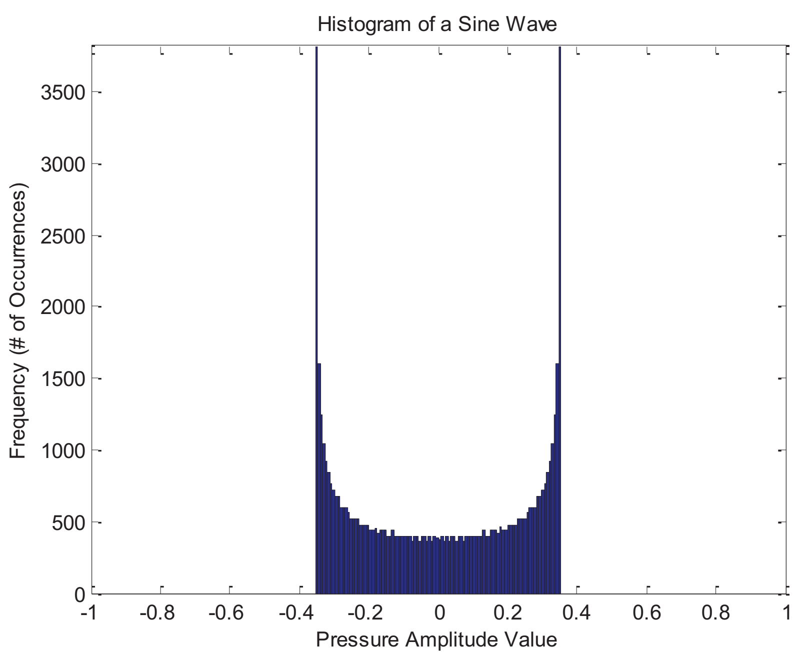

Figure 3.4 Histogram of a sine wave with A = 0.354, σ= 0.25, μ = 0 and Ku = 1.5.

Probability Density Function for Sine Wave plus Gaussian Noise

The Probability Density Function (PDF) of a sine wave plus Gaussian distribution is given by the formula

$$p(x) = \frac{1}{\sigma_n \pi \sqrt{2\pi}} \int_0^{\pi} e^{\left({-(A cos\theta - x)^2} / {(2{\sigma_n}^2)} \right)} d\theta \text{ [28].}$$

σ_n= standard deviation of Gaussian noise

A= amplitude of sine wave

A signal to noise ratio for this PDF

$$\alpha = \frac{A}{\sigma_n \sqrt{2}} \text{ [22].}$$

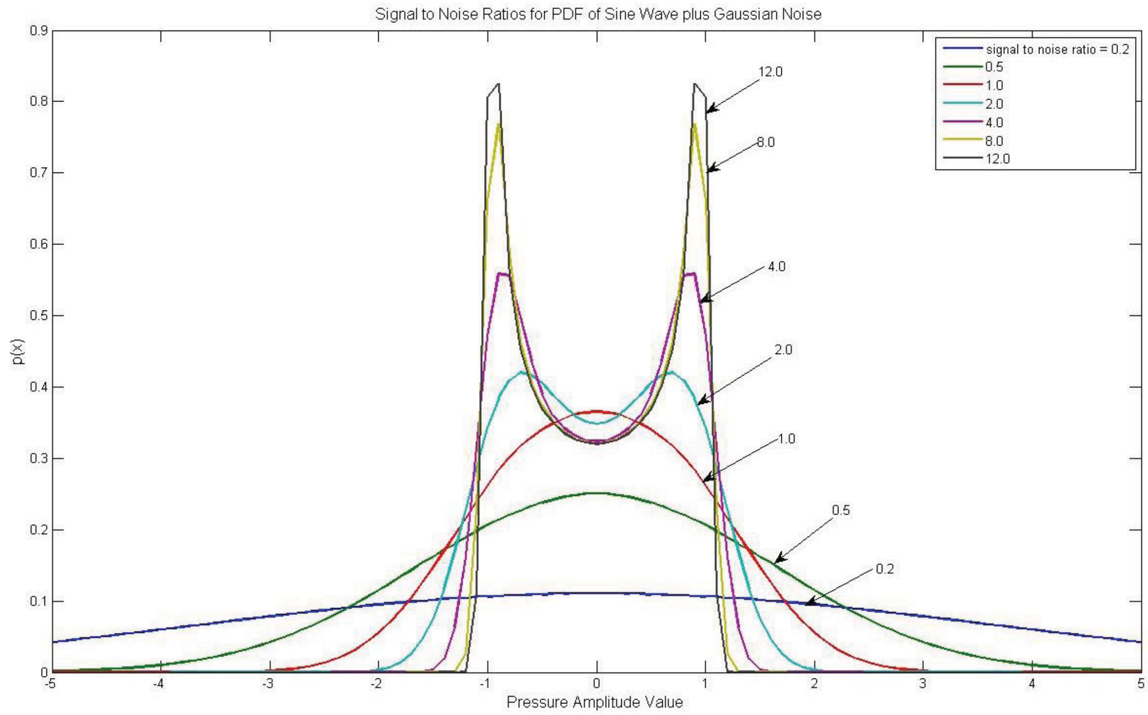

Figure 3.5 Different signal to noise ratios for the sine plus Gaussian Noise PDF function. Notice that the higher the signal to noise ratio, the more bimodal the shape of the curve appears.

From Figure 3.5 it can be seen that the different signal to noise ratios have different kurtosis (Ku) values associated with them. For a high signal to noise ratio of 12, the kurtosis is 1.5. For low signal to noise ratios, the kurtosis is closer to 3.0, which is that of a Gaussian distribution.

CHAPTER FOUR

MODE MATCHING ALGORITHM

The goal of analyzing combustion instability data at the PRC is to determine the mode, dominant frequency, amplitude, and node line angular location. The first pressure transducer is labeled P1, the second pressure transducer P2, and the third pressure transducer is P3. These follow the same layout of the combustion chamber as shown in Figure 1.12. All node angle locations use P1 as the reference. Figure 4.1 shows what a 2-T mode pressure distribution would look like in the combustion chamber from a top view.

To explain the development of the automated methodology, a 2-T mode with a node of angle of 10° from P1 will be used as an example. This is shown in Figure 4.2 as the distribution of the absolute amplitude of pressure over time from the top view. Figure 4.3 shows what the pressure over time plot for each of the three pressure transducers would look like for the first 2.5 milliseconds. Notice that each of the pressure transducers does not detect the same amplitude of signal due to their location with respect to the node lines of the mode.

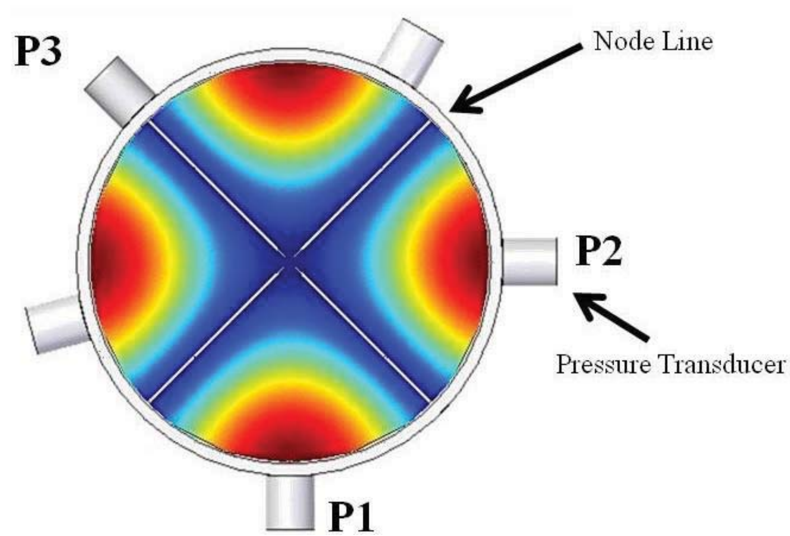

Figure 4.1 The pressure amplitude distribution of a 2-T mode within the combustion chamber.

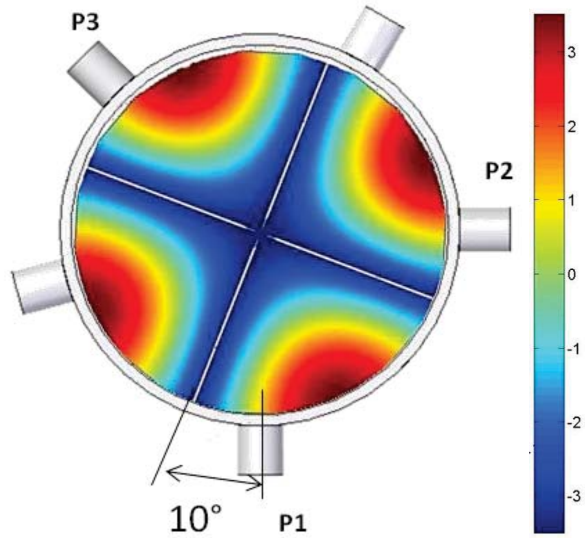

Figure 4.2 Top view of a 2-T mode with a node angle of 10 degrees with respect to P1.

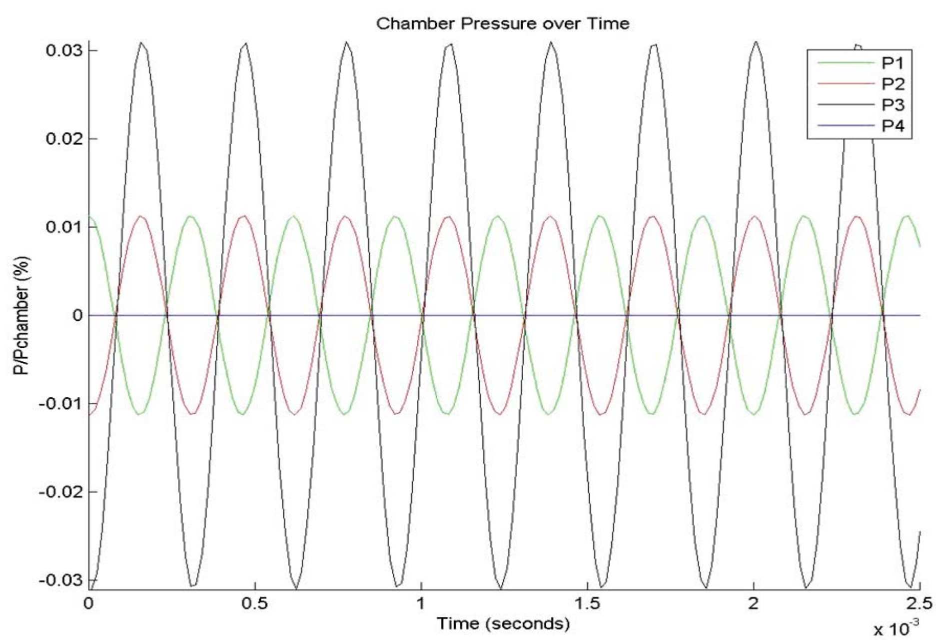

Figure 4.3 The expected pressure plot for the various pressure transducers within the combustion chamber for a 2-T mode at 10° from P1.

Dominant Frequency and Amplitude Ratios

In order to determine the dominant frequency the Fast Fourier Transform (FFT) of the signal is taken for each pressure transducer. This is done using the FFT command in Matlab. The FFT converts a signal from the time domain to the frequency domain, allowing for easy determination of the frequencies that compose a signal. The maximum amplitude for any of the pressure transducers is considered the dominant frequency. This frequency is assumed to be the frequency with the active mode in the chamber, and is the one considered for further analysis. The dominant frequency for the example 2-T mode at 10 is 3250 Hz. An FFT of the example mode data has been taken, and the results for the three pressure transducers are shown in Figure 4.4. The FFT verifies that the 3250 Hz signal is the dominant frequency.

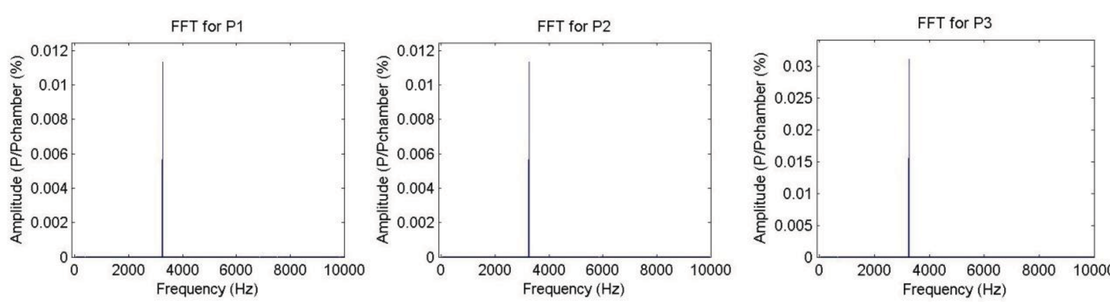

Figure 4.4 FFT of a theoretical 2-T mode at a node angle of 10°.

The next parameter to consider is the amplitude of the signal at each pressure transducer. For this purpose, it is taken directly from the FFT. The amplitude of the dominant frequency is considered the amplitude for the signal. As a way to nondimensionalized the amplitudes (since all tests will have different amplitudes), ratios between the amplitude of the various pressure transducers are found.

$$\frac{\text{P1}}{\text{P2}} = \frac{FFT(A_{P1})}{FFT(A_{P2})},$$

$$\frac{\text{P2}}{\text{P3}} = \frac{FFT(A_{P2})}{FFT(A_{P3})},$$

$$\frac{\text{P1}}{\text{P3}} = \frac{FFT(A_{P1})}{FFT(A_{P3})}.$$

Where FFT($A_{P\#}$) = the amplitude determined from the FFT for pressure transducer # at the dominant frequency.

For example, the amplitude ratios (ARs) for the 2-T mode at 10° are

$$\frac{\text{P1}}{\text{P2}} = 1.000,$$

$$\frac{\text{P2}}{\text{P3}} = 0.3640,$$

$$\frac{\text{P1}}{\text{P3}} = 0.3640.$$

These amplitude ratios have been found for all modes, at all node angle locations varying from 0 to 360 degrees. The value for all of these amplitude ratios are shown graphically in Appendix A for all modes.

Phase between Signals

From the FFT of the data, the phase information can found. This is done using the angle command in Matlab, which returns the phase angles in radians of complex elements. The angle command takes the arctangent of the imaginary portion of the FFT divided by the real portion of the FFT.

$$\text{Phase Spectrum in radians } = \text{phase } [FFT(A)] = arctangent\left(\frac{imag[FFT(A)]}{real[FFT(A)]}\right)$$

The phase difference is then found between P1-P2, P2-P3, and P1-P3.

$$\begin{aligned} Phase\ [P1 - P2] \\ &= \left[arctangent\left(\frac{imag[FFT(A_{P1})]}{real[FFT(A_{P1})]}\right)\right. \\ &\left. -\ arctangent\left(\frac{imag[FFT(A_{P2})]}{real[FFT(A_{P2})]}\right)\right] \end{aligned}$$

$$\begin{aligned} Phase\ [P2 - P3] \\ &= \left[arctangent\left(\frac{imag[FFT(A_{P2})]}{real[FFT(A_{P2})]}\right)\right. \\ &\left. - arctangent\left(\frac{imag[FFT(A_{P3})]}{real[FFT(A_{P3})]}\right)\right] \end{aligned}$$

$$\begin{aligned} Phase\ [P1 - P3] \\ &= \left[arctangent\left(\frac{imag[FFT(A_{P1})]}{real[FFT(A_{P1})]}\right)\right. \\ &\left. - arctangent\left(\frac{imag[FFT(A_{P3})]}{real[FFT(A_{P3})]}\right)\right] \end{aligned}$$

- $0° \rightarrow$ Completely in phase
- $180° \rightarrow$ Completely out of phase

For the example 2-T mode at 10°, the expected phase differences are

$$Phase\ [P1 - P2] = 180°,$$

$$Phase\ [P2 - P3] = 0°,$$

$$Phase\ [P1 - P3] = 180°.$$

These phase differences have been found for all modes, at all node angle locations varying from 0 to 360 degrees. The value for all of these phase differences are shown graphically in Appendix B for all modes.

At this point, the dominant frequency, the three amplitude ratios and the three phase differences are all known. This information can now be compared to the theoretical values determined in the section above. To do this a matching algorithm was developed in Matlab. The command used to determine matches is 'intersect'. The possible node lines and modes that match the AR of the signal are reported in an excel file. Next the possible node lines and modes that match the phase of the signal are reported in the excel file. The node lines and modes that match in both AR and phase are then determined. Finally, the results are filtered through the cut on frequencies listed in the table in the previous section. Only modes that have dominant frequencies greater than the cut on frequency are reported. The entire matching code is given in Appendix C. The algorithm has been given the name Acoustic Mode Analysis Program (AMAP). Figure 4.5 provides a flowchart that fully describes how this methodology works.

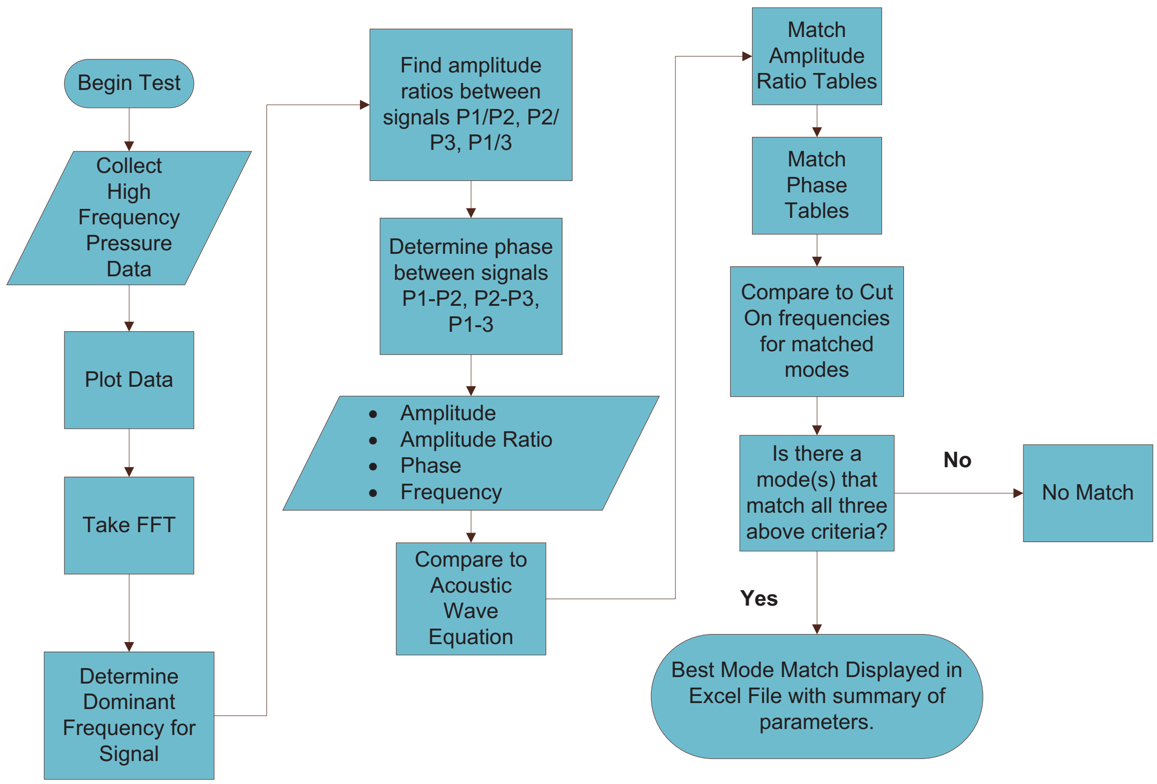

Figure 4.5 Analysis methodology flowchart.

Maximum Amplitude in Chamber

The last parameter determined is the maximum amplitude experienced in the entire chamber when a mode is active. Once the node angle is known, the relationship between this node angle and the maximum amplitude location is also known. Ratios between all possible node angle locations and the maximum amplitude location have been determined. When the node angle location is determined, it is multiplied by this ratio to get an estimate of what the maximum pressure experienced in the chamber is. For this paper, this estimated value is termed “calculated max amplitude in chamber”. From

Figure 4.6, which shows the location of the maximum pressure and the location of the node, it is easy to see how the ratio between the two amplitudes can be obtained.

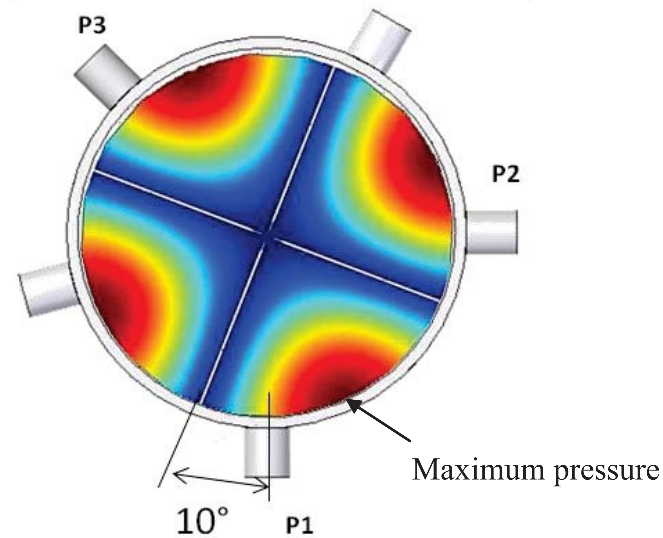

Figure 4.6 Location of maximum amplitude in the chamber compared to the node angle.

CHAPTER FIVE

VERIFICATION TESTING OF MATCHING ALGORITHM

In this section, artificial test data is created using Equation (2.4), for each mode type. The equation is used is shown again below. This test data is created for a given mode, at a given node location. All node locations are referenced based upon the location of the first pressure transducer, P1. The test data is then processed through the mode-matching program to verify the correct matching algorithms are employed in this program.

$$P(x,r,\theta,t) = \frac{1}{2}A_{mn}J_m(\mathrm{k_{mn}r})\cos(\omega t - \mathrm{m\theta}) + \frac{1}{2}A_{mn}J_m(\mathrm{k_{mn}r})\cos(\omega t + \mathrm{m\theta})$$

Test 1 Verification of the 1-T Mode at Node Angle = 10°

Using Equation (2.4) a 1-T mode has been modeled inside of a cylinder that has the same diameter as the combustion chamber. This is shown in Figure 5.1. The z-axis shows the absolute amplitude of pressure over time experienced within the combustion chamber. Figure 5.2 shows the pressure over time that would be experienced by the pressure transducers around the chamber if a 1-T mode at 10° was active.

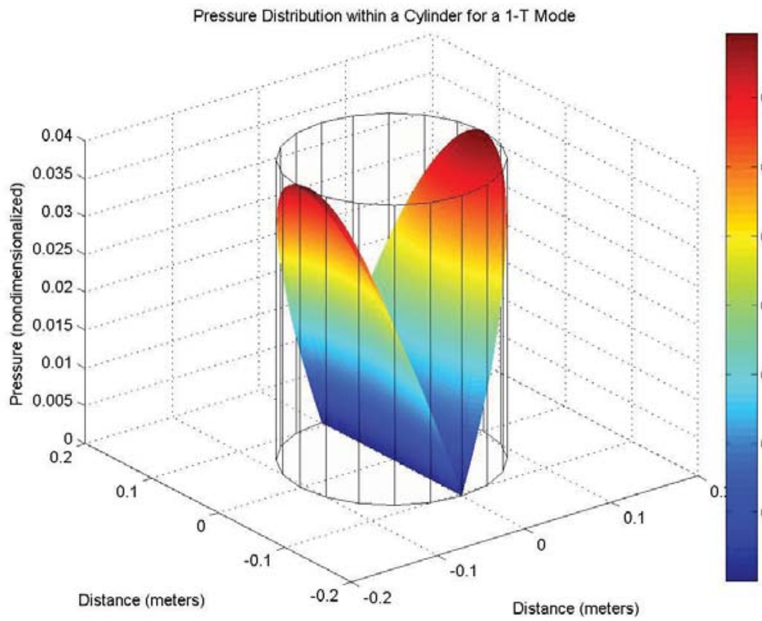

Figure 5.1 Expected pressure distribution within the combustion chamber for a 1-T mode.

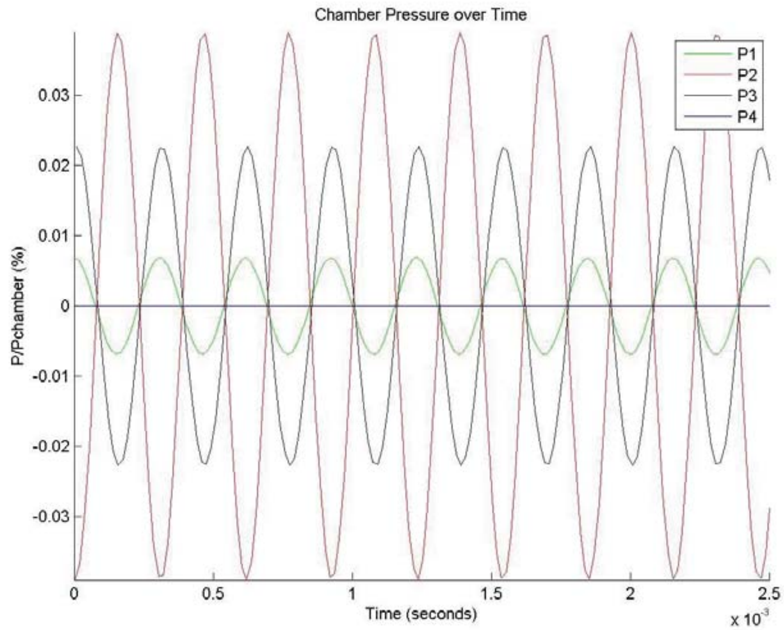

Figure 5.2 Pressure with respect to time for a 1-T mode at a node angle of 10° from P1.

The program requires an input for P4 because for the real test data there is pressure data for P4. Due to the location of P4 at a different longitudinal position on combustion chamber, P4 is useful for detecting longitudinal modes. However, since the combustion chamber is open at the top, longitudinal modes are not considered in this analysis. The data from P4 is included for completeness only. Therefore, for these verification tests, P4 is input as a very low amplitude cosine wave. Table 1.1 shows the results of the program. A 1-T mode is correctly identified at a node angle of 10 degrees.

It also lists a match for 190 degrees. This is because there is one node line and the mode shape is repeated every 180 degrees.

Table 5.1 Summary of results after running theoretical data through the Acoustic Mode Analysis Program for a 1-T mode.

	P1/P2	P2/P3	P1/P3	Node Angle	Matches Freq, AR and Phase
Dominant Frequency (Hz)	3250	3250	3250	10	1-T Mode
Amp Ratios from FFT	0.176327	1.71696	0.302746	190	1-T Mode
Phase Diff (degrees)	180	180	7.82E-15		
Calculated Max Amplitude in Chamber (P/PChamber)	0.039582				
Actual Amplitude (P/PChamber)	0.0396				

Test 2 Verification of the 2-T Mode at Node Angle = 10°

Using the same method described for the 1-T Mode Verification, equations were written for the three different pressure transducer locations for the 2-T Mode. The absolute pressure experienced in the combustion chamber is shown in the figure below, and the output of the program is shown in the table. The pressure over time that would be experienced by the pressure transducers around the chamber if this mode were active is shown graphically in the appendix. The program is able to accurately determine the existence of a 2-T mode at the correct node line locations.

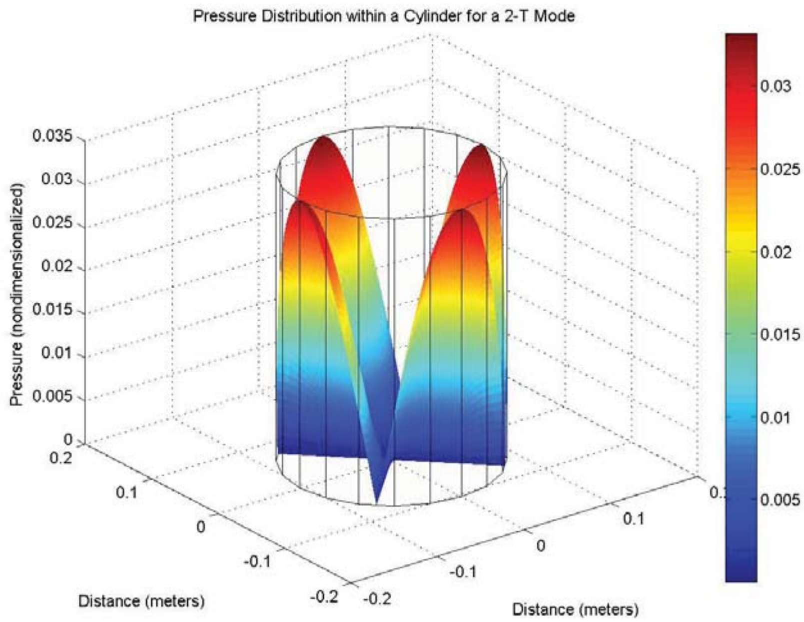

Figure 5.3 Expected pressure distribution within the combustion chamber for a 2-T mode.

Table 5.2 Summary of results after running theoretical data through the Acoustic Mode Analysis Program for a 2-T mode.

	P1/P2	P2/P3	P1/P3	Node Angle	Matches Freq, AR and Phase
Dominant Frequency (Hz)	3250	3250	3250	10	2-T Mode
Amp Ratios from FFT	1	0.36397	0.36397	100	2-T Mode
Phase Diff (degrees)	180	0	180	190	2-T Mode
Calculated Max Amplitude in Chamber (P/PChamber)	0.033093			280	2-T Mode
Actual Amplitude (P/PChamber)	0.0331				

Test 3 Verification of the 3-T Mode at Node Angle = 10°

Using the same method described for the 1-T Mode Verification, equations were written for the three different pressure transducer locations for the 3-T Mode. The absolute pressure experienced in the combustion chamber is shown in the figure below, and the output of the program is shown in the table. The pressure over time that would be experienced by the pressure transducers around the chamber if this mode were active is shown graphically in the appendix. The program is able to accurately determine the existence of a 3-T mode at the correct node line locations.

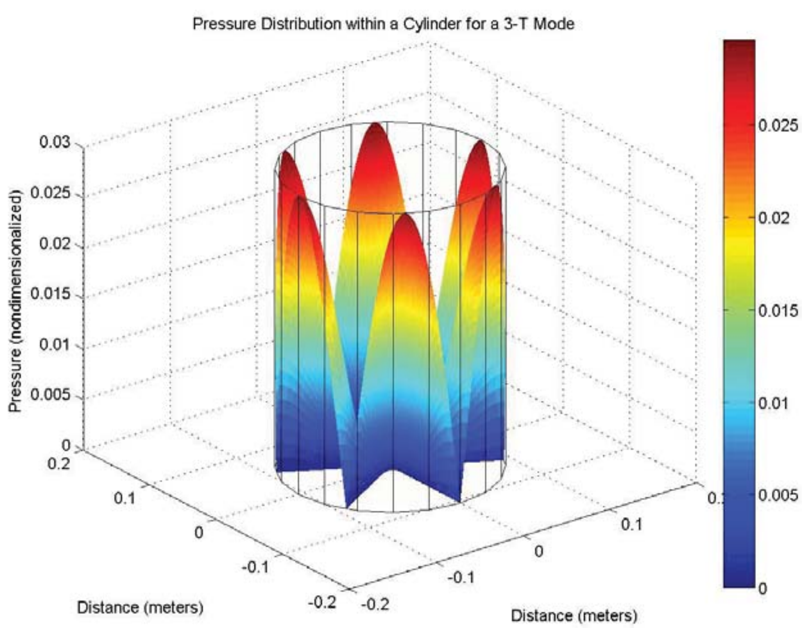

Figure 5.4 Expected pressure distribution within the combustion chamber for a 3-T mode.

Table 5.3 Summary of results after running theoretical data through the Acoustic Mode Analysis Program for a 3-T mode.

	P1/P2	P2/P3	P1/P3	Node Angle	Matches Freq, AR and Phase
Dominant Frequency (Hz)	3250	3250	3250	10 70 130 190 250 310	3-T Mode 3-T Mode 3-T Mode 3-T Mode 3-T Mode 3-T Mode
Amp Ratios from FFT	0.57735	0.896575	0.517638		
Phase Diff (degrees)	2.07E-15	2.32E-14	2.52E-14		
Calculated Max Amplitude in Chamber (P/PChamber)	0.029547				
Actual Amplitude (P/PChamber)	0.0295				

Test 4 Verification of the 4-T Mode at Node Angle = 10°

Using the same method described for the 1-T Mode Verification, equations were written for the three different pressure transducer locations for the 4-T Mode. The absolute pressure experienced in the combustion chamber is shown in the figure below, and the output of the program is shown in the table. The pressure over time that would be experienced by the pressure transducers around the chamber if this mode were active is shown graphically in the appendix. The program was able to determine that it was a 4-T mode. However, it was not able to determine the node line location. To determine the node line location, for this and any higher order mode, more pressure transducers would be required.

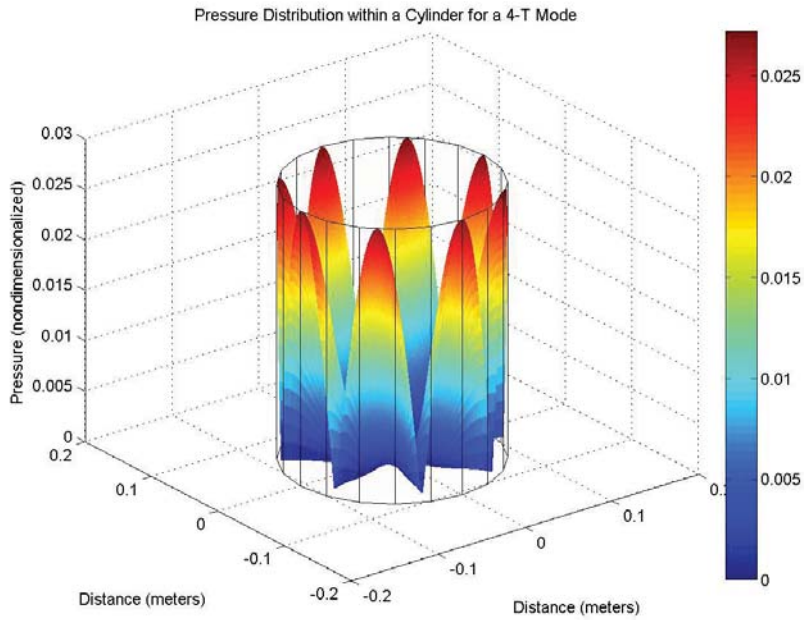

Figure 5.5 Expected pressure distribution within the combustion chamber for a 4-T mode.

Table 5.4 Summary of results after running theoretical data through the Acoustic Mode Analysis Program for a 4-T mode.

	P1/P2	P2/P3	P1/P3	Node Angle	Matches Freq, AR and Phase
Dominant Frequency (Hz)	3500	3500	3500	1 to 360 Matches	4-T Mode for all node angles
Amp Ratios from FFT	1	1	1		
Phase Diff (degrees)	1.2E-14	180	180		
Calculated Max Amplitude in Chamber (P/PChamber)	0.479529				
Actual Amplitude (P/PChamber)	0.0272				

Test 5 Verification of the 5-T Mode at Node Angle = 10°

Using the same method described for the 1-T Mode Verification, equations were written for the three different pressure transducer locations for the 5-T Mode. The absolute pressure experienced in the combustion chamber is shown in the figure below, and the output of the program is shown in the table. The pressure over time that would be experienced by the pressure transducers around the chamber if this mode were active is shown graphically in the appendix. The program was able to determine that a 5-T mode existed at the correct node line locations.

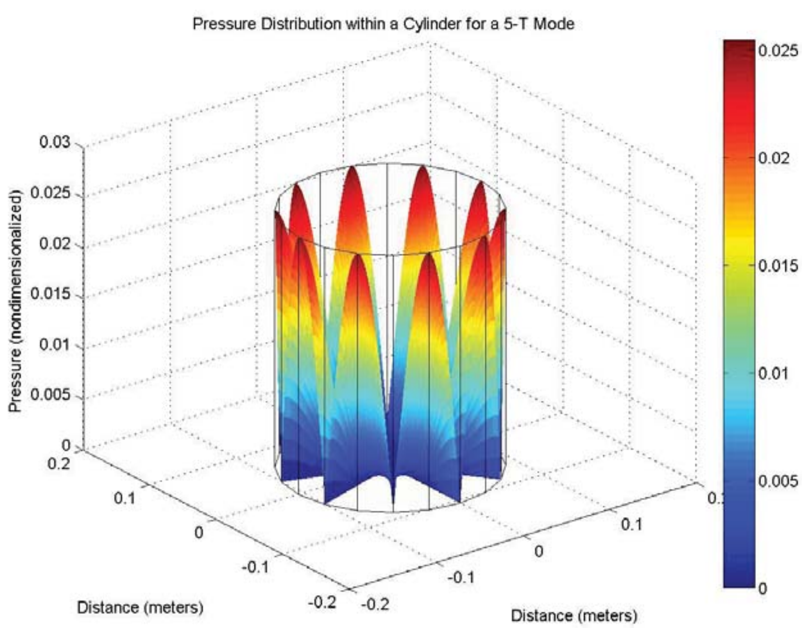

Figure 5.6 Expected pressure distribution within the combustion chamber for a 5-T mode.

Table 5.5 Summary of results after running theoretical data through the Acoustic Mode Analysis Program for a 5-T mode.

	P1/P2	P2/P3	P1/P3	Node Angle	Matches Freq, AR and Phase
Dominant Frequency (Hz)	4500	4500	4500	10 46 82	5-T Mode 5-T Mode 5-T Mode
Amp Ratios from FFT	1.191754	7.375161	8.789374	118 154	5-T Mode 5-T Mode
Phase Diff (degrees)	180	180	3.81E-14	190 226	5-T Mode 5-T Mode
Calculated Max Amplitude in Chamber (P/PChamber)	0.022506			262 298 334	5-T Mode 5-T Mode 5-T Mode
Actual Amplitude (P/PChamber)	0.0254				

Test 6 Verification of the 6-T Mode at Node Angle = 10°

Using the same method described for the 1-T Mode Verification, equations were written for the three different pressure transducer locations for the 6-T Mode. The absolute pressure experienced in the combustion chamber is shown in the figure below, and the output of the program is shown in the table. The pressure over time that would be experienced by the pressure transducers around the chamber if this mode were active is shown graphically in the appendix. The program was able to determine the mode, but not the node line location. To determine the node line location, for this and any higher order mode, more pressure transducers would be required.

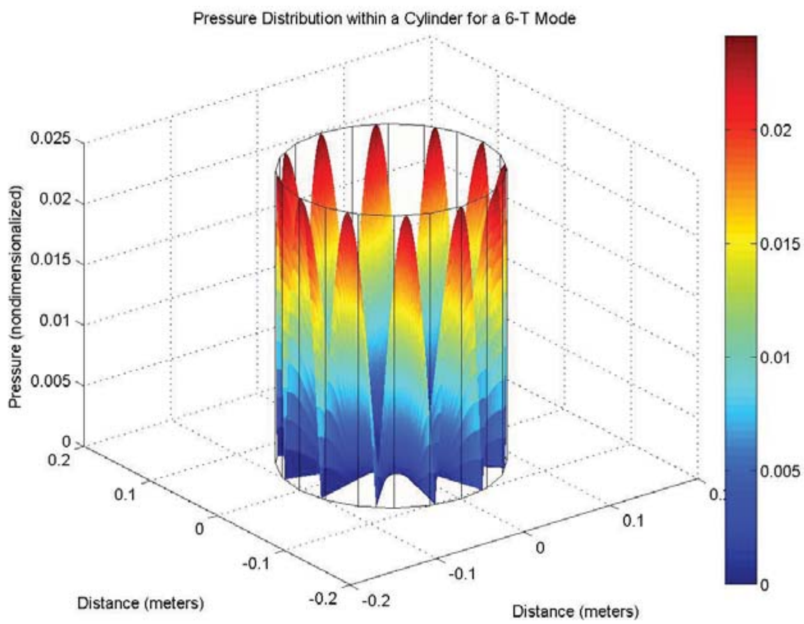

Figure 5.7 Expected pressure distribution within the combustion chamber for a 6-T mode.

Table 5.6 Summary of results after running theoretical data through the Acoustic Mode Analysis Program for a 6-T mode.

	P1/P2	P2/P3	P1/P3
Dominant Frequency (Hz)	5500	5500	5500
Amp Ratios from FFT	1	1.7320	1.73205
Phase Diff (degrees)	180	180	2.25E-14
Calculated Max Amplitude in Chamber (P/PChamber)	0.02362		
Actual Amplitude (P/PChamber)	0.0241		

Node Angle	Matches Freq, AR and Phase	Node Angle	Matches Freq, AR and Phase
59	2-T Mode	239	1-R/2-T Mode
60	2-T Mode	240	1-R/2-T Mode
61	2-T Mode	241	1-R/2-T Mode
149	2-T Mode	329	1-R/2-T Mode
150	2-T Mode	330	1-R/2-T Mode
151	2-T Mode	331	1-R/2-T Mode
239	2-T Mode	10	6-T Mode
240	2-T Mode	40	6-T Mode
241	2-T Mode	70	6-T Mode
329	2-T Mode	100	6-T Mode
330	2-T Mode	130	6-T Mode
331	2-T Mode	160	6-T Mode
59	1-R/2-T Mode	190	6-T Mode
60	1-R/2-T Mode	220	6-T Mode
61	1-R/2-T Mode	250	6-T Mode
149	1-R/2-T Mode	280	6-T Mode
150	1-R/2-T Mode	310	6-T Mode
151	1-R/2-T Mode	340	6-T Mode

Test 7 Verification of the 1-R Mode

Using the same method described for the 1-T Mode Verification, equations were written for the three different pressure transducer locations for the 1-R Mode. The absolute pressure experienced in the combustion chamber is shown in the figure below, and the output of the program is shown in the table. The pressure over time that would be experienced by the pressure transducers around the chamber if this mode were active is shown graphically in the appendix. The program was able to determine that it was a 1-R mode.

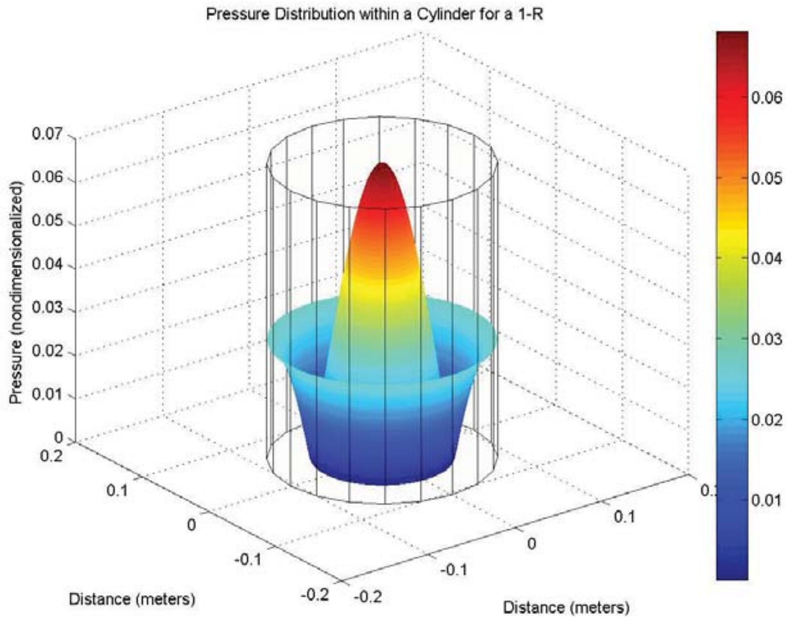

Figure 5.8 Expected pressure distribution within the combustion chamber for a 1-R mode.

Table 5.7 Summary of results after running theoretical data through the Acoustic Mode Analysis Program for a 1-R mode.

	P1/P2	P2/P3	P1/P3	Node Angle	Matches Freq, AR and Phase
Dominant Frequency (Hz)	2500	2500	2500	N/A	Radial Mode Matches 1-R Mode
Amp Ratios from FFT	1	1	1		
Phase Diff (degrees)	0	0	0		
Calculated Max Amplitude in Chamber (P/PChamber)	0.0274				
Actual Amplitude (P/PChamber)	0.027393				

Test 8 Verification of the 2-R Mode

Using the same method described for the 1-T Mode Verification, equations were written for the three different pressure transducer locations for the 2-R Mode. The absolute pressure experienced in the combustion chamber is shown in the figure below, and the output of the program is shown in the table. The pressure over time that would be experienced by the pressure transducers around the chamber if this mode were active is shown graphically in the appendix. The program determined this to be either a 1-R or 2-R mode.

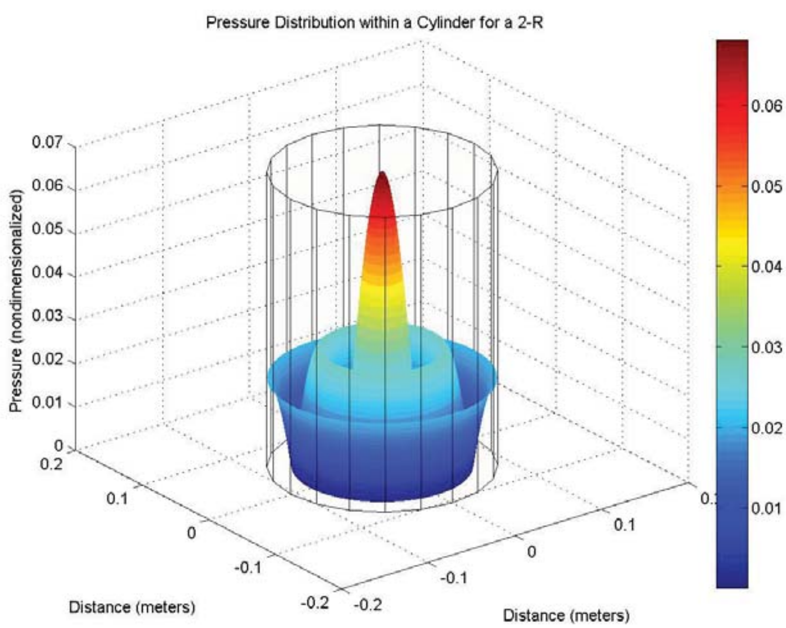

Figure 5.9 Expected pressure distribution within the combustion chamber for a 2-R mode.

Table 5.8 Summary of results after running theoretical data through the Acoustic Mode Analysis Program for a 2-R mode.

	P1/P2	P2/P3	P1/P3	Node Angle	Matches Freq, AR and Phase
Dominant Frequency (Hz)	5000	5000	5000	N/A	Radial Mode Matches 1-R Mode 2-R Mode
Amp Ratios from FFT	1	1	1		
Phase Diff (degrees)	0	0	0		
Calculated Max Amplitude in Chamber (P/PChamber)	0.020402				
Actual Amplitude (P/PChamber)	0.0204				

Test 9 Verification of the 3-R Mode

Using the same method described for the 1-T Mode Verification, equations were written for the three different pressure transducer locations for the 3-R Mode. The absolute pressure experienced in the combustion chamber is shown in the figure below, and the output of the program is shown in the table. The pressure over time that would be experienced by the pressure transducers around the chamber if this mode were active is shown graphically in the appendix. The program determined this to be a 1-R, 2-R, or 3-R mode.

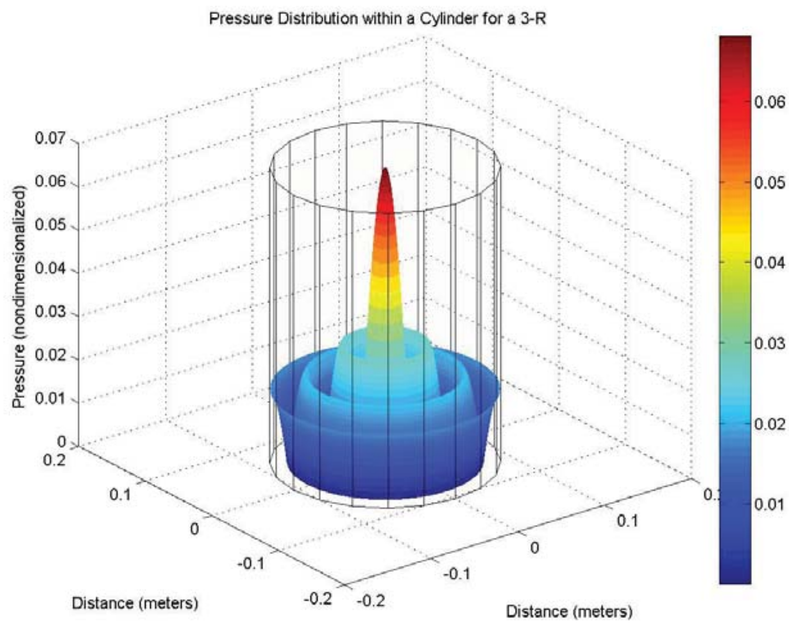

Figure 5.10 Expected pressure distribution within the combustion chamber for a 3-R mode.

Table 5.9 Summary of results after running theoretical data through the Acoustic Mode Analysis Program for a 3-R mode.

	P1/P2	P2/P3	P1/P3	Node Angle	Matches Freq, AR and Phase
Dominant Frequency (Hz)	7000	7000	7000	N/A	Radial Mode Matches 1-R Mode 2-R Mode 3-R Mode
Amp Ratios from FFT	1	1	1		
Phase Diff (degrees)	0	0	0		
Calculated Max Amplitude in Chamber (P/PChamber)	0.016963				
Actual Amplitude (P/PChamber)	0.017				

Test 10 Verification of the 1-R, 1-T Mode at Node Angle = 10°

Using the same method described for the 1-T Mode Verification, equations were written for the three different pressure transducer locations for the 1-R,1-T Mode. The absolute pressure experienced in the combustion chamber is shown in the figure below, and the output of the program is shown in the table. The pressure over time that would be experienced by the pressure transducers around the chamber if this mode were active is shown graphically in the appendix. The program determined this to be either a 1-T or 1-R, 1-T mode at the correct node angles.

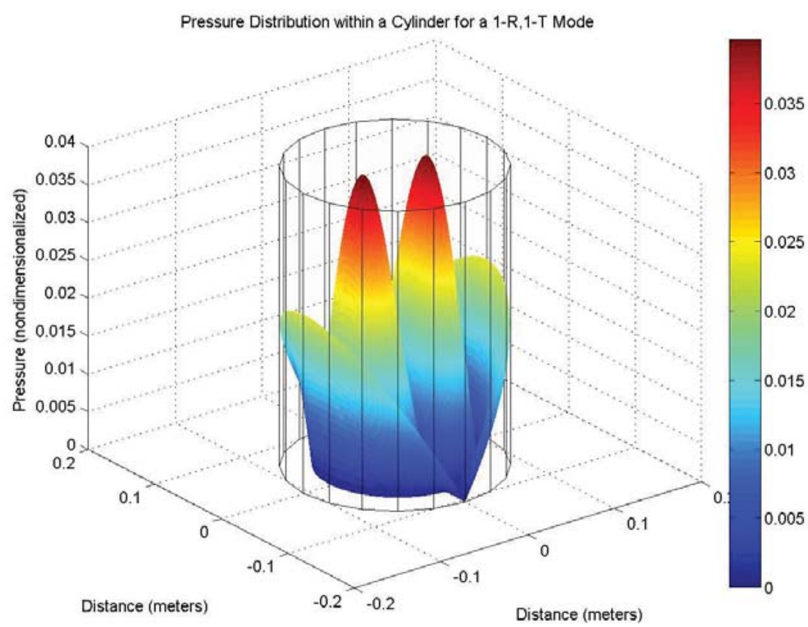

Figure 5. 11 Expected pressure distribution within the combustion chamber for a 1-R, 1-T mode.

Table 5.10 Summary of results after running theoretical data through the Acoustic Mode Analysis Program for a 1-R, 1-T mode.

	P1/P2	P2/P3	P1/P3	Node Angle	Matches Freq, AR and Phase
Dominant Frequency (Hz)	3500	3500	3500	10	1-T Mode
Amp Ratios from FFT	0.176327	1.71696	0.302746	190	1-T Mode
Phase Diff (degrees)	180	180	0	10	1-R/1-T Mode
Calculated Max Amplitude in Chamber (P/PChamber)	0.023537			190	1-R/1-T Mode
Actual Amplitude (P/PChamber)	0.0235				

Test 11 Verification of the 1-R, 2-T Mode at Node Angle = 10°

Using the same method described for the 1-T Mode Verification, equations were written for the three different pressure transducer locations for the 1-R,2-T Mode. The absolute pressure experienced in the combustion chamber is shown in the figure below, and the output of the program is shown in the table. The pressure over time that would be experienced by the pressure transducers around the chamber if this mode were active is shown graphically in the appendix. The program determined this to be either a 1-T or 1-R, 2-T mode at the correct node angles.

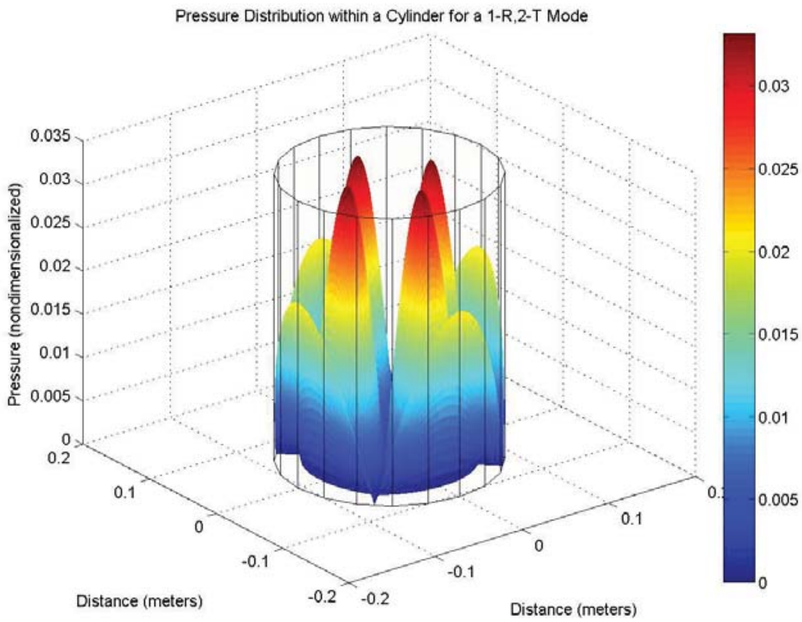

Figure 5.12 Expected pressure distribution within the combustion chamber for a 1-R, 2-T mode.

Table 5.11 Summary of results after running theoretical data through the Acoustic Mode Analysis Program for a 1-R, 2-T mode.

	P1/P2	P2/P3	P1/P3	Node Angle	Matches Freq, AR and Phase
Dominant Frequency (Hz)	4500	4500	4500	10 100	2-T Mode 2-T Mode
Amp Ratios from FFT	1	0.36397	0.36397	190 280	2-T Mode 2-T Mode
Phase Diff (degrees)	180	1.27E-14	180	10 100	1-R/2-T Mode 1-R/2-T Mode
Calculated Max Amplitude in Chamber (P/PChamber)	0.021317			190 280	1-R/2-T Mode 1-R/2-T Mode
Actual Amplitude (P/PChamber)	0.0213				

Test 12 Verification of the 1-R, 3-T Mode at Node Angle = 10°

Using the same method described for the 1-T Mode Verification, equations were written for the three different pressure transducer locations for the 1-R,3-T Mode. The absolute pressure experienced in the combustion chamber is shown in the figure below, and the output of the program is shown in the table. The pressure over time that would be experienced by the pressure transducers around the chamber if this mode were active is shown graphically in the appendix. The program determined this to be a 3-T, 5-T, or 1-R, 3-T mode. To precisely determine this mode, more pressure transducers would be required.

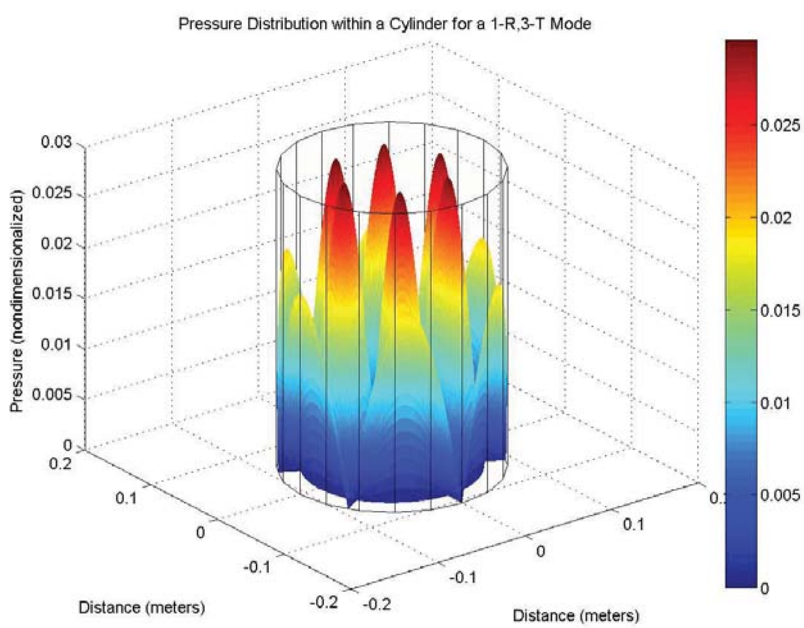

Figure 5.13 Expected pressure distribution within the combustion chamber for a 1-R, 3-T mode.

Table 5.12 Summary of results after running theoretical data through the Acoustic Mode Analysis Program for a 1-R, 3-T mode.

	P1/P2	P2/P3	P1/P3	Node Angle	Matches Freq, AR and Phase	Node Angle	Matches Freq, AR and Phase
				10	3-T Mode	282	5-T Mode
				70	3-T Mode	318	5-T Mode
Dominant Frequency (Hz)	5500	5500	5500	130	3-T Mode	354	5-T Mode
				190	3-T Mode	10	1-R,3-T Mode
				250	3-T Mode	70	1-R,3-T Mode
Amp Ratios from FFT	0.57735	0.89657	0.51763	310	3-T Mode	130	1-R,3-T Mode
				30	5-T Mode	190	1-R,3-T Mode
				66	5-T Mode	250	1-R,3-T Mode
Phase Diff (degrees)	2.54E-14	1.02E-13	7.63E-14	102	5-T Mode	310	1-R,3-T Mode
				138	5-T Mode		
				174	5-T Mode		
Calculated Max Amp. in Chamber (P/PChamber)	0.01979			210	5-T Mode		
				246	5-T Mode		
Actual Amplitude (P/PChamber)	0.0198						

Test 13 Verification of the 1-R, 4-T Mode at Node Angle = 10°

Using the same method described for the 1-T Mode Verification, equations were written for the three different pressure transducer locations for the 1-R,4-T Mode. The absolute pressure experienced in the combustion chamber is shown in the figure below, and the output of the program is shown in the table. The pressure over time that would be experienced by the pressure transducers around the chamber if this mode were active is shown graphically in the appendix. The program determined this to be either a 4-T or 1-R, 4-T mode and could not identify the node angle. To determine the node line location, more pressure transducers would be required.

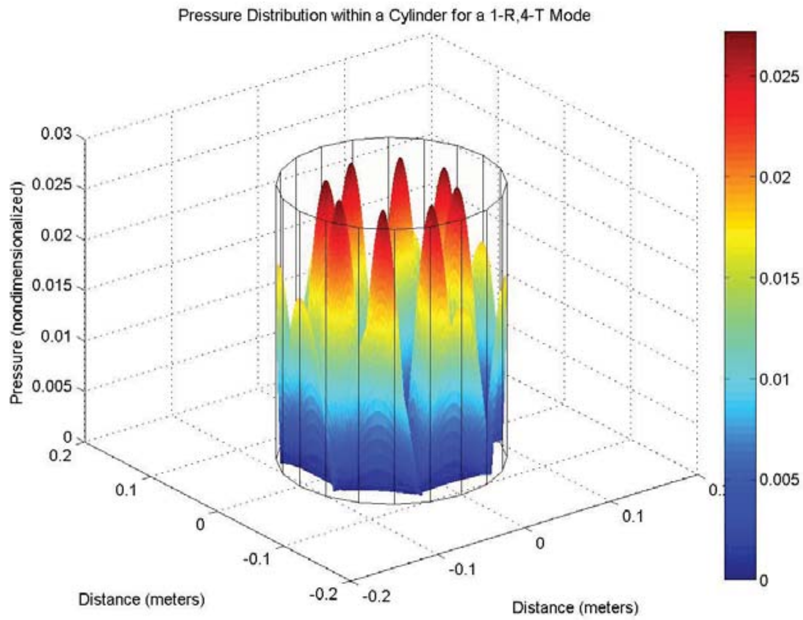

Figure 5.14 Expected pressure distribution within the combustion chamber for a 1-R, 4-T mode.

Table 5.13 Summary of results after running theoretical data through the Acoustic Mode Analysis Program for a 1-R, 4-T mode.

	P1/P2	P2/P3	P1/P3	Node Angle	Matches Freq, AR and Phase
Dominant Frequency (Hz)	6000	6000	6000	All node angles 1-360	4-T Mode and 1-R, 4-T Mode at all node angles
Amp Ratios from FFT	1	1	1		
Phase Diff (degrees)	2.54E-14	180	180		
Calculated Max Amplitude in Chamber (P/PChamber)	0.328962				
Actual Amplitude (P/PChamber)	0.0186				

Test 14 Verification of the 2-R, 1-T Mode at Node Angle = 10°

Using the same method described for the 1-T Mode Verification, equations were written for the three different pressure transducer locations for the 2-R, 1-T Mode. The absolute pressure experienced in the combustion chamber is shown in the figure below, and the output of the program is shown in the table. The pressure over time that would be experienced by the pressure transducers around the chamber if this mode were active is shown graphically in the appendix. The program determined this to be a 1-T; 1-R, 1-T or 2-R, 1-T mode at the correct node angles.

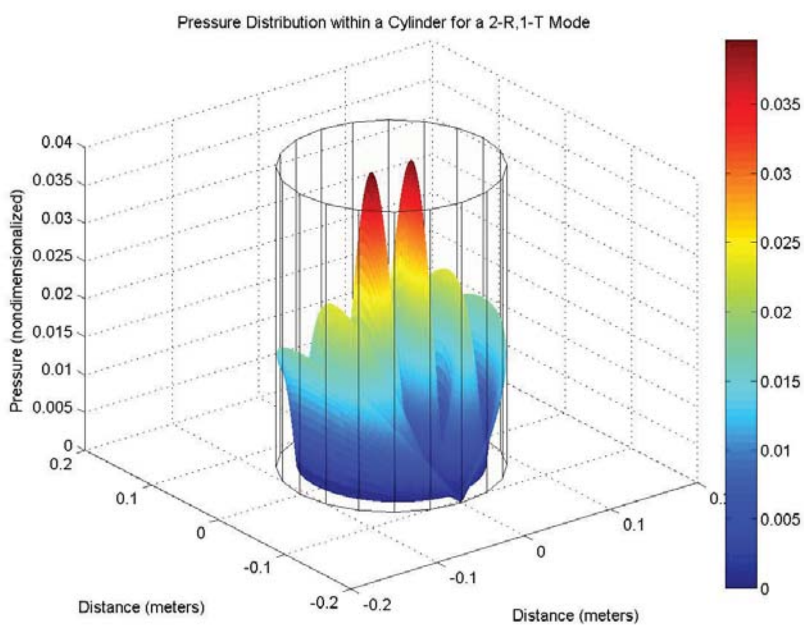

Figure 5.15 Expected pressure distribution within the combustion chamber for a 2-R, 1-T mode.

Table 5.14 Summary of results after running theoretical data through the Acoustic Mode Analysis Program for a 2-R, 1-Tmode.

	P1/P2	P2/P3	P1/P3	Node Angle	Matches Freq, AR and Phase
Dominant Frequency (Hz)	5500	5500	5500	10	1-T Mode
Amp Ratios from FFT	0.176327	1.71696	0.302746	190	1-T Mode
Phase Diff (degrees)	180	180	3.61E-14	10	1-R/1-T Mode
Calculated Max Amplitude in Chamber (P/PChamber)	0.018574			190 10	1-R/1-T Mode 2-R,1-T Mode
Actual Amplitude (P/PChamber)	0.0186			190	2-R,1-T Mode

Test 15 Verification of the 2-R, 2-T Mode at Node Angle = 10°

Using the same method described for the 1-T Mode Verification, equations were written for the three different pressure transducer locations for the 2-R, 2-T Mode. The absolute pressure experienced in the combustion chamber is shown in the figure below, and the output of the program is shown in the table. The pressure over time that would be experienced by the pressure transducers around the chamber if this mode were active is shown graphically in the appendix. The program determined this to be a 2-T; 1-R, 2-T or 2-R, 2-T mode at the correct node angles.

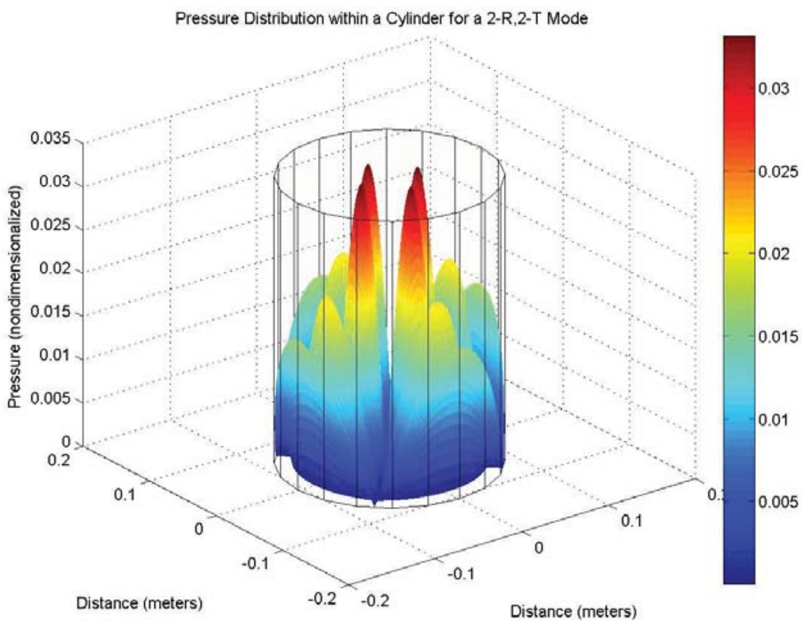

Figure 5.16 Expected pressure distribution within the combustion chamber for a 2-R, 2-T mode.

Table 5.15 Summary of results after running theoretical data through the Acoustic Mode Analysis Program for a 2-R, 2-T mode.

	P1/P2	P2/P3	P1/P3	Node Angle	Matches Freq, AR and Phase
Dominant Frequency (Hz)	6500	6500	6500	10	2-T Mode
Amp Ratios from FFT	1	0.36397	0.36397	100	2-T Mode
Phase Diff (degrees)	180	2.54E-14	180	190	2-T Mode
Calculated Max Amplitude in Chamber (P/PChamber)	0.017307			280	2-T Mode
				10	1-R/2-T Mode
Actual Amplitude (P/PChamber)	0.0173			100	1-R/2-T Mode
				190	1-R/2-T Mode
				280	1-R/2-T Mode
				10	2-R,2-T Mode
				100	2-R,2-T Mode
				190	2-R,2-T Mode
				280	2-R,2-T Mode

2-T Mode with Gaussian Noise

Many of the tests performed at the Combustion Instability Test Facility to date have had a high level of noise present in the pressure data that has been collected. Any methodology used to analyze this data must be able to provide accurate results, even in the presence of a high level of noise. To do determine the program's ability to do this, two tests were devised. The first test had a signal with a constant amplitude level, and then the noise was increased until the noise was greater than the signal. In the second test, there was a constant level of noise and the amplitude of the signal was decreased less than the noise level.

2-T Mode with Constant Amplitude and Noise

In this test, the 2-T mode at a node angle of 10° was created along with Gaussian noise varying in amplitude from Signal to Noise Ratios (S/N Ratios) of 0.5 to 50. The same zero-mean Gaussian noise distribution was added to each pressure signal. A very high S/N Ratio represents a strong signal, while a very low S/N Ratio represents a signal that is dominated by noise. The results are summarized Table 5.16. A 2-T mode was uniquely identified in all test cases. The node angle was also correctly identified in most cases, except for the two lowest S/N ratio cases, 0.5 and 1. These results are surprising, and show the robustness of using the FFT to determine the amplitude ratios between the signals. The FFT is able to isolate the frequency of the signal within the noise. The zero mean Gaussian noise is several orders of magnitude lower than that of the signal when detected on the FFT. The FFTs are shown in Figure 5.17.

Table 5.16 Summary of results for 2-T constant amplitude test.

S/N Ratio	2-T Mode Identified?	Node Angle Identified?
50	Yes	Yes
25	Yes	Yes
12	Yes	Yes
8	Yes	Yes
4	Yes	Yes
2	Yes	Yes
1	Yes	No
0.5	Yes	No

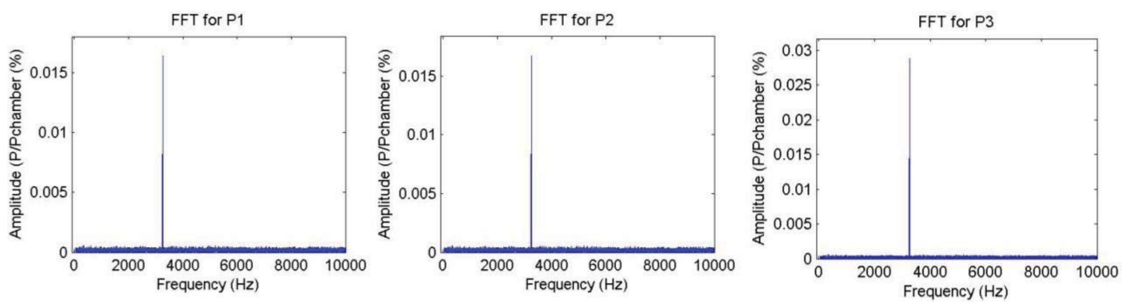

Figure 5.17 FFT results for the three pressure transducers for when the signal to noise ratio = 1. When detected by the FFT, the zero mean Gaussian noise is several orders of magnitude lower than that of the signal.

To visualize what the mode shape may look like with noise, the 2-T mode absolute pressure distribution with different noise levels has been modeled within the combustion chamber. These are shown with signal to noise ratios of eight and 1 in Figure 5.18 and Figure 5.19. The statistical parameters for these tests followed as expected. For a signal to noise ratio of 50 the kurtosis was 1.51 showing the signal is dominated by a sine wave. For a signal to noise ratio of 0.5, the kurtosis was 2.99 showing that the signal is dominated by Gaussian noise. Histograms for these tests are shown in Figure 5.20 and Figure 5.21

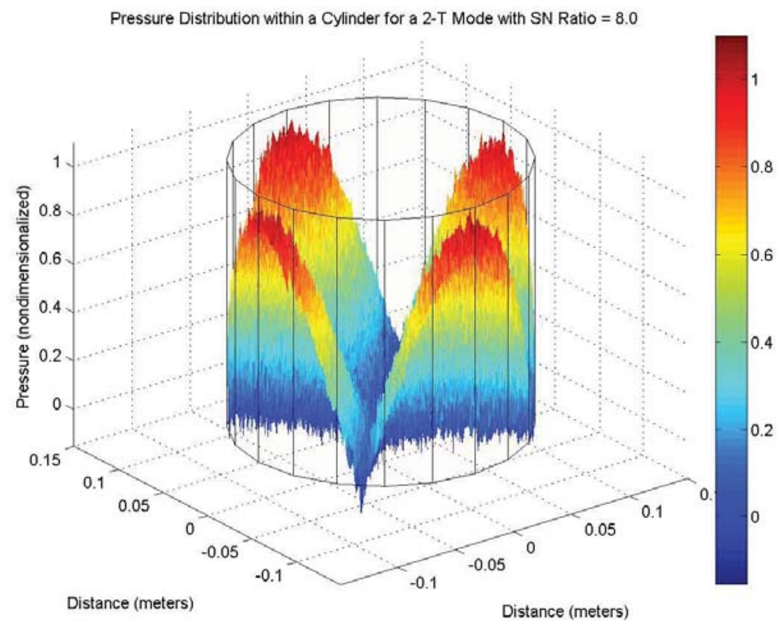

Figure 5.18 2-T mode with a signal to noise ratio of 8.

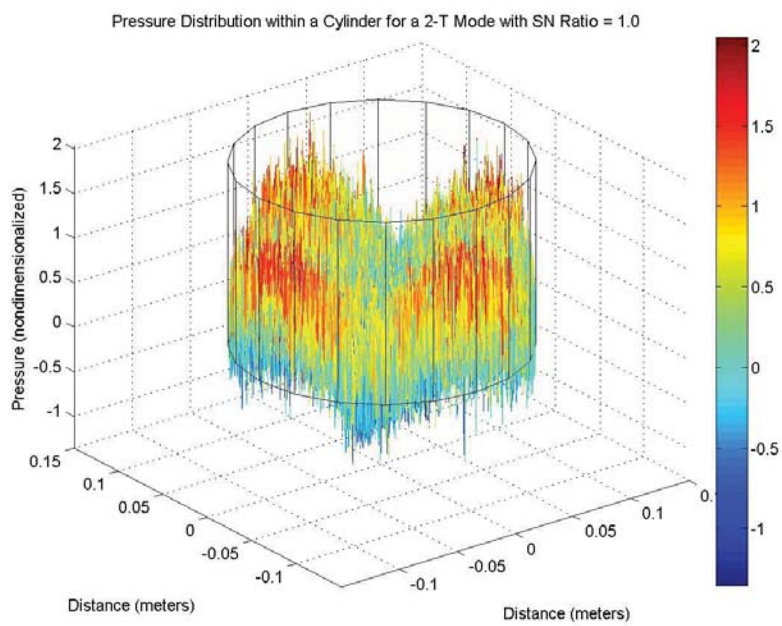

Figure 5.19 2-T mode with a signal to noise ratio of 1.

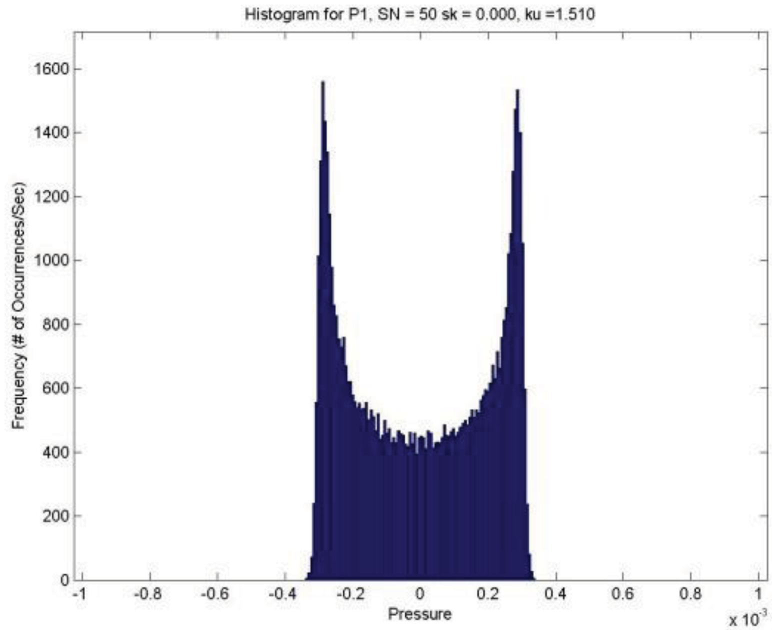

Figure 5.20 Histogram of 2-T mode with a signal to noise ratio of 50.

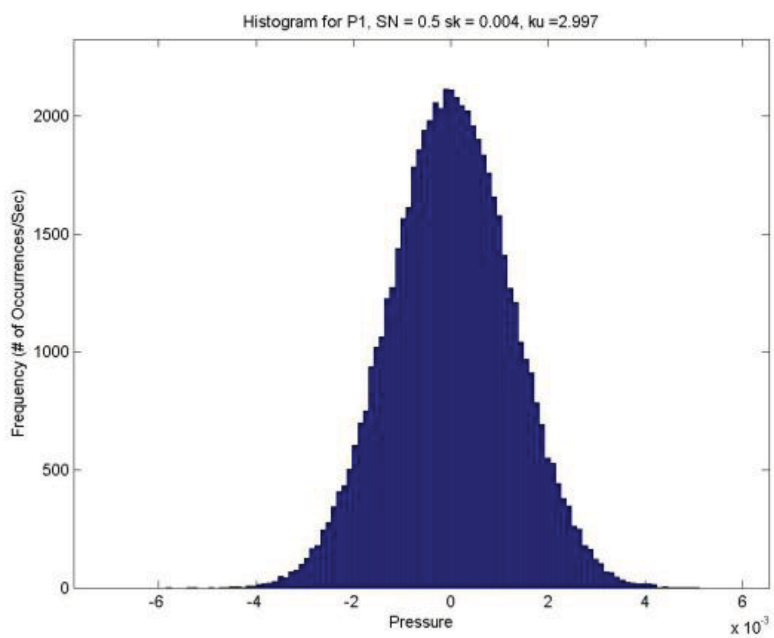

Figure 5.21 Histogram of a 2-T mode with a signal to noise ratio of 0.5.

2-T Mode with Constant Noise Level

In this test, the 2-T mode at a node angle of 10° was created with a constant level of Gaussian noise. The amplitude was adjusted to vary the signal to noise ratios (S/N ratios) from 0.5 to 50. The same zero-mean Gaussian noise distribution was added to each pressure signal. The results here are similar to the results in the previous test case. The program is able to correctly identify the mode as a 2-T for all signal to noise ratios. The node angle is correctly identified in all cases except for when the signal to noise ratios is less than one. The results are summarized in Table 5. 17.

Table 5. 17 Summary of results for 2-T constant level of noise test.

S/N Ratio	2-T Mode Identified?	Node Angle Identified?	Max Chamber Amplitude Predicted Correctly?
50	Yes	Yes	Yes
25	Yes	Yes	Yes
12	Yes	Yes	Yes
8	Yes	Yes	Yes
4	Yes	Yes	Yes
2	Yes	Yes	Yes
1	Yes	Yes	Yes
0.5	Yes	No	No

2-T Mode Test at all Node Locations in Chamber

For this test, a 2-T mode was created at nodes angles from 1-360 degrees with respect to P1 and processed through the Acoustic Mode Analysis Program. The program was able to identify a 2-T mode at all node angle locations except when one of the node lines was at a pressure transducer location. Whenever a node line is at one of the pressure transducers, the amplitude detected by the pressure transducer is zero. This causes the amplitude ratios to become undefined and the matching scheme becomes unreliable. Also, it was not always able to correctly identify the node angle. The program was able to determine the node angle of the mode within a few degrees of what the actual was input was. Figure 5.22 shows the top view of a 2-T mode, with the pressure transducers and the node lines.

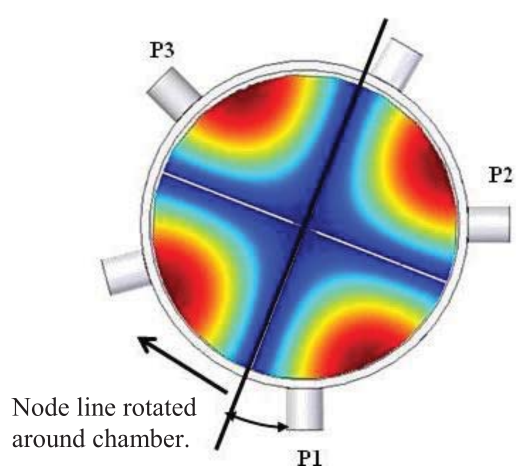

Figure 5.22 Top view of a 2-T mode in the combustion chamber. For this test, the node lines were created at all possible node angles from 0-360 degrees around the chamber.

The calculated maximum amplitude from the program vs. the actual maximum amplitude of the mode is shown in Figure 5.23. The red line represents the actual amplitude and the blue line represents the calculated maximum amplitude. The maximum amplitude is calculated in the program as a function of the node angle. Therefore, when the node is not determined correctly, the maximum amplitude is also not determined correctly. The calculated amplitude usually is very close to the actual amplitude, except when a pressure transducer is near a node line. When this happens, the calculated amplitude becomes zero.

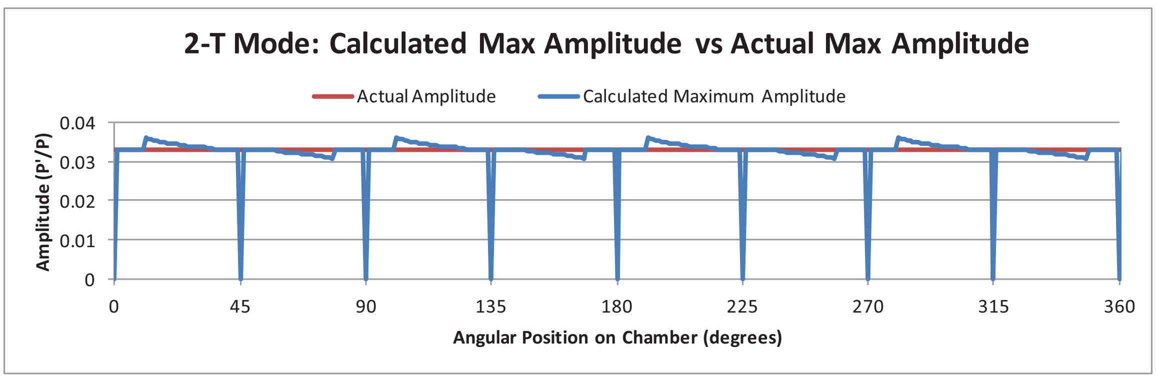

Figure 5.23 Results for rotating the 2-T mode 360° around the chamber. The program is unable to identify the mode correctly when there is a node line at one of the pressure transducers.

Summary of Verification Results

From the results of the test cases, the Acoustic Mode Analysis Program has been shown to work very well for detecting the correct mode when theoretical data is used for analysis. Here is a summary of all of the important results.

- Using this methodology the mode, node angle, and maximum predicted amplitude can be uniquely identified for 1-T, 2-T, 3-T, and 1-R modes.
- The node angle for a 4-T mode cannot be identified. This is because the amplitude ratio between the pressure transducers is the same regardless of the mode orientation. This could be solved with the addition of more pressure transducers.
- Higher order modes 5-T and above cannot be uniquely identified. This is because only three pressure transducers are used in this methodology. If more pressure transducers were employed, higher order modes could be detected. When the program detects the possibility of higher order modes, both the higher order mode and lower order mode matches are given.
- Combined modes cannot be uniquely identified. They will be given as either the tangential mode, or the combined radial and tangential mode.
- If a strong signal is present, the program can detect it even in the presence of a high level of noise.
- Signals with a kurtosis of near 3.0 have a low signal to noise ratio and represent a Gaussian distribution. Signals with a kurtosis near 1.5 have a high signal to noise ratio and represent a strong sinusoidal signal.
- The program cannot detect modes when the node line is at one of the pressure transducers.

CHAPTER SIX

APPLICATION OF ANALYSIS METHOD TO TEST DATA

The methodology used in the Acoustic Mode Matching Program has been shown to work very well on artificially simulated data in the previous chapter. Does this methodology represent an acceptable approach for analyzing test data collected at the Propulsion Research Center Combustion Instability Test Facility? To answer this question data from two different types of injectors has been examined. First data from a 45 degree impinging pentad injector will be discussed, and then data from a shear coaxial injector. The full output of the Acoustic Mode Matching Program for all of the tests discussed in this section is provided in Appendix E.

Pentad Injector Test Results

The first set of tests to be discussed used an impinging jet injector. These types of injectors "are the preferred injector geometry for rocket engines that use storable propellants or liquid hydrocarbons" [3]. Generally, they have low fabrication costs and good atomization and mixing characteristics. However, the improved performance also decreases the combustion stability characteristics. Consequently, at the PRC most of the high amplitude combustion instability results have come from tests using impinging jet injectors. A diagram of the impinging jet injector used in the tests discussed below is shown in Figure 6.1.

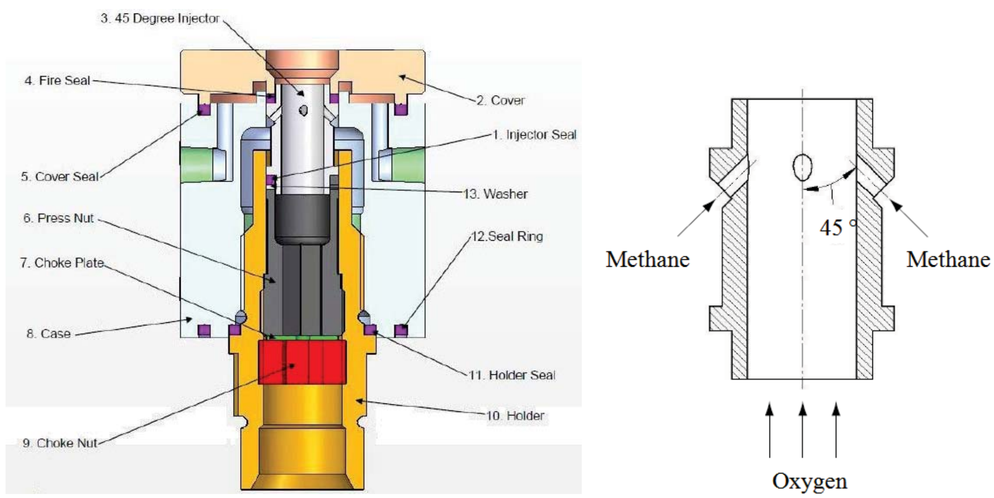

Figure 6.1 45° impinging jet injector schematic (left) and propellant flow paths through injector (right) [10].

Set Point JPP-E

The first test to be analyzed was published in the Journal of Propulsion and Power in 2010 by Robert Byrd and labeled test E [16]. Here it will be referred to as JPP-E. This test had one of the strongest amplitudes found in his testing. His analysis, which considered the phase and amplitude relationships between the pressure transducers during the test, concluded that a 2-T mode was active.

The pressure data for JPP-E was analyzed using the Acoustic Mode Analysis program. The program was able to verify Byrd's conclusion that a 2-T mode was active. The most likely orientation is a node line of 38° to 39° from P1. The amplitude ratios closely match what would be expected, varying 3.5% to 21.9% from the theoretical values. The phase difference was off from between 7° to 32°. The results for this analysis are summarized in Table 6.1 and Table 6.2.

Table 6.1 Summary of results for JPP-E.

	P1/P2	P2/P3	P1/P3
Dominant Frequency (Hz)	1733	1733	1733
Amp Ratios from FFT	0.8499	4.8877	4.1542
Phase Diff (degrees)	211.9537	24.92702	187.0267
Calculated Max Amplitude in Chamber (P'/PChamber), %	0.551866		

Node Angle	Matches Freq, AR and Phase
38	2-T Mode
39	2-T Mode
128	2-T Mode
129	2-T Mode
218	2-T Mode
219	2-T Mode
308	2-T Mode
309	2-T Mode

Table 6.2 Actual results from JPP-E compared to theoretical results for a 2-T mode at a node angle of 38 degrees.

	P1/P2	P2/P3	P1/P3
Amp Ratios (actual)	.850	4.888	4.154
Amp Ratios (expected)	1.000	4.0108	4.0108
Percent Difference	15%	21.9%	3.5%
Phase Difference (actual)	211.95°	24.93°	187.03°
Phase Difference (expected)	180°	0°	180°
Phase Difference (actual – expected)	31.95°	24.93°	7.03°

The pressure time history for both the experimental data and the theoretical data are shown in Figure 6.2. The theoretical graph does not have the same scale for pressure. The graphs are very similar, and verify that a strong 2-T mode was in fact active. The FFT (Figure 6.3) for the data also matches very well. The experimental data shows one distinct peak at a frequency of 1733 Hz. The histograms of JPP-E are shown in Figure 6.4. It was hypothesized that strong instabilities would have a kurtosis of approximately 1.5. Here P1 and P2 the kurtosis is 1.56 and 1.55, respectively. These two pressure transducers showed a strong bimodal distribution, indicating a strong sine wave with minimal noise. For P3, the kurtosis was slightly higher at 2.29, indicating that the distribution was slightly more Gaussian and thus had more noise.

This test confirms both the analysis performed by Byrd on test point JPP-E and the validity of the acoustic analysis mode methodology developed here. The Acoustic Mode Analysis Program appears to provide the same results that were done using other proven methods developed at the PRC.

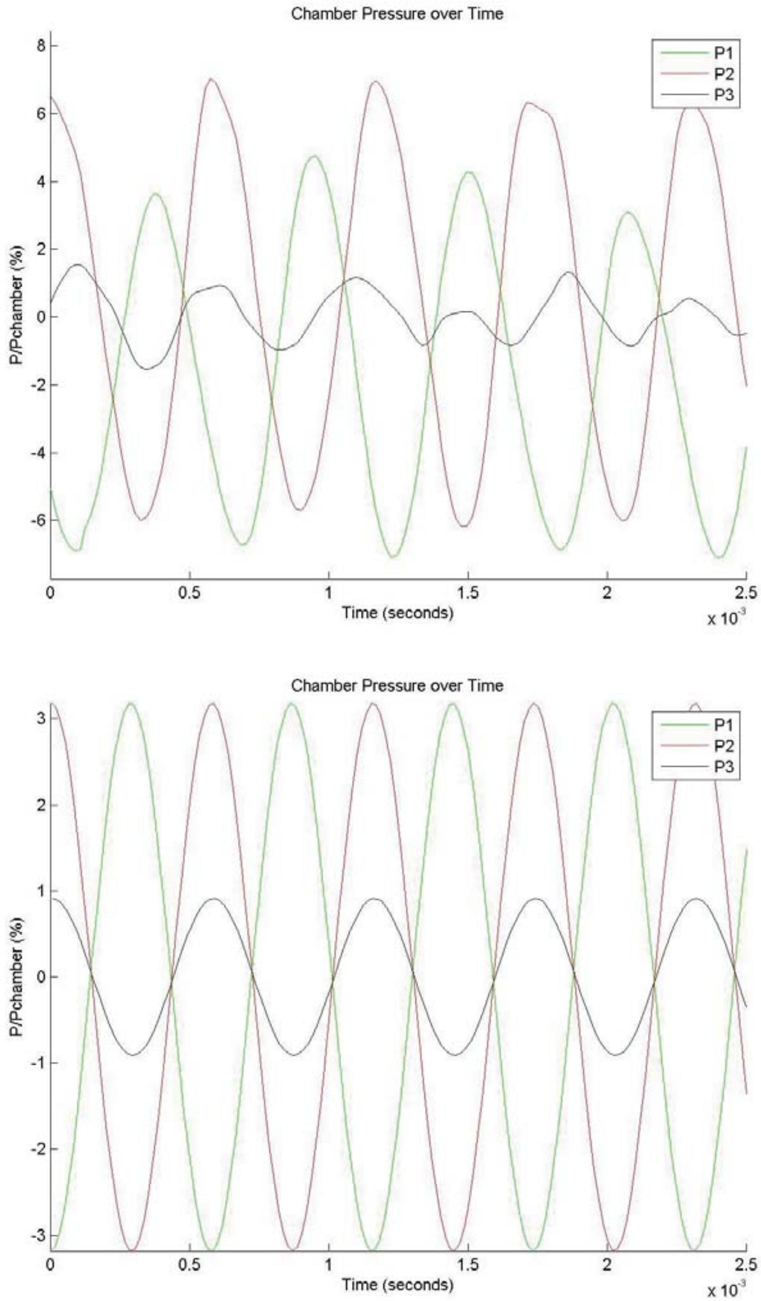

Figure 6.2 Time history for the pressure detected in the JPP-E test (top) compared to the expected time history using theoretically generated data (bottom).

FFT from actual test data

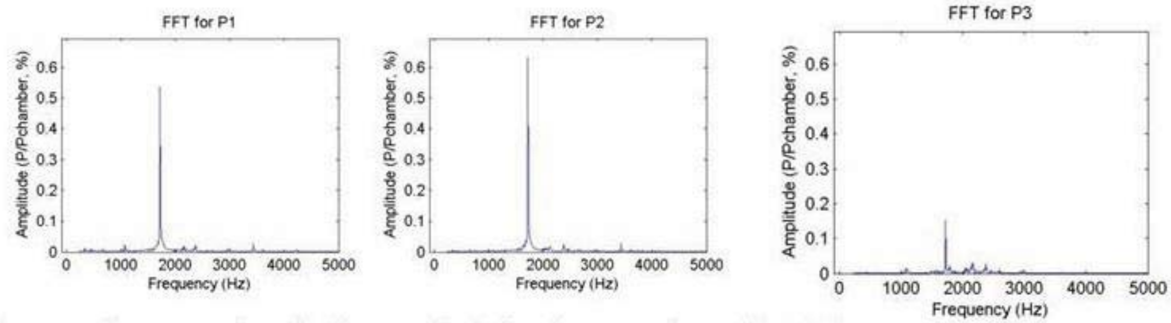

FFT from theoretical data at a node angle of 38°

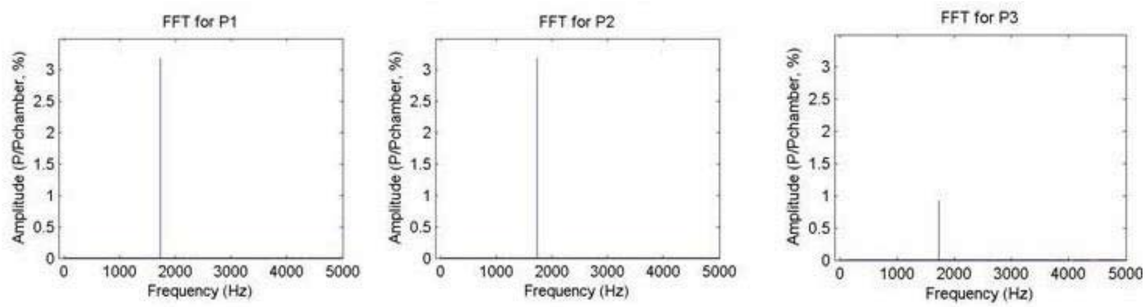

Figure 6.3 FFT of the test data for set point JPP-E (top) vs. FFT of the theoretical data. Notice that the amplitude ratio between the signals is very similar for both the test data and the theoretical.

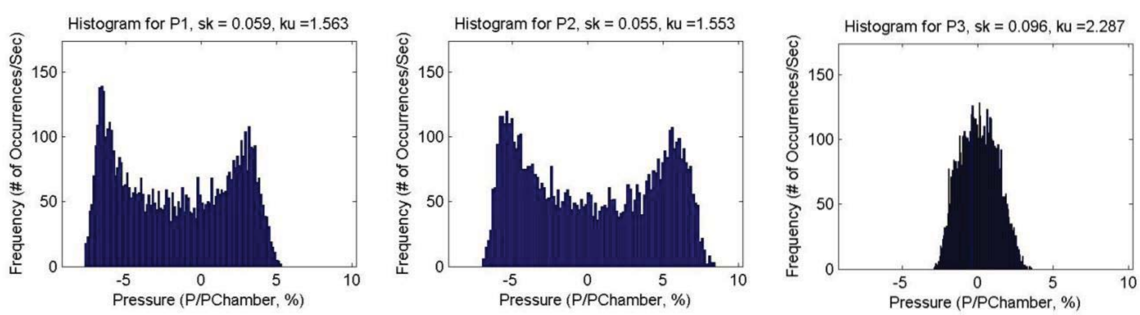

Figure 6.4 Histogram and statistical parameters for set point JPP-E.

Analysis of other Impinging Jet Injector Test Data

Figure 6.5 below summarizes the data collected by Robert Byrd at the UAH Propulsion Research Center in 2008 [10]. Many of these tests had high-sustained amplitudes. A robust analysis of the most interesting data collected in these tests is provided by Byrd [10]. To verify the acoustic mode matching methodology, the 13 test set points (SP) that make up Test 3.5 were selected. These had a fixed mass flow rate of 0.379 g/s of methane and an oxygen mass flow rate that varied from 0.720 g/s at SP1 up to 3.054 g/s at SP13. These tests were run with the injector 1.0" from the combustion chamber wall.

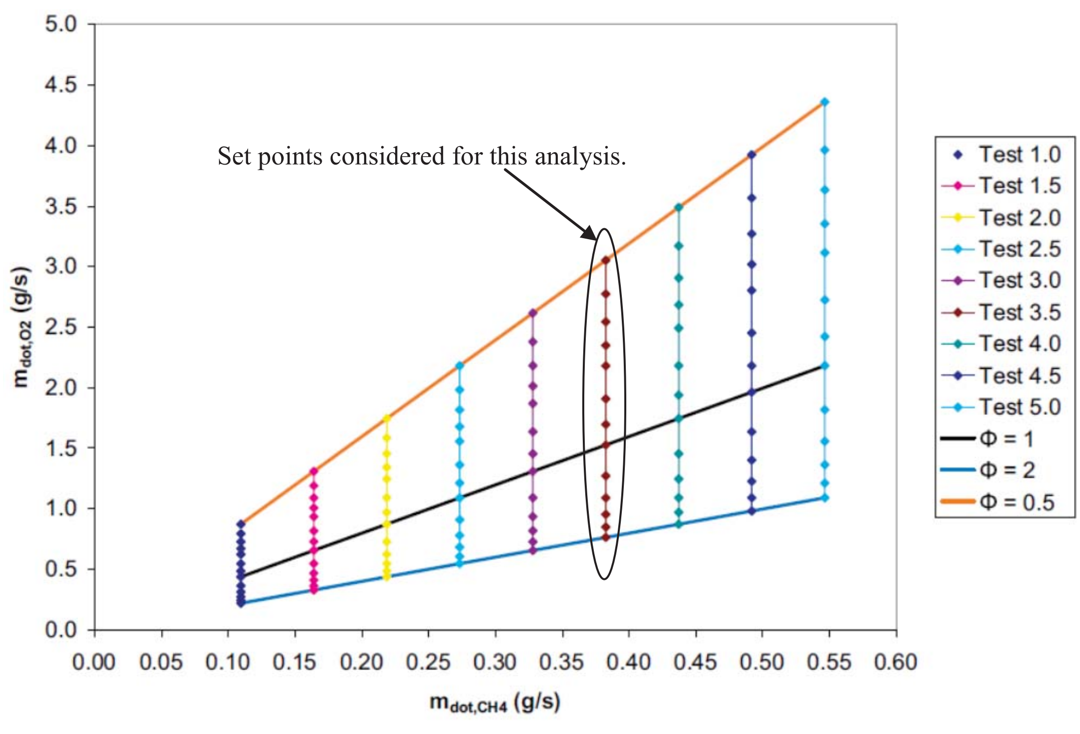

Figure 6.5 Test matrix used for collecting data by Robert Byrd in 2008 [10]. Test 3.5 is analyzed in this section.

The data for these tests was analyzed using the Acoustic Mode Analysis Program. The results are summarized in Table 6.3 and

Table 6.4. Only one out of the thirteen tests had modes identified. This gives a match rate of about 7.7%. A 1-T or 1-R, 1-T mode was identified in SP13 and had a maximum predicted amplitude of 0.57%. The kurtosis average for the tests with a mode match was 2.66, while the average value for all the tests without mode matches was 2.64. This is unexpected, as it was hypothesized that tests with mode matches would have a kurtosis value closer to 1.5.

Table 6.3 Analysis results for Test 3.5.

Set Point	Mode	Dominant Frequency (Hz)	Max FFT Amplitude (P'/PChamber, %)	Max Calculated Amplitude (P'/PChamber, %)	Kurtosis		
					P1	P2	P3
1	-	2205	0.0357	-	4.711	2.970	2.377
2	-	2220	0.0201	-	2.637	2.714	2.150
3	-	1746	0.0776	-	3.301	2.603	1.968
4	-	2145	0.3113	-	2.770	2.156	1.836
5	-	1739	0.2599	-	3.403	2.291	2.573
6	-	2140	0.3229	-	3.106	2.171	2.046
7	-	2123	0.3582	-	2.546	2.291	2.190
8	-	2118	0.5452	-	3.669	2.133	2.352
9	-	2970	0.3591	-	2.364	2.402	2.681
10	-	2101	0.2661	-	2.307	2.116	2.429
11	-	3064	0.3858	-	2.249	2.416	2.485
12	-	3095	0.1433	-	2.771	3.483	4.497
13	1-T or 1-R,1-T	3069	0.3547	0.5731	2.417	3.114	2.460

Table 6.4 Summary of analysis results for Test 3.5.

	P1	P2	P3	Average Kurtosis of P1, P2, P3
Average Kurtosis – Tests with Modes Detected	3.4535	2.9305	2.29	2.66
Average Kurtosis - Tests without modes	3.017909	2.457455	2.494	2.64
Max Calculated Amplitude (P'/PChamber), %	0.5731			
Number of modes Detected	1			
Number of Tests	13			
Percent Match	7.7%			

It was observed that in the test data for the cases that had a mode match one strong, distinct peak was observed on the FFT. Test JPP-E in particular had a very strong distinct peak (see Figure 6.3). This is different from the test cases where there was no match, which had multiple strong peaks. In Figure 6.6 a comparison is made between SP13 that matched a 1-T or a 1-R, 1-T with that of SP7, which had no match. SP7 has two peak frequencies of nearly the same amplitude, while SP13 has only one large amplitude peak with several others that are several orders of magnitude smaller.

Set point 13 – 1-T or 1-R, 1-T Match

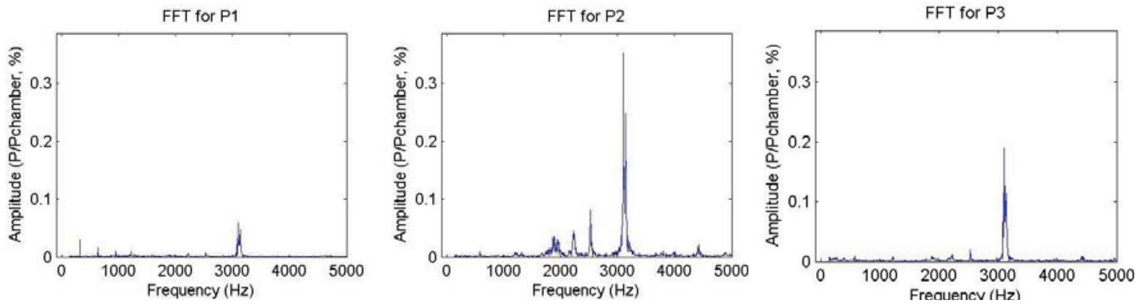

Set point 7 – No Match

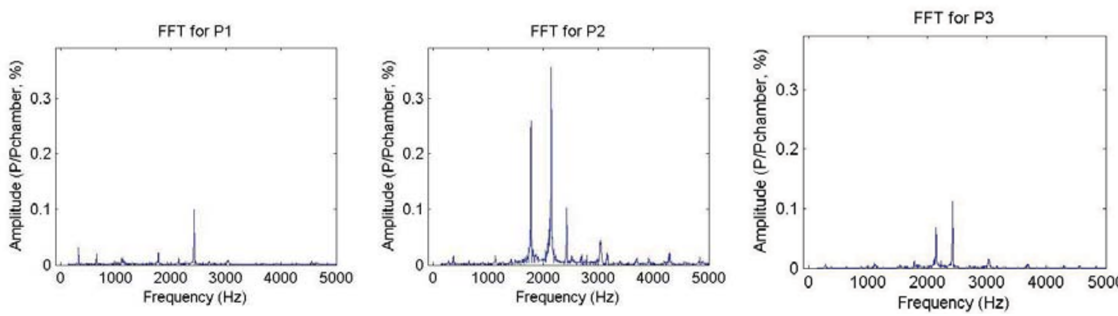

Figure 6.6 FFTs for test cases that had a strong match (top) compared to FFTs for test cases that did not have a match (bottom).

Shear Coaxial Injector Test Results

A shear coaxial injector was tested at the Combustion Instability Test Facility from the 13th to the 21st of September, 2011. Two different injector lengths were tested and the injector was tested both at a center location, and near the wall of the combustion chamber. Test parameters for these set points are summarized in Table 6.5.

The shear coaxial injector has relatively smooth flow of the propellants compared to the impinging jet injector. The oxygen flows through the center oxygen post to the fire face while the methane flows coaxially around the oxygen post Figure 6.7 shows a diagram of the shear coaxial injector used in these tests.

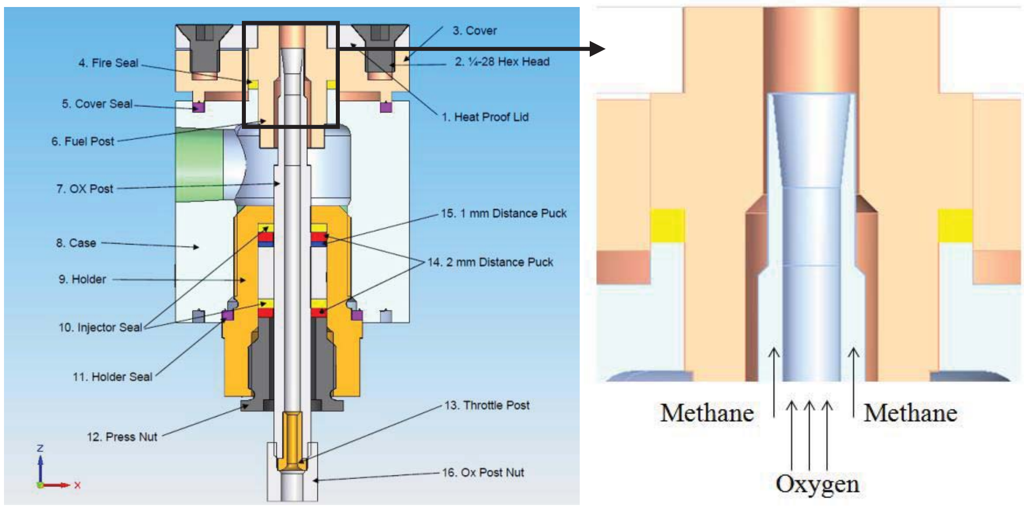

Figure 6.7 Shear coaxial injector schematic (left) and propellant flow paths through injector (right) [11].

The data collected has been analyzed using the Acoustic Mode Analysis Program. The only detected modes were 1-R and 2-T modes. The detected dominate frequencies varied from 1694 to 3002 Hz. The maximum calculated amplitude for the entire chamber for any test was 0.1266 ($P'/P_{Chamber}$) which was from set point 19 tested on September 19^{th}. In total, 33 set points were tested and the analysis code was able to detect acoustic modes in 20. This is a 60.9% successful match rate. Table 6.6 shows the results for all of the tests.

Table 6.5 Test parameters for the shear coaxial injector tests.

Set Point #	$\dot{m}_{ox}$ (g/s)	$\dot{m}_{fuel}$ (g/s)	$\dot{m}_{N2}$ (g/s)	T_{fuel} (°C)	$\dot{Q}_{fuel}$ (cm^3/s)	$\dot{Q}_{ox}$ (cm^3/s)	Equivalence Ratio	Velocity Ratio	Momentum Ratio	Density Ratio	Area Ratio
11	0.469	0.132	0.246	300	793.8	358.8	1.13	7.799	6.6816	0.387	3.522
12	0.463	0.137	0.255	300	814	361.9	1.16	7.929	6.9061	0.387	3.525
19	0.431	0.170	0.316	300	1033	329.5	1.58	11.05	13.416	0.387	3.525
20	0.461	0.143	0.265	300	875.4	353	1.24	8.742	8.3951	0.387	3.525
22	0.437	0.145	0.270	300	881.2	334.3	1.33	9.292	9.485	0.387	3.525
27	0.467	0.137	0.255	300	900.6	356.9	1.18	8.895	8.6923	0.387	3.525
28	0.350	0.187	0.348	300	1197.6	268	2.14	15.75	27.259	0.387	3.525
30	0.458	0.144	0.268	300	764.1	350.2	1.26	7.691	6.4988	0.387	3.525
31	0.480	0.142	0.265	300	807.3	367	1.19	7.754	6.6054	0.387	3.525
32	0.526	0.142	0.264	300	642.4	402.6	1.08	5.624	3.4756	0.387	3.525

Table 6.6 Analysis results for the shear coaxial injector tests.

Set Point	Injector	Center	Position	Mode Match	Dominant Frequency (Hz)	Max FFT Amplitude (P'/PChamber), %	Max Predicted Amplitude (P'/PChamber),%	Kurtosis		
								P1	P2	P3
11	9/13/11	Custom	Centered	1-R	2235	0.0745	0.0745	2.711	2.683	2.659
	9/14/11	Custom	Wall	-	2559	0.0294	-	2.322	2.599	2.534
	9/19/11	Rocketdyne	Centered	2-T	2302	0.0739	0.0891	2.885	2.821	2.945
	9/21/11	Rocketdyne	Wall	-	2978	0.0541	-	2.820	3.006	2.865
12	9/13/11	Custom	Centered	1-R	2264	0.0617	0.0617	2.819	2.627	2.590
	9/14/11	Custom	Wall	1-R	2255	0.0914	0.0914	2.746	2.788	2.760
	9/19/11	Rocketdyne	Centered	-	2348	0.0524	-	2.885	2.779	2.987
	9/21/11	Rocketdyne	Wall	-	2374	0.0536	-	2.807	2.904	2.752
19	9/13/11	Custom	Centered	N/A	N/A	N/A	N/A	N/A	N/A	N/A
	9/14/11	Custom	Wall	1-R	2249	0.0949	0.0949	2.871	2.916	2.895
	9/19/11	Rocketdyne	Centered	2-T	2368	0.0911	0.1266	2.987	2.936	2.981
	9/21/11	Rocketdyne	Wall	-	1738	0.0562	-	2.88	2.989	2.939
20	9/13/11	Custom	Centered	N/A	N/A	N/A	N/A	N/A	N/A	N/A
	9/14/11	Custom	Wall	1-R	2569	0.019	0.019	2.424	2.563	2.560
	9/19/11	Rocketdyne	Centered	-	2378	0.0478	-	2.834	2.761	3.023
	9/21/11	Rocketdyne	Wall	-	1749	0.0534	-	2.759	3.003	2.801
22	9/13/11	Custom	Centered	1-R	2261	0.0415	0.0415	2.917	2.633	2.586
	9/14/11	Custom	Wall	1-R	2406	0.0427	0.0427	2.743	2.822	2.784
	9/19/11	Rocketdyne	Centered	-	1694	0.0701	-	2.807	2.832	2.890
	9/21/11	Rocketdyne	Wall	-	2338	0.0716	-	2.831	2.861	2.955
27	9/13/11	Custom	Centered	N/A	N/A	N/A	N/A	N/A	N/A	N/A
	9/14/11	Custom	Wall	1-R	2455	0.0272	0.0272	2.988	2.921	3.309
	9/19/11	Rocketdyne	Centered	-	1721	0.0643	-	3.139	2.874	2.918
	9/21/11	Rocketdyne	Wall	-	2981	0.0621	-	2.879	2.854	2.883

Table 6.7 (Continued)

Set Point	Injector	Center	Position	Mode Match	Dominant Frequency (Hz)	Max FFT Amplitude (P'/PChamber), %	Max Predicted Amplitude (P'/PChamber),%	Kurtosis		
								P1	P2	P3
28	9/13/11	Custom	Centered	N/A	N/A	N/A	N/A	N/A	N/A	N/A
	9/14/11	Custom	Wall	1-R	2290	0.0664	0.0664	3.005	3.070	3.021
	9/19/11	Rocketdyne	Centered	2-T	1730	0.0588	0.0672	2.871	2.876	3.035
	9/21/11	Rocketdyne	Wall	2-T	1733	0.0576	0.0853	2.871	2.975	2.986
30	9/13/11	Custom	Centered	N/A	N/A	N/A	N/A	N/A	N/A	N/A
	9/14/11	Custom	Wall	1-R	2289	0.0807	0.0807	2.829	2.887	2.851
	9/19/11	Rocketdyne	Centered	2-T	1726	0.0598	0.0642	2.808	2.819	2.980
	9/21/11	Rocketdyne	Wall	1-R	2374	0.0465	0.0465	2.878	2.861	2.852
31	9/13/11	Custom	Centered	N/A	N/A	N/A	N/A	N/A	N/A	N/A
	9/14/11	Custom	Wall	1-R	2466	0.0306	0.0306	2.620	2.775	2.742
	9/19/11	Rocketdyne	Centered	-	1701	0.0558	-	2.840	2.842	2.802
	9/21/11	Rocketdyne	Wall	-	3002	0.055	-	2.847	2.853	2.788
32	9/13/11	Custom	Centered	N/A	N/A	N/A	N/A	N/A	N/A	N/A
	9/14/11	Custom	Wall	1-R	2282	0.0853	0.0853	2.804	2.831	2.860
	9/19/11	Rocketdyne	Centered	2-T	1708	0.064	0.0553	2.714	2.879	2.935
	9/21/11	Rocketdyne	Wall	2-T	1733	0.0518	0.0781	2.846	2.817	2.777

Table 6.8 Summary of analysis results for shear coaxial tests.

	P1	P2	P3	Average Kurtosis of P1, P2, P3
Average Kurtosis – Tests with Modes Detected	2.816	2.825	2.855	2.832
Average Kurtosis - Tests without modes	2.819	2.858	2.856	2.844
Max Predicted Amplitude (P'/PChamber),%	0.1266			
Number of 2-T Matches	7			
Number of 1-R Matches	13			
Number of modes Detected	20			
Number of Tests	33			
Percent Match	60.9%			

Observations for Shear Coaxial Injector

The 2-T mode was most often identified when the injector was placed near the wall, while 1-R modes were generated when the injector was placed in the center. This is consistent with previous research. The kurtosis for these tests was not indicative of a strong sign wave. The average kurtosis for tests that had matches was 2.83 and for tests without matches was 2.84, virtually identical. This was not expected. It was expected that when modes were identified in the combustion chamber, the kurtosis would drop to nearly 1.5. It would seem that these tests did not have strong modes, or that there was a large amount of noise present in the signal. The amplitudes for these tests tended to be rather low, and the noise could be what caused the higher kurtosis value. The average kurtosis for each pressure transducer, averaged across all 33 tests is shown in Table 6.8.

.

When modes are active, the pressure within the combustion chamber is expected to spike. The average pressure amplitude for tests when a 1-R mode was identified was 0.0586% and for tests 2-T modes the average was 0.0589%. This is a 5.0% and 5.5% increase over the average pressure of tests that did not have mode identified, 0.0558%. This is a modest increase, but these results appear to support the theory as expected. A comparison of the average pressures of all the tests sorted by mode is shown in Figure 6.8.

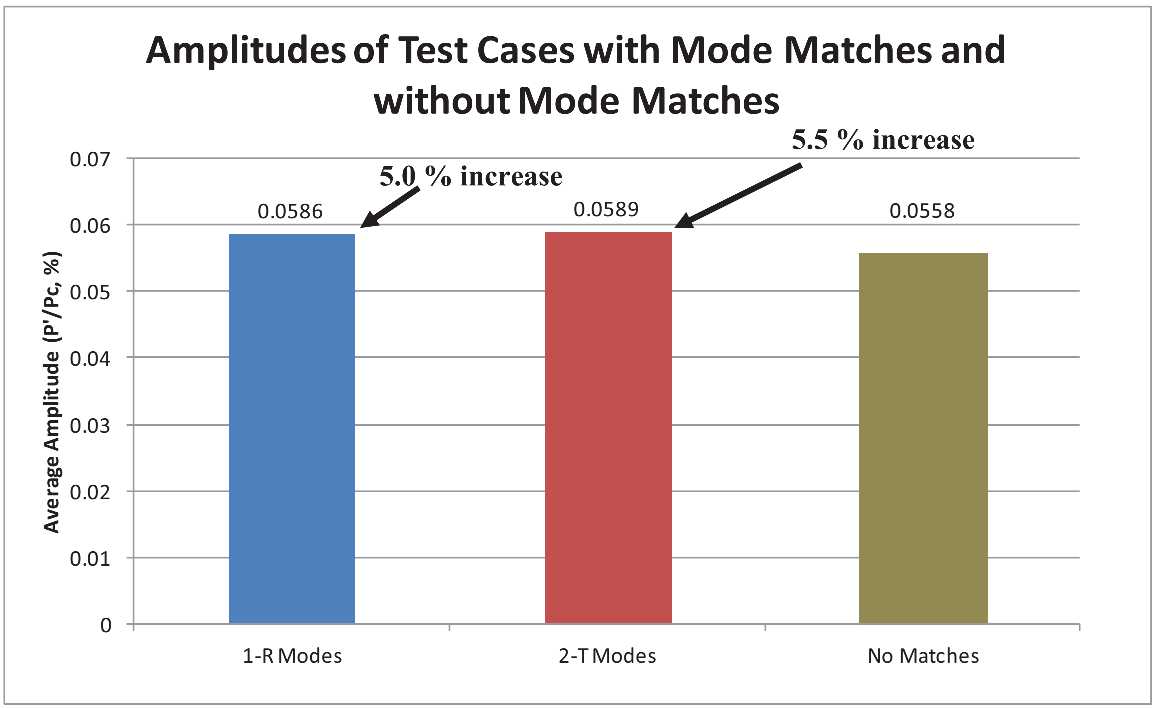

Figure 6.8 Average amplitude for the types of modes found, and the tests cases that had no match for the shear coaxial injector.

CHAPTER SEVEN

CONCLUSIONS AND FUTURE WORK

Conclusions

The analysis methodology developed worked extremely well for all test cases. The notable exceptions are the higher order modes where using only three pressure transducers to collect data provides insufficient resolution to uniquely identify the modes. In order to precisely determine modes 4-T and higher, more pressure transducers must be used. More pressure transducers located circumferentially around the chamber will provide higher resolution of mode orders. When a node line is at a pressure transducer, this method cannot accurately find a match for the mode. This is because when a node line is at a pressure transducer, the amplitude detected by the pressure transducer is zero and the amplitude ratios become undefined. This causes the mode-matching algorithm to become unreliable. The program was also shown to work very well in detecting a sinusoidal signal even in the presence of high levels of noise (up to a signal to noise ratio of one).

Test JPP-E showed the strongest amplitude of all of the tests. Analyzing this data using the Acoustic Mode Analysis Program verified the previous analysis that this test had a strong 2-T mode. It also verified that the Acoustic Mode Analysis Program provides the same results as other proven methods used at the PRC. This mode matched very well with the theoretical data. For the other impinging jet injector tests, only 1 out of 13 or 7.7% of the test cases had a match with an acoustic mode. For the shear coaxial injector 60.9% of the tests matched acoustic modes. The test cases that had matches tended to have one dominant, discrete peak frequency on the FFT. Test cases that did not have matches tended to have multiple frequencies on the FFT with similar amplitudes.

The shear coaxial injector was tested at two different locations: at the center of the combustion chamber and near the combustion chamber wall. There were 13 1-R modes found and 7 2-T modes found. Only 1-R modes occurred at the injector centered location. One 1-R mode was found at the near wall location, this occurred in SP30 taken on 9/21/11. All seven of the 2-T modes were found at the near wall injector location. The average amplitude of tests with 1-R modes showed a 5.0% increase and for 2-T modes, a 5.5% increase in pressure compared to tests that had no matches. This is expected based upon combustion instability theory. However, more test cases should be analyzed to verify this trend.

Future Work

Combustion instability research will continue at the Propulsion Research Center. The methodology developed and described in this thesis should be implemented into a real time analysis code, which can process data from the Instability Testing Facility as tests are being run. This would be an invaluable tool, allowing for the search of specific modes by changing parameters such as flow rate during the test.

Test JPP-E showed the strongest amplitude and correspondingly showed a bimodal distribution of the data when plotted as a histogram. This signal had an average kurtosis of 1.79 when for a perfect sine wave the kurtosis is 1.50. This indicates that this test had a high signal to noise ratio. This trend was expected to fit all data that had a mode match. However, this was not the case. For all of the rest of the test cases analyzed, the kurtosis varied between 2.65 to 2.90. This kurtosis is much higher than expected because a kurtosis of 3.0 represents a signal composed entirely of Gaussian noise. More work should be done to characterize the statistical properties of the combustion instability signals in tests performed at the PRC.

The next thing to be implemented at the test facility is a converging nozzle section that will be placed on top of the combustion chamber. This is currently being fabricated. Adding a converging nozzle will help prevent air entrainment from the surround environment. This should also increase the uniformity in chamber properties, such as air temperature. Consideration of longitudinal modes was neglected in this analysis because of the open top arrangement of the setup. With the addition of a converging nozzle, longitudinal modes should be considered.

The testing of different types of injectors will also be done, allowing more in depth study of the geometric effects of injector design on instability. The next setup will also use propane for fuel, instead of methane. Other propellant combinations can be tested at this facility.

APPENDICES

APPENDIX A

MODE AMPLITUDE RATIO GRAPHS

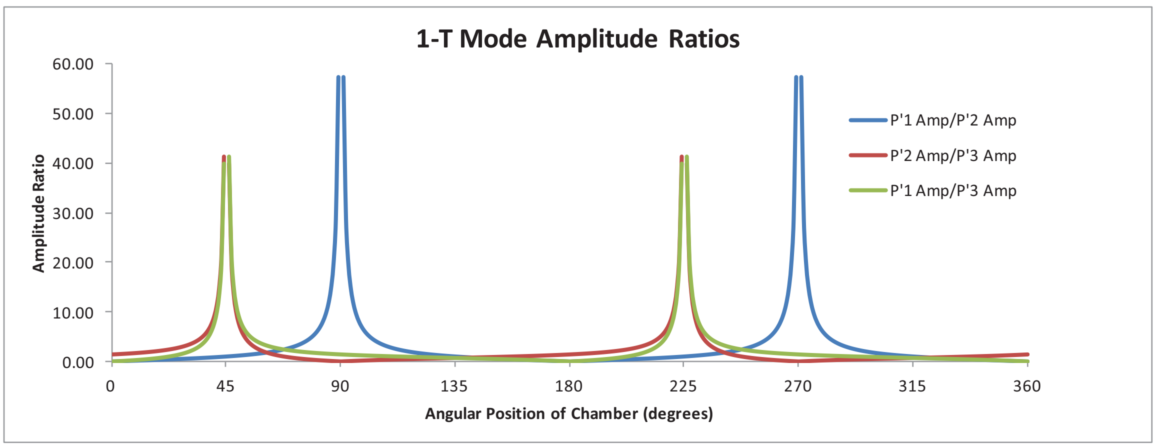

Figure A.1 1-T Mode Amplitude Ratio Graph.

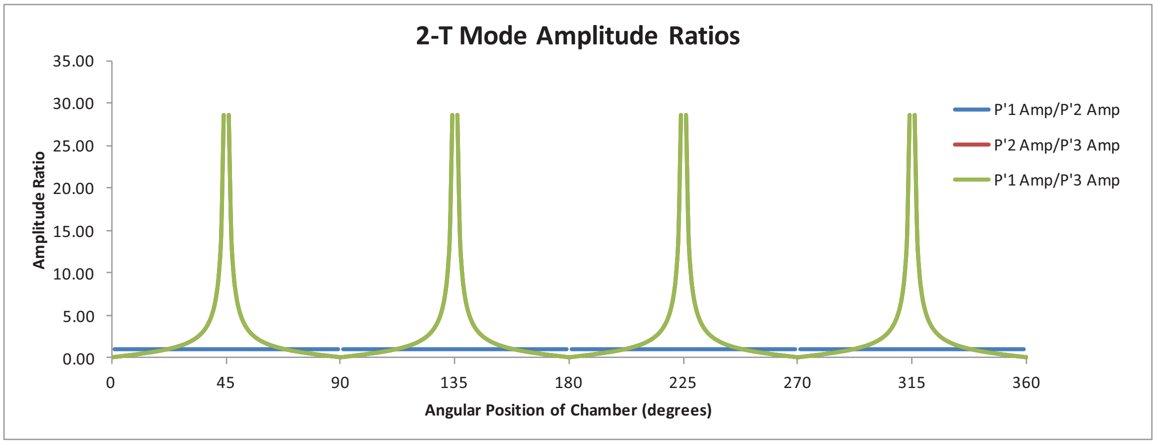

Figure A.2 2-T Mode Amplitude Ratio Graph.

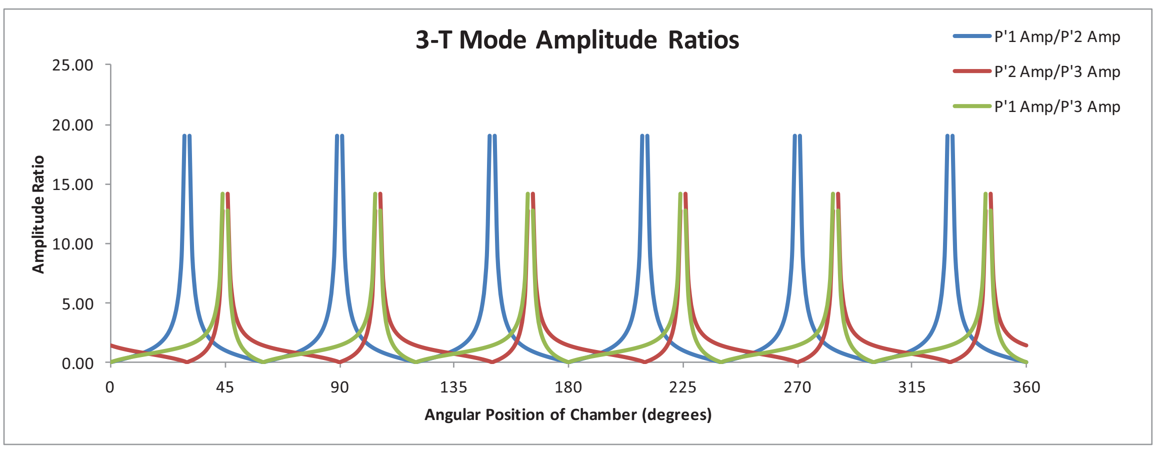

Figure A.3 3-T Mode Amplitude Ratio Graph.

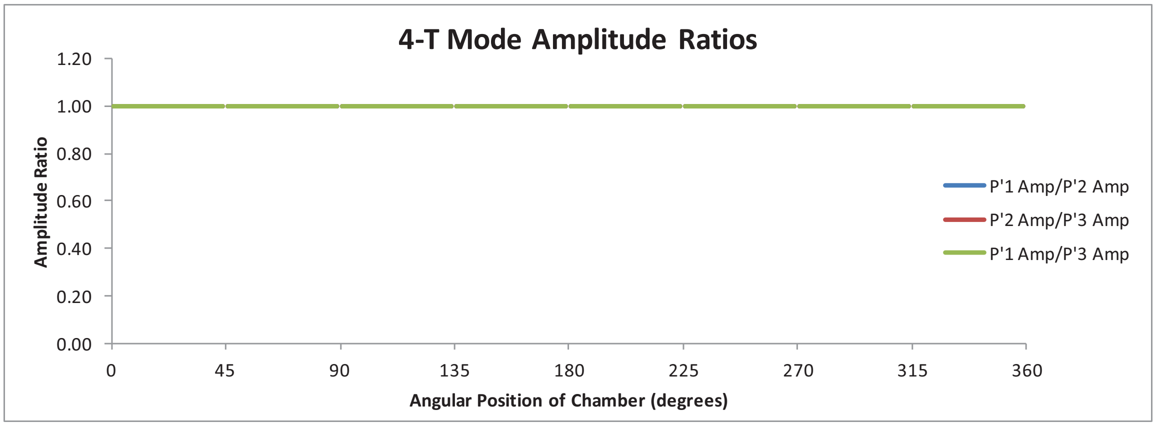

Figure A.4 4-T Mode Amplitude Ratio Graph.

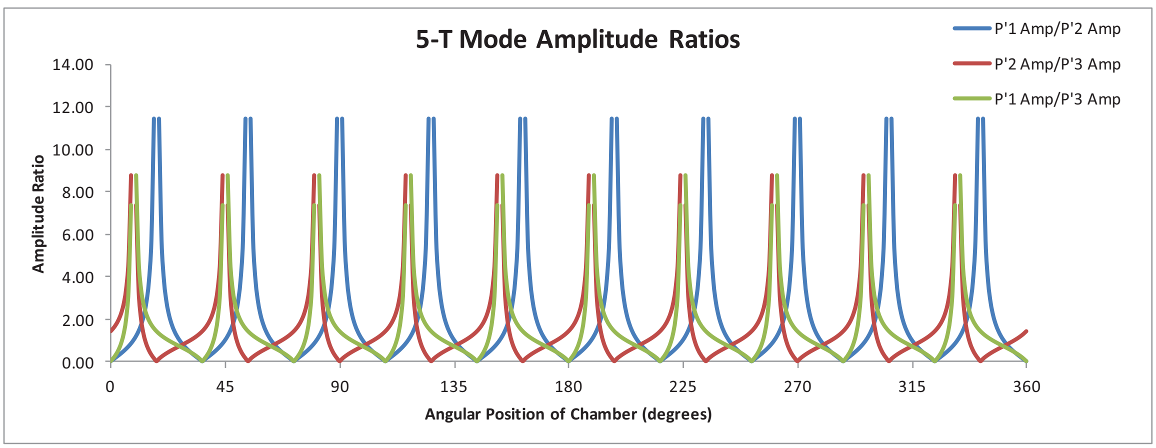

Figure A.5 5-T Mode Amplitude Ratio Graph.

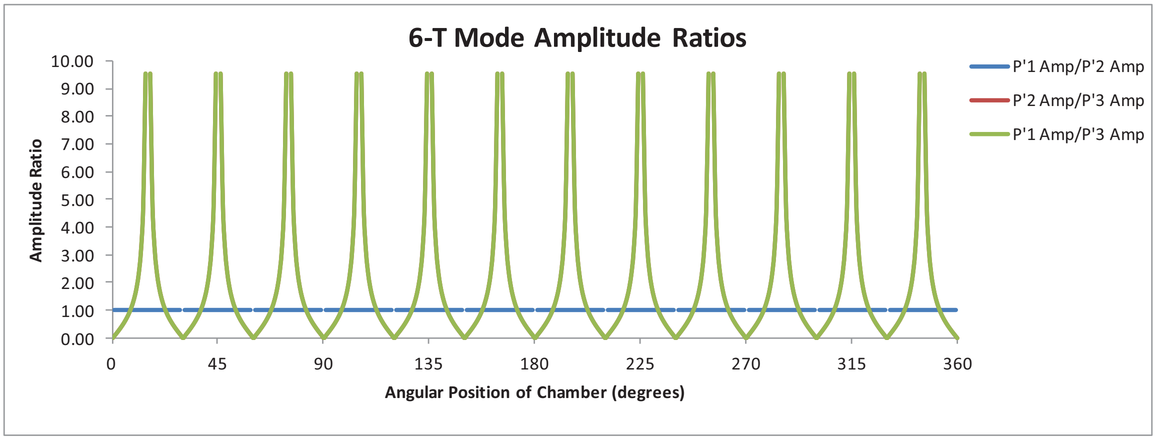

Figure A.6 6-T Mode Amplitude Ratio Graph.

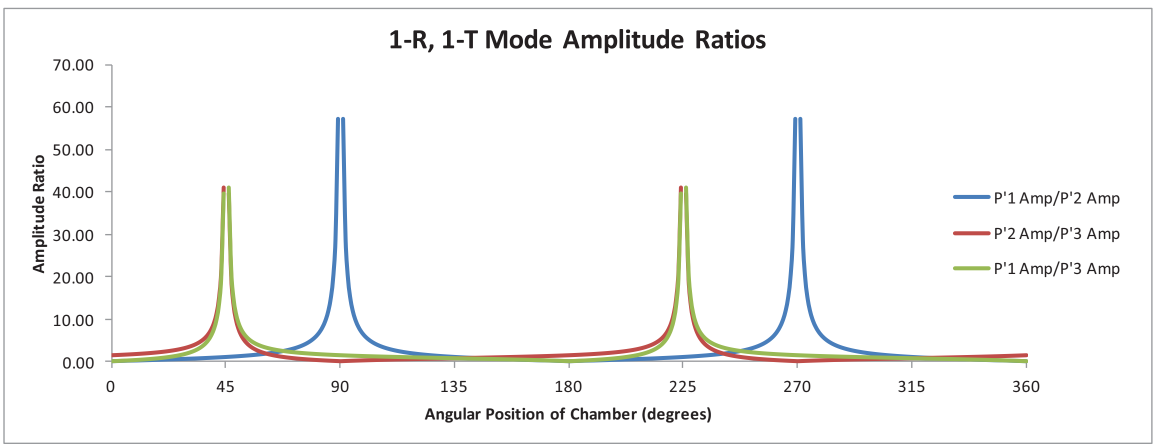

Figure A.7 1-R, 1-T Mode Amplitude Ratio Graph.

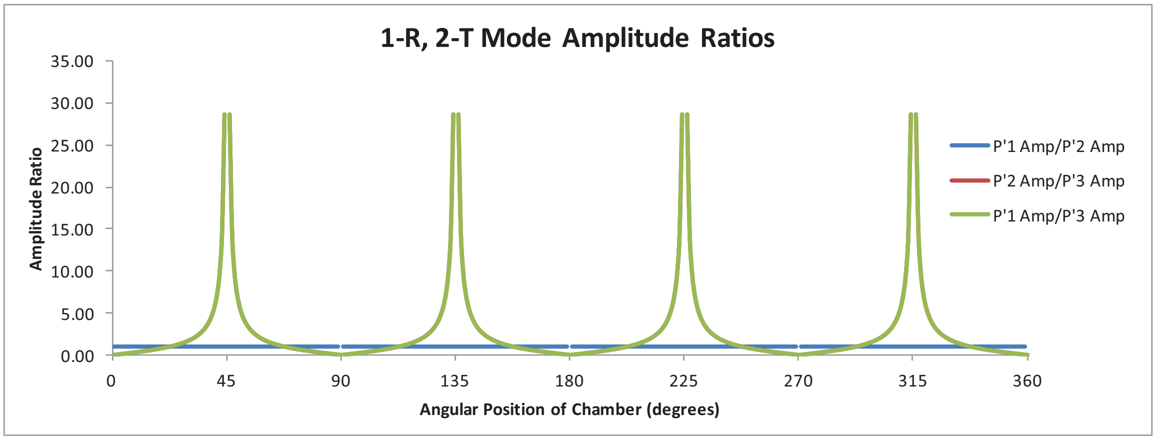

Figure A.8 1-R, 2-T Mode Amplitude Ratio Graph.

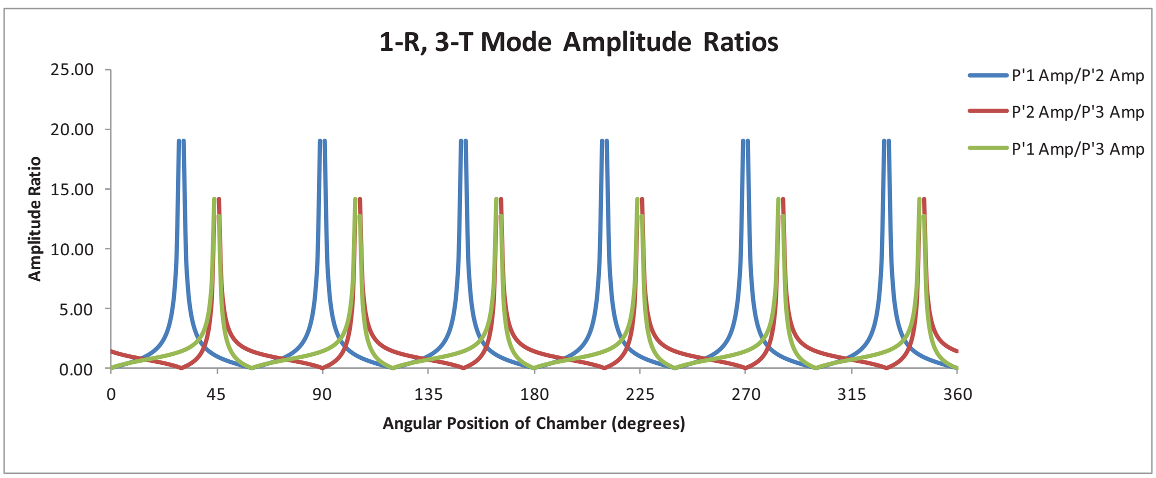

Figure A.9 1-R, 3-T Mode Amplitude Ratio Graph.

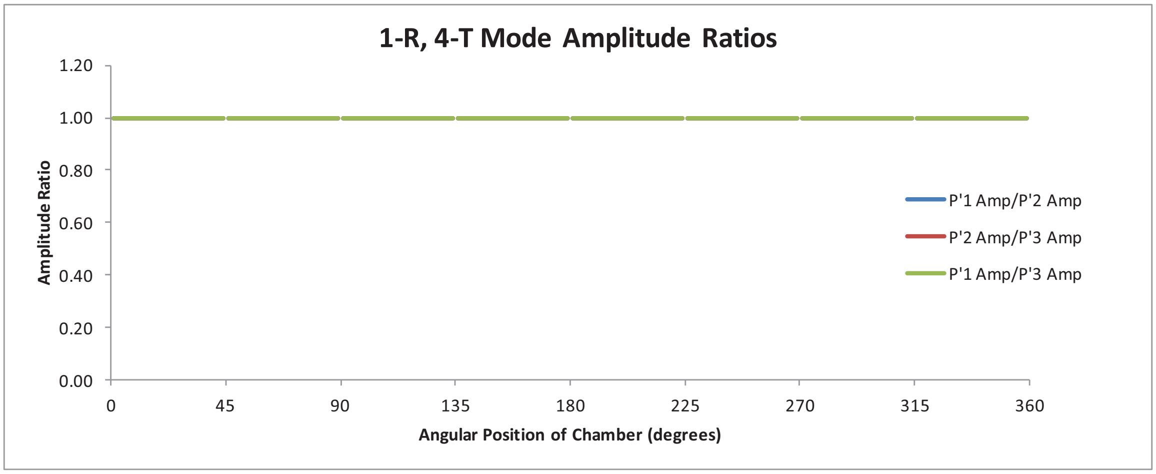

Figure A.10 1-R, 4-T Mode Amplitude Ratio Graph.

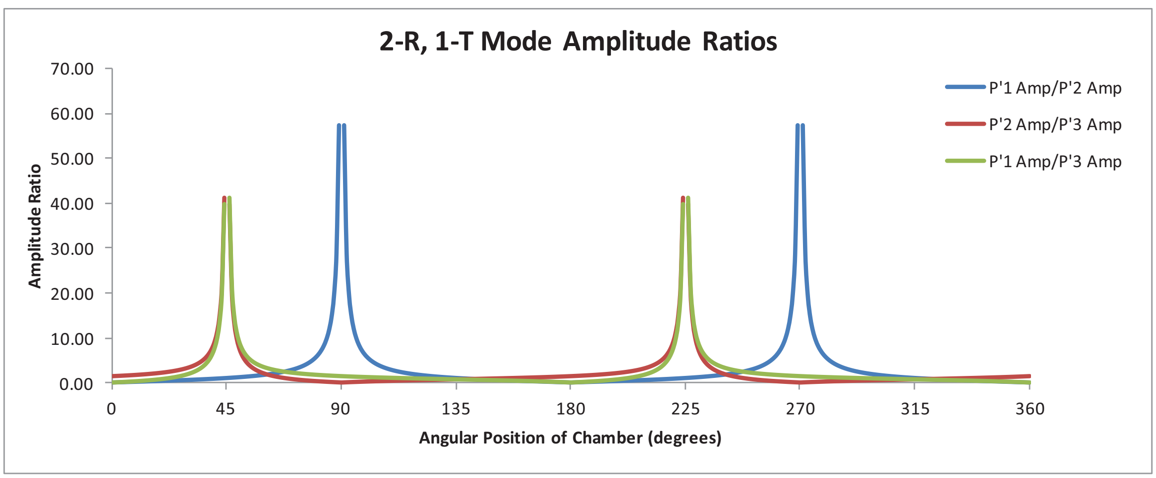

Figure A.11 2-R, 1-T Mode Amplitude Ratio Graph.

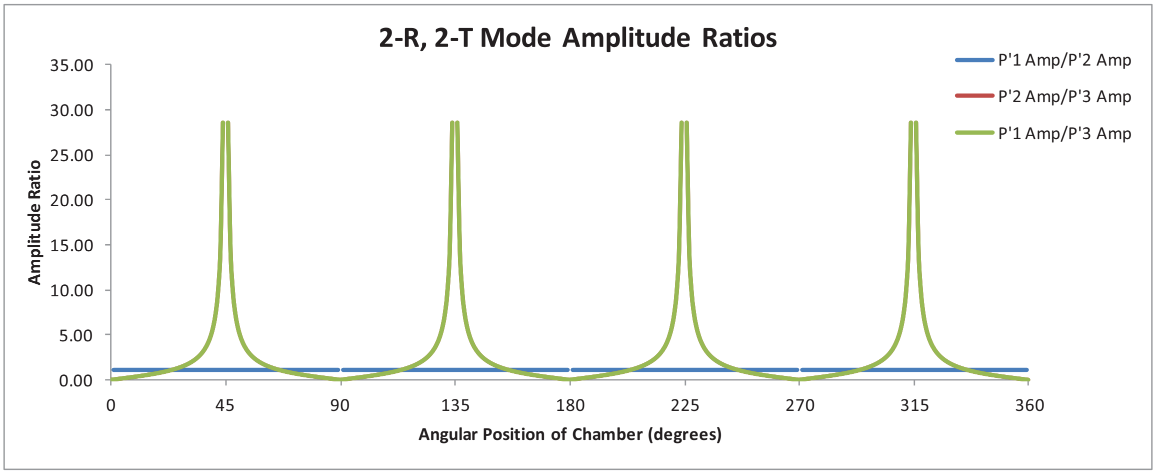

Figure A.12 2-R, 2-T Mode Amplitude Ratio Graph.

APPENDIX B

MODE PHASE GRAPHS

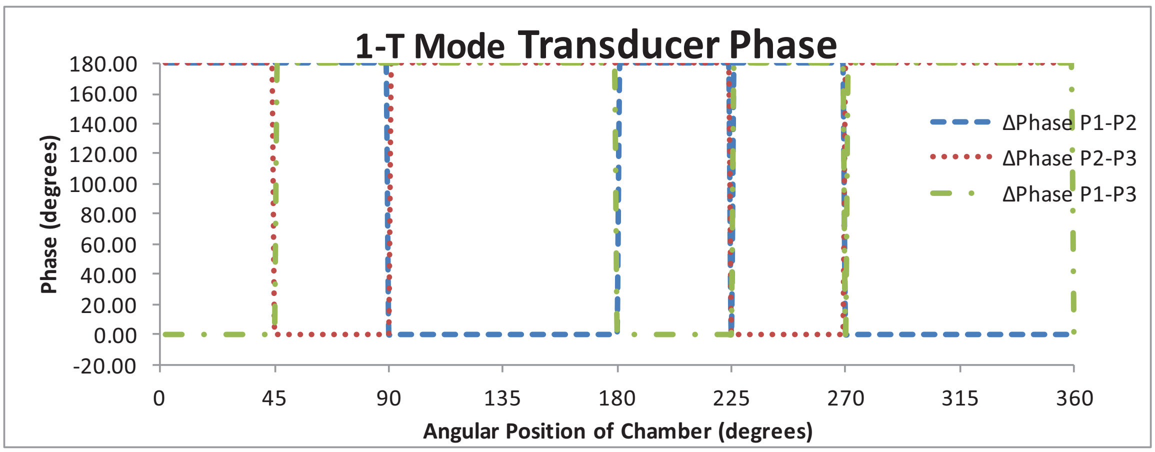

Figure B.1 1-T Mode Transducer Phase.

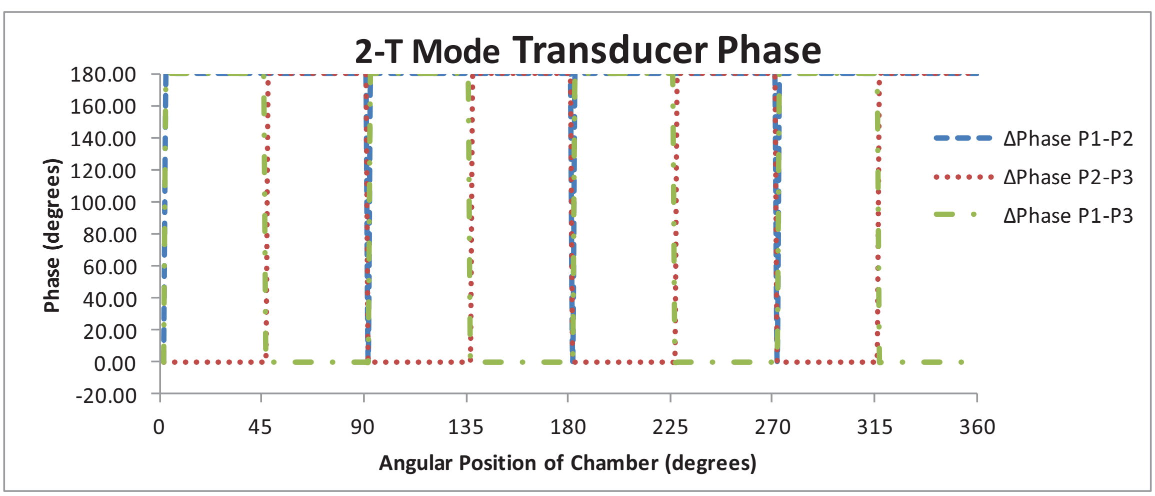

Figure B.2 2-T Mode Transducer Phase.

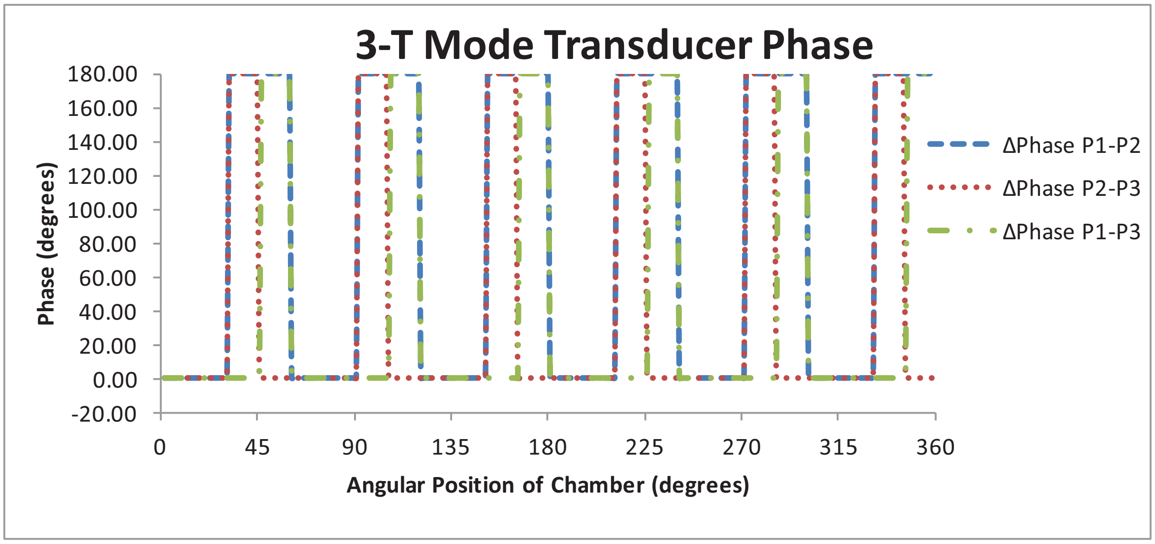

Figure B.3 3-T Mode Transducer Phase

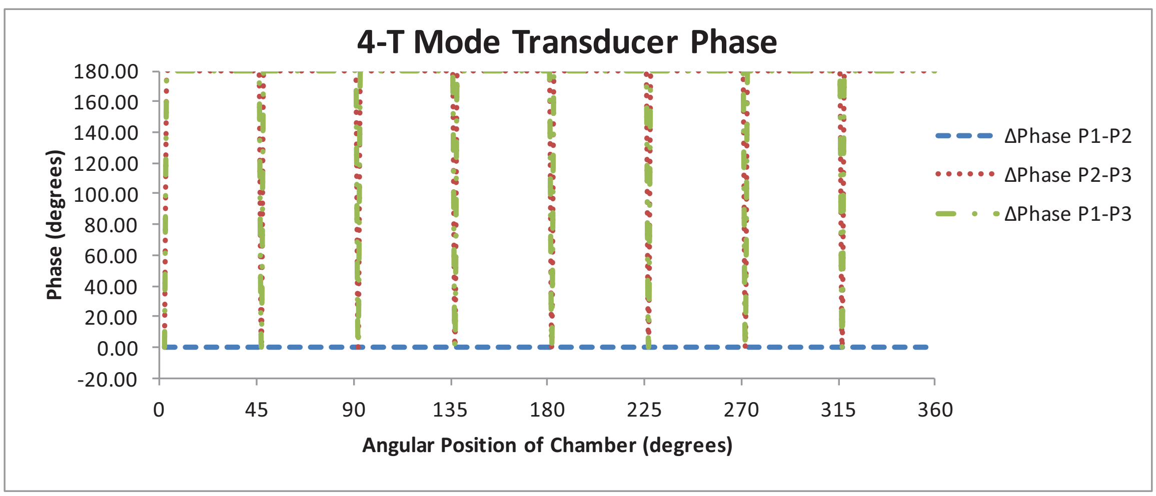

Figure B.4 4-T Mode Transducer Phase.

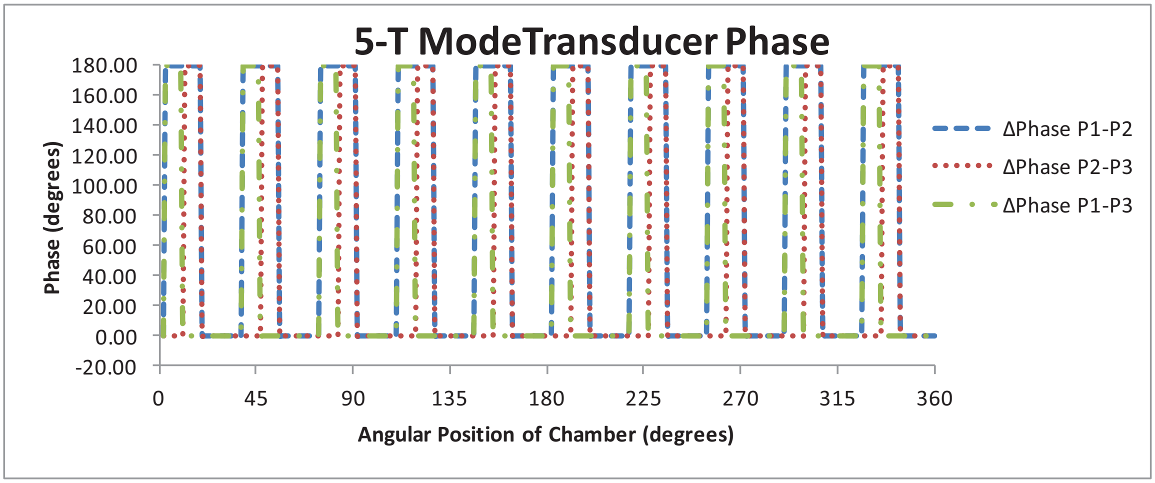

Figure B.5 5-T Mode Transducer Phase.

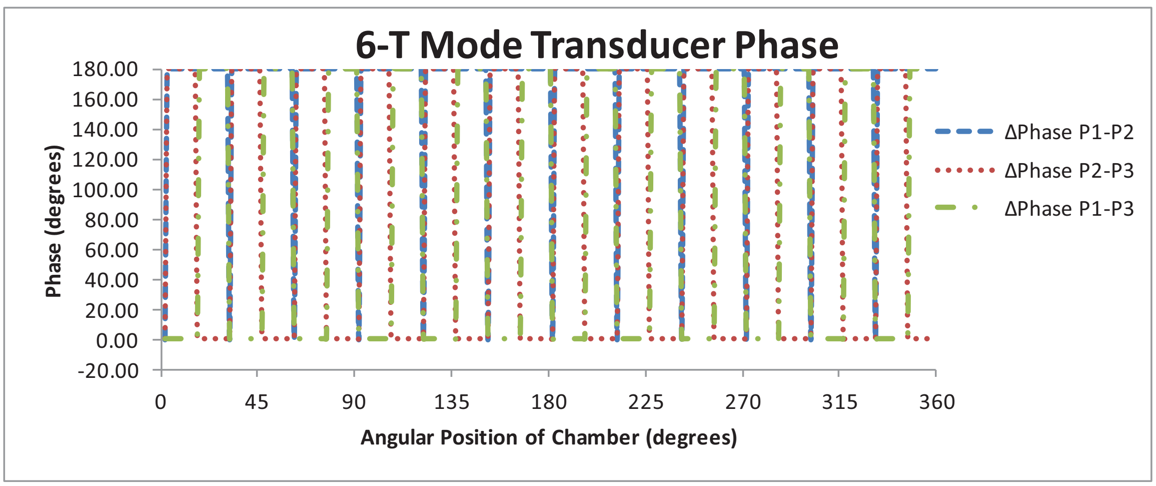

Figure B.6 6-T Mode Transducer Phase.

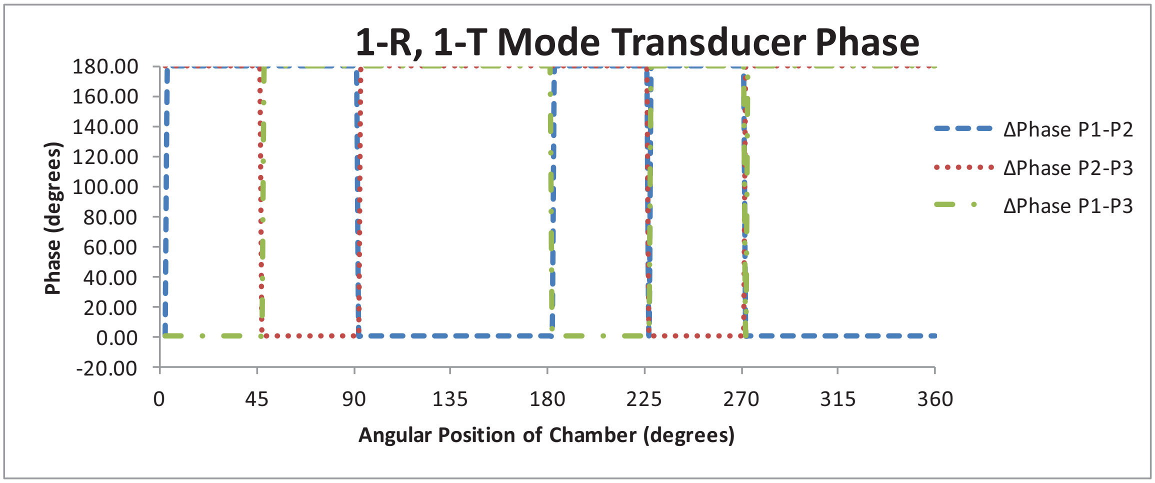

Figure B.7 1-R, 1-T Mode Transducer Phase.

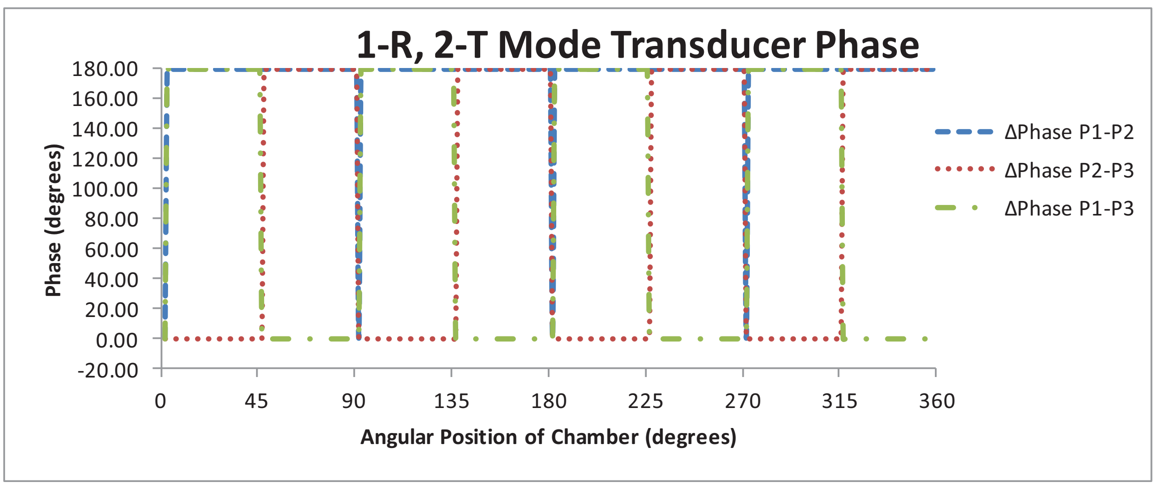

Figure B.8 1-R, 2-T Mode Transducer Phase.

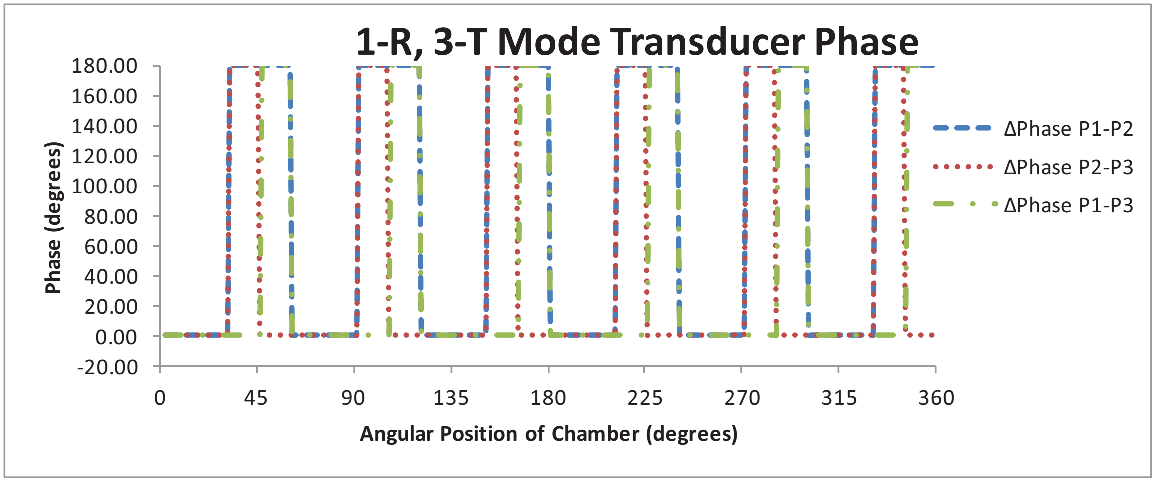

Figure B.9 1-R, 3-T Mode Transducer Phase.

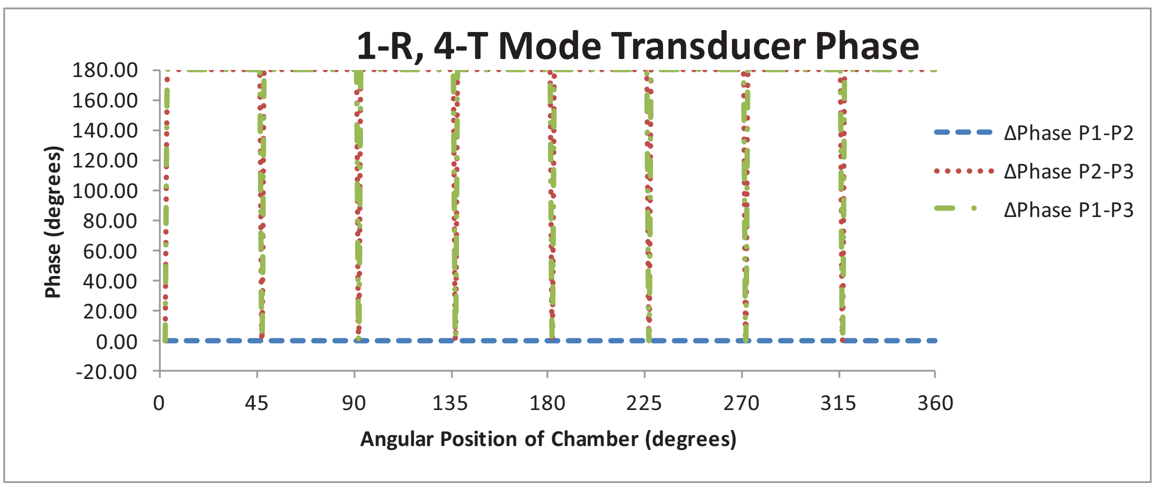

Figure B.10 1-R, 4-T Mode Transducer Phase.

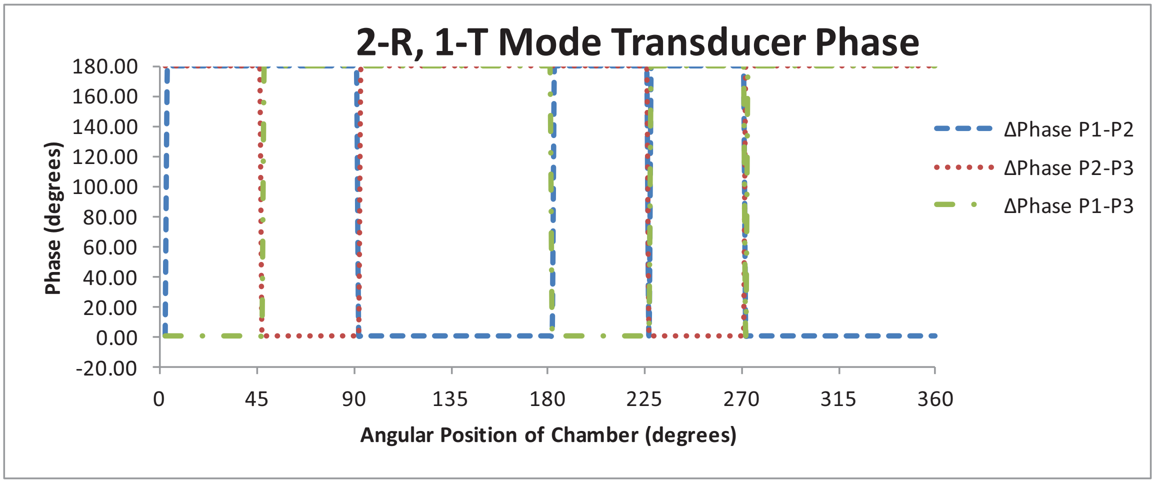

Figure B.11 2-R, 1-T Mode Transducer Phase.

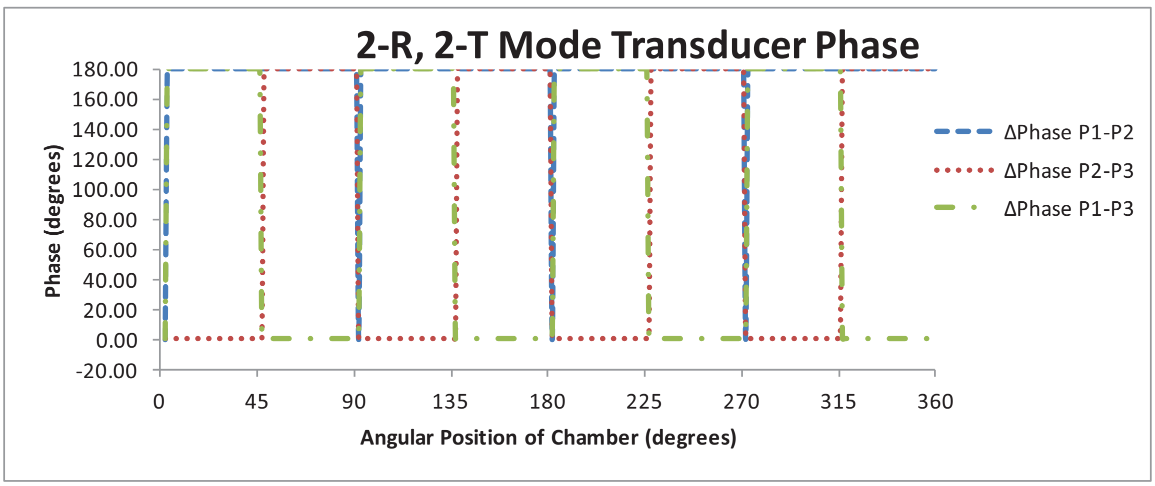

Figure B.12 2-R, 2-T Mode Transducer Phase.

APPENDIX C

PRESSURE VS. TIME GRAPHS FOR MODES

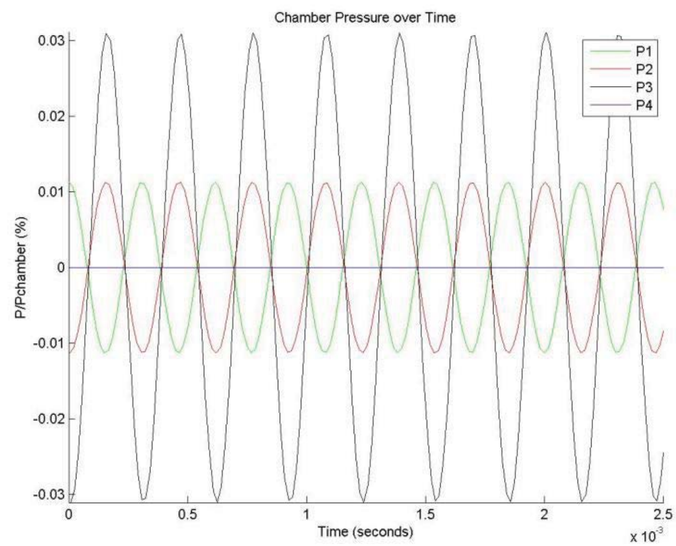

Figure C.1 Theoretical pressure vs. time graph for a 2-T mode at a node angle of 10°.

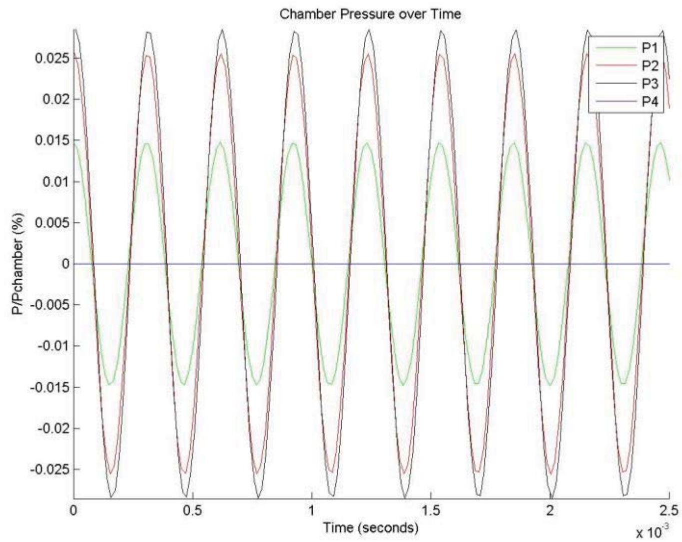

Figure C.2 Theoretical pressure vs. time graph for a 3-T mode at a node angle of 10°.

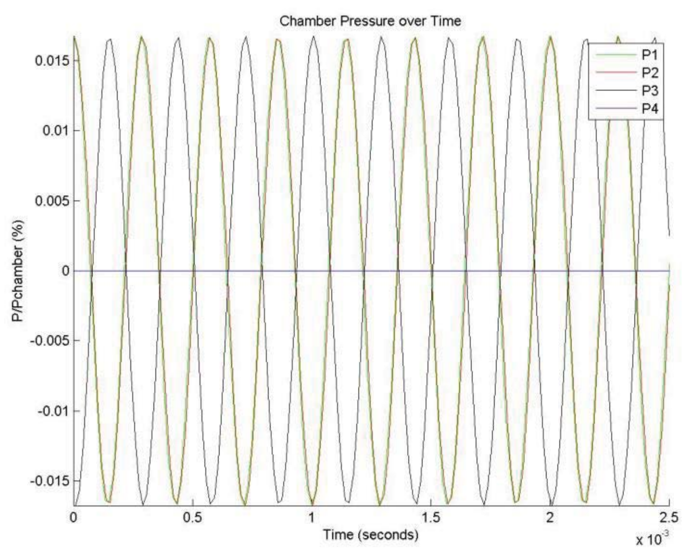

Figure C.3 Theoretical pressure vs. time graph for a 4-T mode at a node angle of 10°.

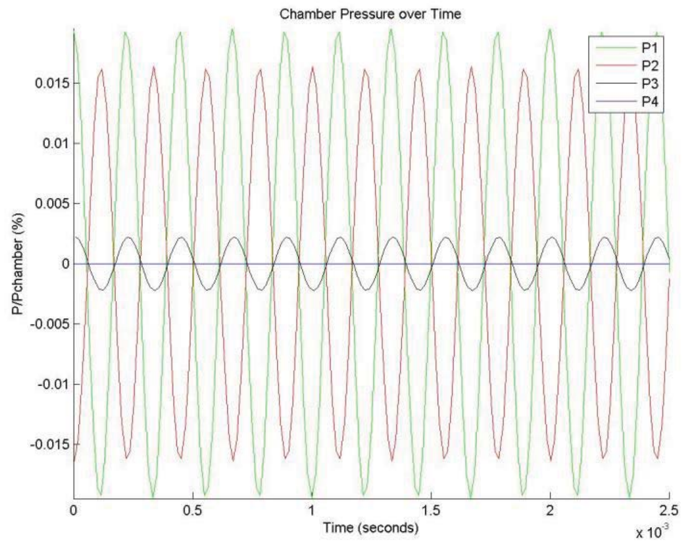

Figure C.4 Theoretical pressure vs. time graph for a 5-T mode at a node angle of 10°.

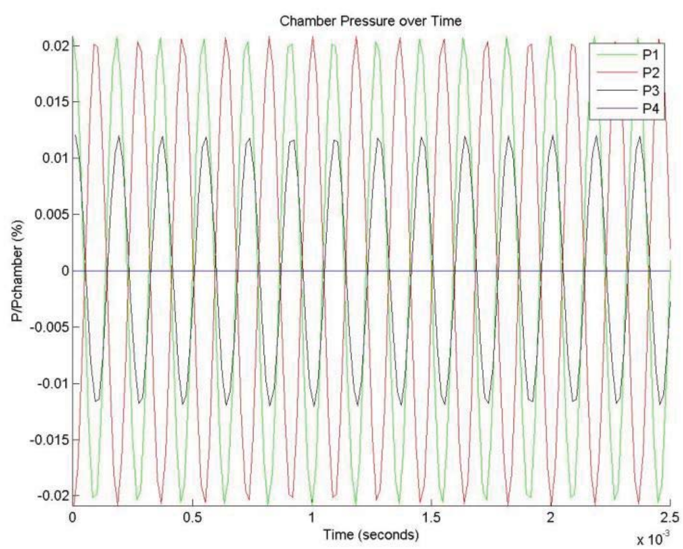

Figure C.5 Theoretical pressure vs. time graph for a 6-T mode at a node angle of 10°.

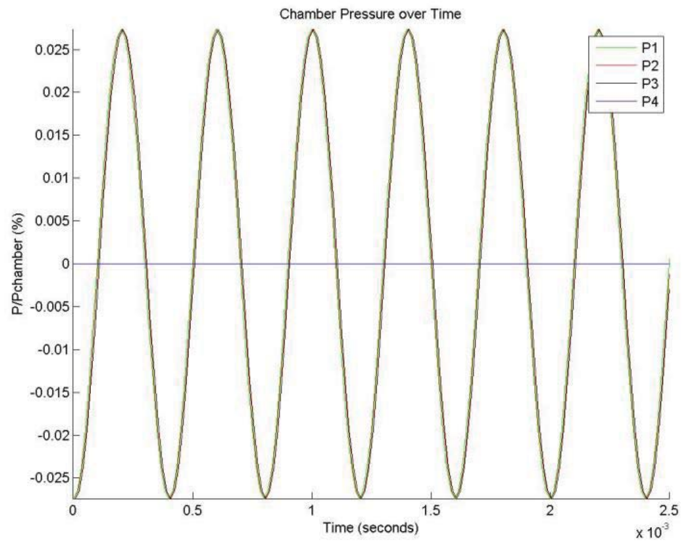

Figure C.6 Theoretical pressure vs. time graph for a 1-R mode.

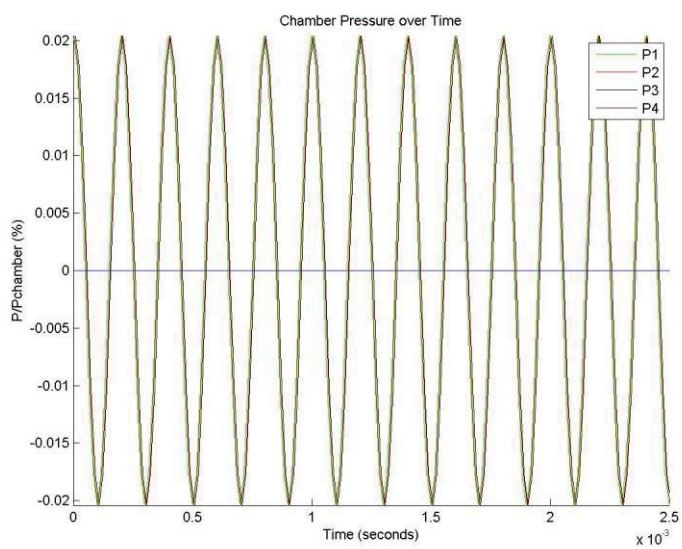

Figure C.7 Theoretical pressure vs. time graph for a 2-R mode.

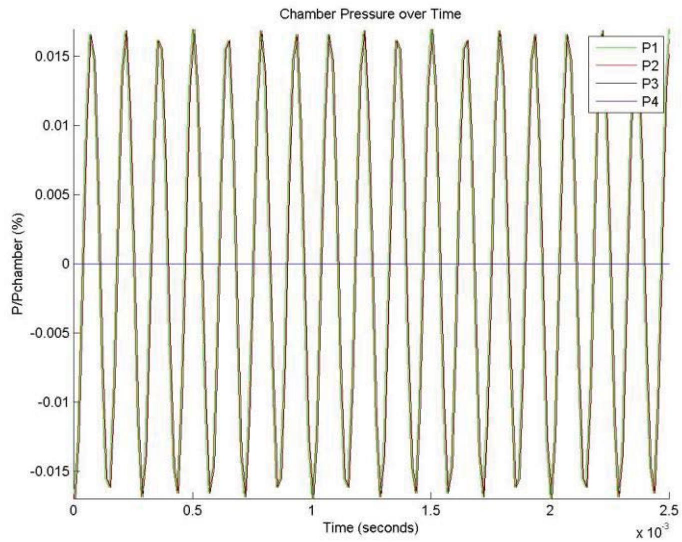

Figure C.8 Theoretical pressure vs. time graph for a 3-R mode.

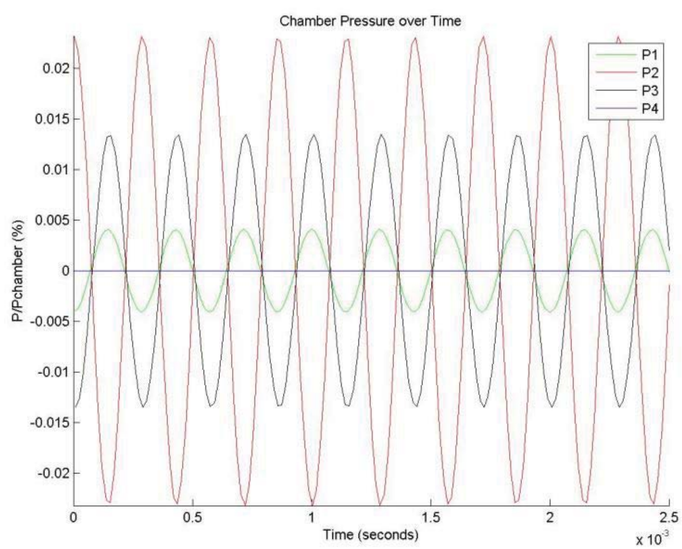

Figure C.9 Theoretical pressure vs. time graph for a 1-R, 1-T mode at a node angle of 10°.

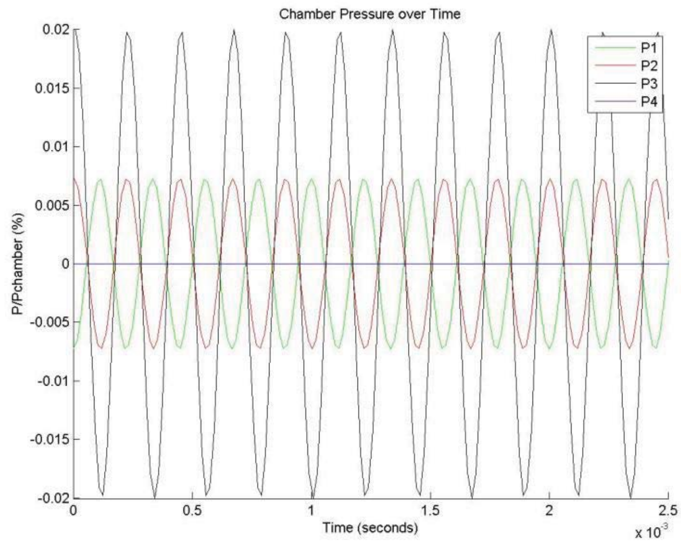

Figure C.10 Theoretical pressure vs. time graph for a 1-R, 2-T mode at a node angle of 10°.

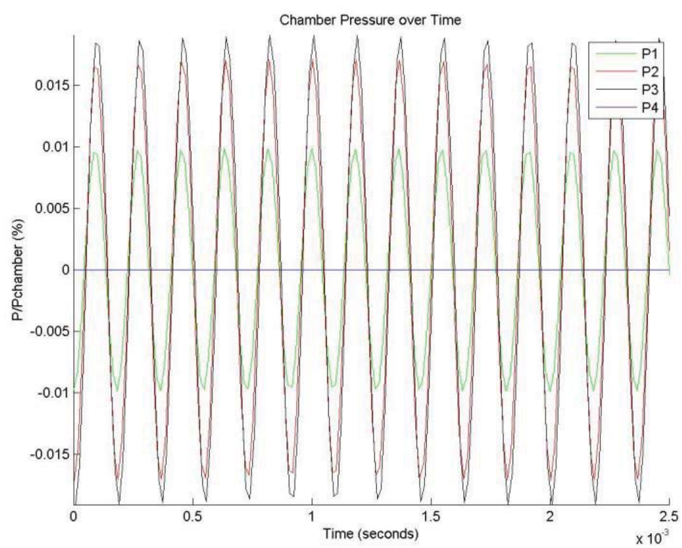

Figure C.11 Theoretical pressure vs. time graph for a 1-R, 3-T mode at a node angle of 10°.

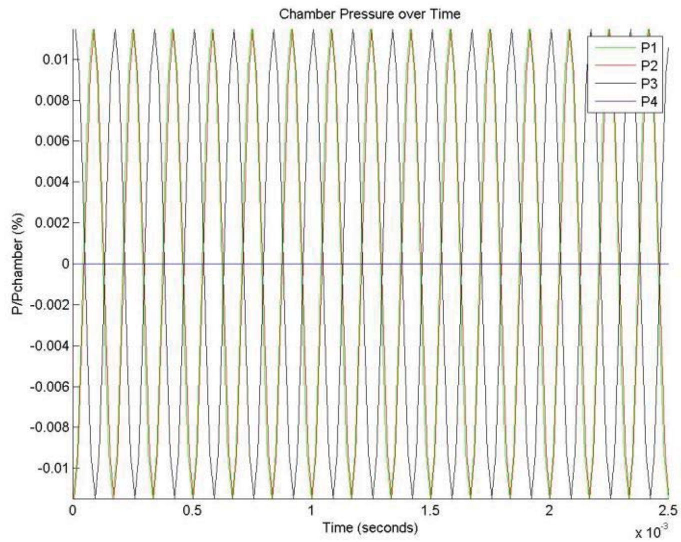

Figure C.12 Theoretical pressure vs. time graph for a 1-R, 4-T mode at a node angle of 10°.

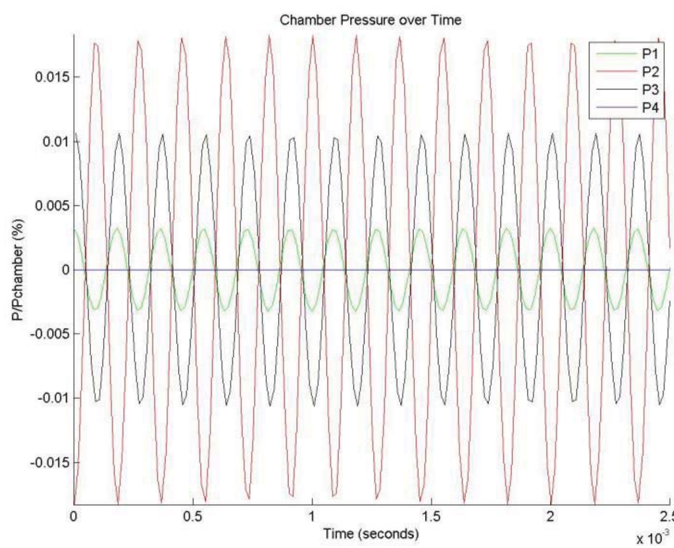

Figure C.13 Theoretical pressure vs. time graph for a 2-R, 1-T mode at a node angle of 10°.

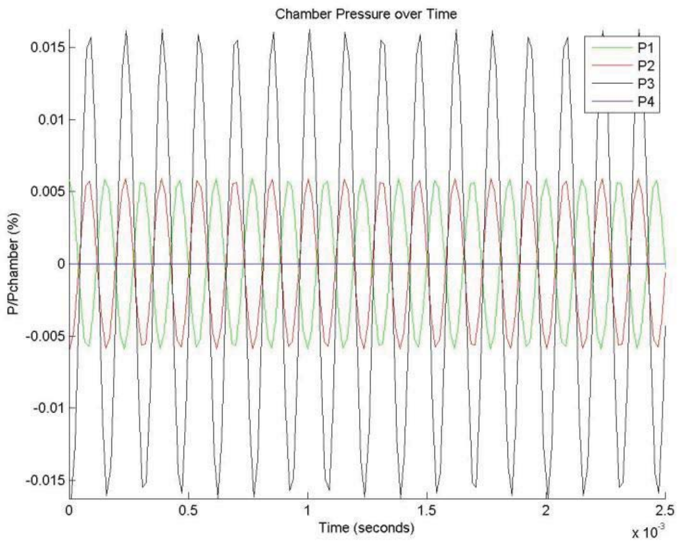

Figure C.14 Theoretical pressure vs. time graph for a 2-R, 2-T mode at a node angle of 10°.

APPENDIX D

Acoustic Analysis Program Matlab Code

```
%Joel Carpenter
%Acoustic Mode Determination Code for a Model Liquid Rocket Engine
close all;
clear all;
clc;
AmpTol = .2;
Phase_Tol = 60 ;
fs = 55500;
data_directory = 'C:\Users\Joel\Desktop\Test Data\' ;
%location of data folder
StartSample = 0;
EndSample = 10000;
NumSamples = EndSample- StartSample;
tsegment = .0025; %set upper limit of time for graph
data_folder = input('Enter the folder with the pressure data
file\n','s');
filename = input('Enter the file name (without the txt
extension)\n','s');
Pressures= importdata([data_directory data_folder '\' filename
'.txt']);
t=StartSample/fs:1/fs:(EndSample/fs-1/fs);
Pressures = Pressures ((StartSample+1):EndSample,1:3);
Tot_Trans = 3; %Number of transducers used in this experiment
%Initialize Arrays to zero
TP=0*ones(length(t),2, Tot_Trans);
y=0*ones(length(t),Tot_Trans);
yshift = 0*ones(length(t), Tot_Trans);
mx=0*ones(length(t), Tot_Trans);
Max_Amplitude=0*ones(1,Tot_Trans);
Stats=0*ones(10,Tot_Trans);
phase=0*ones(length(t),Tot_Trans);
Peak_Frequency = 0*ones(1,Tot_Trans);
Peak_Phase = 0*ones(1,Tot_Trans);
upperbound=0*ones(1,Tot_Trans);
lowerbound=0*ones(1,Tot_Trans);
Graph_i = 1;
Phase_Table_P1P2 = 0*ones(361,12) ;
Phase_Table_P2P3 =0*ones(361,12) ;
Phase_Table_P1P3 = 0*ones(361,12) ;
AR_Table_P1P2=  0*ones(361,12) ;
AR_Table_P2P3= 0*ones(361,12) ;
AR_Table_P1P3= 0*ones(361,12) ;
radial_mode = 0;
%Put time and pressure into one matrix
for NumTrans=1:Tot_Trans
```

```
TP(:,1, NumTrans) = t';
TP(:,2, NumTrans) = Pressures(:,NumTrans);
end
%Divide by atmospheric pressure and time shift.
for NumTrans=1:Tot_Trans
    if fs == 60000
    TP(:,1,NumTrans) = TP(:,1,NumTrans)+0.00001665/4*(NumTrans-1);
    end
    TP(:,2,NumTrans) = TP(:,2,NumTrans)/14.7*100;
end
%Bounds for Graphs
for NumTrans=1:Tot_Trans
upperbound(NumTrans)= max(TP(:,2,NumTrans));
lowerbound(NumTrans)= min(TP(:,2,NumTrans));
end
ub=max(upperbound);
lb=min(lowerbound);
% Graph all four transducers on the same graph
figure (Graph_i)
hold on
plot(TP(:,1,1), TP(:,2,1),'g')
plot(TP(:,1,2), TP(:,2,2),'r')
plot(TP(:,1,3), TP(:,2,3),'black')
% plot(TP(:,1,4), TP(:,2,4),'b')
axis([t(1) (t(1)+tsegment) lb ub])
xlabel('Time (seconds)')
ylabel('P/Pchamber (%)')
title(sprintf( 'Chamber Pressure over Time'))
legend('P1', 'P2', 'P3', 'P4')
hold off
saveas (figure (Graph_i),[data_directory data_folder '\' 'TP_' filename
'.jpg'])
Graph_i = Graph_i+1;
% Graph all four transducers on the same graph - WHOLE SIGNAL
figure (Graph_i)
for plotcount = 1:3
hold on
subplot(3,1,plotcount),plot(TP(:,1,Tot_Trans),
TP(:,2,Tot_Trans),'b',...
    TP(:,1,1), TP(:,2,1),'g',...
    TP(:,1,2), TP(:,2,2),'r',...
    TP(:,1,3), TP(:,2,3),'black')
axis([0+(1/3*(plotcount-1)) 1/3*plotcount 1.5*lb 1.5*ub])
xlabel('Time (seconds)')
ylabel('P/Pchamber (%)')
title(sprintf( 'Chamber Pressure over Time for Test'))
legend('P4', 'P1', 'P2', 'P3')
hold off
end
saveas (figure (Graph_i),[data_directory data_folder '\' 'Whole
Signal_' filename '.jpg'])
Graph_i = Graph_i+1;
%Plot histograms for all transducers
for NumTrans=1:Tot_Trans
figure (Graph_i)
ku=kurtosis(TP(:,2,NumTrans));
sk= skewness(TP(:,2,NumTrans));
```

```
Stats(1,NumTrans) = (sk);
Stats(2,NumTrans) = (ku);
subplot(2,2,NumTrans),hist(TP(:,2,NumTrans),100)
xlabel('Pressure (P/PChamber, %)')
ylabel('Frequency (# of Occurrences/Sec)')
uphist = 1.1*max( max(hist(TP(:,2,1),100),100));
axis([1.2*lb 1.2*ub -Inf uphist])
title(sprintf( 'Histogram for P%d, sk = %.3f, ku =%.3f', NumTrans, sk,
ku))
saveas (figure (Graph_i),[data_directory data_folder '\' 'Histogram_'
filename '.jpg'])
end
Graph_i= Graph_i+1;
%Find FFT
for NumTrans=1:Tot_Trans
%fs defined at the start                                    %sample
frequency (Hz)
m = length(TP(:,2,NumTrans));                          %Window length
y(:,NumTrans) = fft(TP(:,2,NumTrans),m);               %Take FFT
yshift(:,NumTrans) = fftshift(y(:,NumTrans));          %Shift fft amplitudes
so it is centered about 0
fshift = (-m/2:m/2-1)*(fs/m);                          %Shifted frequencies
mx(:,NumTrans)=(2/fs*abs(yshift(:,NumTrans)));
mx(1:NumSamples/2+25,NumTrans) = 0; %ignore the negative half of the
FFT results and the first 50 Hz
if fs == 60000
mx(.8*NumSamples:NumSamples,NumTrans)= 0; %ignore anything over 10k Hz
because of the 10k Hz Butterworth Filter
end
%Finds the max amplitude
Max_Amplitude(:,NumTrans) = max (mx(:,NumTrans));
end
%Determines which signal has the max amplitude
[row_Max_Amp col_Max_Amp ] =
ind2sub(size(Max_Amplitude(:,1:3)),find(Max_Amplitude(:,1:3)==max(Max_A
mplitude(:,1:3))));
for NumTrans=1:NumTrans
 %Finds the location of the max amplitude
[row(:,NumTrans) col(:,NumTrans)] =
ind2sub(size(mx(:,NumTrans)),find(mx(:,NumTrans)==Max_Amplitude(:,NumTr
ans)));
end
% Sets Peak_Frequency to the frequency of the pressure transducer with
the max amplitude
Peak_Frequency(:,:) = fshift(row(:,col_Max_Amp));
for NumTrans=1:Tot_Trans
%Plot all 4 FFTs in the same figure
figure (Graph_i)
subplot(2,2,NumTrans),plot(fshift,mx(:,NumTrans), 'markersize', 16);
xlabel('Frequency (Hz)')
ylabel('Amplitude (P/Pchamber, %)')
title(sprintf( 'FFT for P%d', NumTrans))
axis([-100 5000 0 1.1*max(Max_Amplitude)])
saveas (figure (Graph_i),[data_directory data_folder '\' 'FFT_'
filename '.jpg'])
end
Graph_i=Graph_i +1;
```

```
%Plot Phase
for NumTrans=1:Tot_Trans
%Find phase for each transducer
phase(:,NumTrans) = angle(yshift(:,NumTrans));
%Find phase at the frequency with the maximum amplitude
Peak_Phase(:,NumTrans) = phase(row(:,col_Max_Amp),NumTrans);
figure (Graph_i)
subplot(4,1,NumTrans),plot(fshift,phase(:,NumTrans)*180/pi)
xlabel('Frequency (Hz)')
ylabel('Phase (Degrees)')
title(sprintf( 'Phase for P%d, Dominant Frequency %d ', NumTrans,
Peak_Frequency(:, NumTrans)))
axis ([ max(Peak_Frequency)-50 max(Peak_Frequency)+50 -200 200])
grid on
saveas (figure (Graph_i),[data_directory data_folder '\' 'Phase_'
filename '.jpg'])
end
Phase_P1P2=abs(((Peak_Phase(:,1)-Peak_Phase(:,2))*180/pi));
Phase_P2P3=abs(((Peak_Phase(:,2)-Peak_Phase(:,3))*180/pi));
Phase_P1P3=abs(((Peak_Phase(:,1)-Peak_Phase(:,3))*180/pi));
%Statistical Parameters for all Transducers
for NumTrans=1:Tot_Trans
    %Standard Deviation
    Stats(3,NumTrans) = std(TP(:,2,NumTrans));
    %Average of Signal
    Stats(4,NumTrans)= mean(TP(:,2,NumTrans));
end
Stats(5,:) = Max_Amplitude (1,:);
Stats(6,:) = Peak_Frequency(1,:);
%Find Amplitude Ratios
AR_P1P2 = Max_Amplitude(1,1)/Max_Amplitude(1,2);
AR_P2P3 = Max_Amplitude(1,2)/Max_Amplitude(1,3);
AR_P1P3 = Max_Amplitude(1,1)/Max_Amplitude(1,3);
Stats_AR_Phase = {'P1/P2', 'P2/P3', 'P1/P3'; AR_P1P2, AR_P2P3,AR_P1P3;
Phase_P1P2,Phase_P2P3,Phase_P1P3;};
% %Write out the statistical data to excel file
Stat_LabelsH = {'Pressure Transducer', 'P1','P2', 'P3', 'P4'};
Stat_LabelsV =  {'Skewness';'Kurtosis'; 'Standard Deviation
(P/Pchamber)'; 'Average Pressure (P/Pchamber)';...
    ;'Max Amplitude from FFT (P/Pchamber, %)'; 'Dominant Frequency from
FFT(Hz)';...
    ' ';'Amp Ratios from FFT'; 'Phase Diff (degrees)'};
xlswrite([data_directory data_folder '\' 'Mode_Results_' filename
'.xlsx'], Stat_LabelsH, 1, 'A1')
xlswrite([data_directory data_folder '\' 'Mode_Results_' filename
'.xlsx'], Stat_LabelsV , 1, 'A2')
xlswrite([data_directory data_folder '\' 'Mode_Results_' filename
'.xlsx'], Stats(1:6,:), 1, 'B2')
xlswrite([data_directory data_folder '\' 'Mode_Results_' filename
'.xlsx'], Stats_AR_Phase, 1, 'B8')
%Check for Radial Modes
    %First Radial Mode Check, must also match in phase (below) to match
radial mode
     if 1<=AR_P1P2*(1+AmpTol) && 1>=AR_P1P2*(1-AmpTol) &&...
            1<=AR_P2P3*(1+AmpTol) && 1>=AR_P2P3*(1-AmpTol) &&...
            1<=AR_P1P3*(1+AmpTol) && 1>=AR_P1P3*(1-AmpTol)
            radial_mode = 1 ;
```

```
     end
     %Second Radial Mode Check. If true, end program and report radial
mode found
     if 0<=Phase_P1P2+Phase_Tol && 0>=Phase_P1P2-Phase_Tol &&...
            0<=Phase_P2P3+Phase_Tol && 0>=Phase_P2P3-Phase_Tol &&...
            0<=Phase_P1P3+Phase_Tol && 0>=Phase_P1P3-Phase_Tol
            radial_mode = radial_mode+1 ;
     end
 if radial_mode == 2
     ii =1;
     Match = {'Radial Mode Matches'};
       xlswrite([data_directory data_folder '\' 'Mode_Results_'
filename '.xlsx'], Match, 1, 'F1')
               if Peak_Frequency(1) >=2138
                    Match_Frequency(ii,1)  = 1;
                   ii= ii+1;
               end
               if Peak_Frequency(1) >= 3914
                   Match_Frequency(ii,1)  = 2;
                   ii= ii+1;
               end
               if Peak_Frequency(1) >=5675
                    Match_Frequency(ii,1)  = 3;
                   ii= ii+1;
               end
               for Radial_Modeswitchcount =  1: length(Match_Frequency)
                     mode_number_Radial =
Match_Frequency(Radial_Modeswitchcount);
               switch mode_number_Radial
                case 1
                    Radial_Matchnew = {'1-R Mode'};
                case 2
                    Radial_Matchnew = {'2-R Mode'};
                case 3
                    Radial_Matchnew = {'3-R Mode'};
               end
                  Radial_Match(Radial_Modeswitchcount, :) =
Radial_Matchnew;
           end
                  xlswrite([data_directory data_folder '\'
'Mode_Results_' filename '.xlsx'], Radial_Match, 1 , 'F2');
                  xlswrite([data_directory data_folder '\'
'Mode_Results_' filename '.xlsx'], max(Max_Amplitude(1,1:3)), 1 ,
'B11');
                  xlswrite([data_directory data_folder '\'
'Mode_Results_' filename '.xlsx'], {'Max Amplitude for Mode
(P/Pchamber, %)'}, 1 , 'A11');
                  return
 end
%Read in Amplitude Table
AR_Table = xlsread('Mode Amplitude Table.xlsx','Amplitude Ratio Table'
);
%Organize AR_Table for easier searching
for mode = 1:12
AR_Table_P1P2(:,mode) = AR_Table (:,((mode-1)*5)+2);
AR_Table_P2P3(:,mode) = AR_Table (:,((mode-1)*5)+3);
AR_Table_P1P3(:,mode) = AR_Table (:,((mode-1)*5)+4);
```

```
end

%Finds the modes based upon AR
% Determines the row, column location of the match for each amplitude
ratio with the AR table
[iP1P2 jP1P2] =
ind2sub(size(AR_Table_P1P2),find(AR_Table_P1P2<=(AR_P1P2*(1+AmpTol)) &
AR_Table_P1P2>=(AR_P1P2*(1-AmpTol))));
kP1P2 = [iP1P2, jP1P2];
[iP2P3 jP2P3] =
ind2sub(size(AR_Table_P2P3),find(AR_Table_P2P3<=(AR_P2P3*(1+AmpTol)) &
AR_Table_P2P3>=(AR_P2P3*(1-AmpTol))));
kP2P3 = [iP2P3, jP2P3];
[iP1P3 jP1P3] =
ind2sub(size(AR_Table_P1P3),find(AR_Table_P1P3<=(AR_P1P3*(1+AmpTol)) &
AR_Table_P1P3>=(AR_P1P3*(1-AmpTol))));
kP1P3  = [iP1P3, jP1P3];
%Finds the common matches of p1/p3, p2/p3 and p1/p3 from AR_Table
common1 = intersect( kP1P2, kP1P3, 'rows');
commonmodes_AR = intersect( common1, kP2P3, 'rows');
%Finds matches based on AR and saves them to variable AR_Match to be
saved to an excel file
if commonmodes_AR >= 1
for switchcount =  1: length(commonmodes_AR)
     mynumber = commonmodes_AR(switchcount,2);
    switch mynumber
    case 1
        AR_Matchnew = {'1-T Mode'};
    case 2
        AR_Matchnew  = {'2-T Mode'};
    case 3
        AR_Matchnew  = {'3-T Mode'};
    case 4
        AR_Matchnew  = {'4-T Mode'};
    case 5
       AR_Matchnew  = {'1-R/1-T Mode'};
    case 6
        AR_Matchnew  ={'5-T Mode'};
    case 7
        AR_Matchnew  = {'1-R/2-T Mode'};
    case 8
        AR_Matchnew = {'6-T Mode'};
    case 9
         AR_Matchnew  = {'1-R,3-T Mode'};
    case 10
         AR_Matchnew  = {'2-R,1-T Mode'};
    case 11
        AR_Matchnew  = {'1-R, 4-T Mode'};
    case 12
        AR_Matchnew  = {'2-R,2-T Mode'};
    otherwise
        AR_Matchnew  = {'No Match'};
    end
    AR_Match(switchcount,1) = AR_Matchnew;
end
else
    AR_Match = {'No Matches'};
```

```
    commonmodes_AR(1,1) = 0;
end
    Label = {'Node Angle', 'Matches Freq, AR and Phase','Node
Angle','Matches AR and Phase', 'Node Angle', 'Matches - AR', 'Node
Angle', 'Matches - Phase'};
    xlswrite([data_directory data_folder '\' 'Mode_Results_' filename
'.xlsx'], Label, 1, 'G1')
    xlswrite([data_directory data_folder '\' 'Mode_Results_' filename
'.xlsx'], commonmodes_AR(:,1)-1, 1, 'K2') %-1 because Angles in table
begin at 0
    xlswrite([data_directory data_folder '\' 'Mode_Results_' filename
'.xlsx'], AR_Match, 1, 'L2')
%Finds modes based on phase
%Read in Phase Table
Phase_Table = xlsread('Phase.xlsx','Phase Table' );
%Organize Phase_Table for easier searching
for mode = 1:12
Phase_Table_P1P2(:,mode) = Phase_Table (:,((mode-1)*5)+2);
Phase_Table_P2P3(:,mode) = Phase_Table (:,((mode-1)*5)+3);
Phase_Table_P1P3(:,mode) = Phase_Table (:,((mode-1)*5)+4);
end
% Determines the row, column location of the match for each amplitude
ratio with the phase table
[xP1P2 yP1P2] =
ind2sub(size(Phase_Table_P1P2),find(Phase_Table_P1P2<=Phase_P1P2+Phase_
Tol & Phase_Table_P1P2>=Phase_P1P2-Phase_Tol));
zP1P2 = [xP1P2, yP1P2];
[xP2P3 yP2P3] =
ind2sub(size(Phase_Table_P2P3),find(Phase_Table_P2P3<=Phase_P2P3+Phase_
Tol & Phase_Table_P2P3>=Phase_P2P3-Phase_Tol));
zP2P3 = [xP2P3, yP2P3];
[xP1P3 yP1P3] =
ind2sub(size(Phase_Table_P1P3),find(Phase_Table_P1P3<=Phase_P1P3+Phase_
Tol & Phase_Table_P1P3>=Phase_P1P3-Phase_Tol));
zP1P3  = [xP1P3, yP1P3];
%Finds the common matches of p1/p3, p2/p3 and p1/p3 for Phase Table
common2 = intersect( zP1P2, zP1P3, 'rows');
commonmodes_Phase = intersect( common2, zP2P3, 'rows');
%Find matches in phase and writes to Excel file
if commonmodes_Phase >= 1
    for phaseswitchcount =  1: length(commonmodes_Phase)
     mode_number_phase = commonmodes_Phase(phaseswitchcount,2);
       switch mode_number_phase
        case 1
            Phase_Matchnew = {'1-T Mode'};
        case 2
            Phase_Matchnew  = {'2-T Mode'};
        case 3
            Phase_Matchnew  = {'3-T Mode'};
        case 4
            Phase_Matchnew  = {'4-T Mode'};
        case 5
            Phase_Matchnew  = {'1-R/1-T Mode'};
        case 6
            Phase_Matchnew   ={'5-T Mode'};
        case 7
          Phase_Matchnew  = {'1-R/2-T Mode'};
```

```
          case 8
             Phase_Matchnew = {'6-T Mode'};
          case 9
               Phase_Matchnew   = {'1-R,3-T Mode'};
          case 10
               Phase_Matchnew  = {'2-R,1-T Mode'};
          case 11
              Phase_Matchnew  = {'1-R,4-T Mode'};
          case 12
              Phase_Matchnew   = {'2-R,2-T Mode'};
           otherwise
              Phase_Matchnew  = {'No Match'};
           end
      Phase_Match(phaseswitchcount, :) = Phase_Matchnew;
     end
       else
          Phase_Match = {'No Matches'};
          commonmodes_Phase(1,1) = 0;
end
       xlswrite([data_directory data_folder '\' 'Mode_Results_'
filename '.xlsx'], commonmodes_Phase(:,1)-1, 1, 'M2')%-1 because Angles
in table begin at 0
       xlswrite([data_directory data_folder '\' 'Mode_Results_'
filename '.xlsx'], Phase_Match, 1 , 'N2');
%Finds the modes that match in both AR and Phase
commonmodes_Both = intersect( commonmodes_Phase, commonmodes_AR,
'rows');
if commonmodes_Both >= 1 %If any matches in both AR and Phase write to
excel file, if not end
    for Modeswitchcount =  1: length(commonmodes_Both)
    mode_number = commonmodes_Both(Modeswitchcount,2);
        switch mode_number
            case 1
                All_Matchnew = {'1-T Mode'};
            case 2
                All_Matchnew = {'2-T Mode'};
            case 3
                All_Matchnew = {'3-T Mode'};
            case 4
                All_Matchnew = {'4-T Mode'};
            case 5
                All_Matchnew = {'1-R/1-T Mode'};
            case 6
                All_Matchnew ={'5-T Mode'};
            case 7
                All_Matchnew = {'1-R/2-T Mode'};
            case 8
                All_Matchnew = {'6-T Mode'};
            case 9
                 All_Matchnew = {'1-R,3-T Mode'};
            case 10
                 All_Matchnew = {'2-R,1-T Mode'};
            case 11
                All_Matchnew = {'1-R,4-T Mode'};
            case 12
                All_Matchnew = {'2-R,2-T Mode'};
             otherwise
```

```
                All_Matchnew = {'No Match'};
        end
        All_Match(Modeswitchcount, :) = All_Matchnew;
    end
    else
    All_Match = {'No Matches'};
    commonmodes_Both(1,1) = 0;
   end
        xlswrite([data_directory data_folder '\' 'Mode_Results_'
filename '.xlsx'], All_Match, 1 , 'J2');
        xlswrite([data_directory data_folder '\' 'Mode_Results_'
filename '.xlsx'], commonmodes_Both(:,1)-1, 1, 'I2')%-1 because Angles
in table begin at 0
%% Find modes that match based on frequency
ii = 1;  %counter for frequency matching
% Peak_Frequency %Gives the detected peak frequency for the highest
amplitude signal
               if Peak_Frequency(1) >=1027
                   Match_Frequency(ii,1)  = 1;
                   ii= ii+1;
               end
               if Peak_Frequency(1) >=1700
                    Match_Frequency(ii,1) = 2;
                   ii= ii+1;
               end
               if Peak_Frequency(1) >=2344
                    Match_Frequency(ii,1)  = 3;
                   ii= ii+1;
               end
               if Peak_Frequency(1) >=2966
                    Match_Frequency(ii,1)  = 4;
                   ii= ii+1;
               end
               if Peak_Frequency(1) >=2974
                    Match_Frequency(ii,1)  = 5;
                   ii= ii+1;
               end

               if Peak_Frequency(1) >=3579
                    Match_Frequency(ii,1)  = 6;
                   ii= ii+1;
               end
               if Peak_Frequency(1) >=3741
                    Match_Frequency(ii,1)  = 7;
                   ii= ii+1;
               end
               if Peak_Frequency(1) >=4185
                   Match_Frequency(ii,1)  = 8;
                   ii= ii+1;
               end
               if Peak_Frequency (1)>=4471
                   Match_Frequency(ii,1)  = 9;
                   ii= ii+1;
               end
               if Peak_Frequency(1) >=4762
                    Match_Frequency(ii,1)  = 10;
                   ii= ii+1;
```

```
                end
                if Peak_Frequency(1) >=5178
                    Match_Frequency(ii,1)   = 11;
                    ii= ii+1;
                end
                if Peak_Frequency(1) >=5562
                     Match_Frequency(ii,1)   = 12;
                    ii= ii+1;
                end
%Finds the modes that in match frequency, AR and Phase
 Mode_Final= intersect(commonmodes_Both(:,2),Match_Frequency);
 zz= 1 ;
for jj = 1 : length(Mode_Final)
 for kk = 1:length(commonmodes_Both)
     if commonmodes_Both (kk,2) == Mode_Final(jj)
     commonmodes_Final(zz,:) = commonmodes_Both(kk,:);
     zz = zz+1;
     end
 end
end
if Mode_Final >= 1 %If any matches in both AR and Phase write to excel
file, if not end
    for Final_Modeswitchcount =  1: length(commonmodes_Final)
    mode_number_Final = commonmodes_Final(Final_Modeswitchcount,2);
        switch mode_number_Final
            case 1
                Final_Matchnew = {'1-T Mode'};
            case 2
                Final_Matchnew = {'2-T Mode'};
            case 3
                Final_Matchnew = {'3-T Mode'};
            case 4
                Final_Matchnew = {'4-T Mode'};
            case 5
                Final_Matchnew = {'1-R/1-T Mode'};
            case 6
                Final_Matchnew ={'5-T Mode'};
            case 7
                Final_Matchnew= {'1-R/2-T Mode'};
            case 8
                Final_Matchnew = {'6-T Mode'};
            case 9
                 Final_Matchnew = {'1-R,3-T Mode'};
            case 10
                 Final_Matchnew = {'2-R,1-T Mode'};
            case 11
                Final_Matchnew = {'1-R,4-T Mode'};
            case 12
                Final_Matchnew = {'2-R,2-T Mode'};
             otherwise
                Final_Matchnew = {'No Match'};
        end
        Final_Match(Final_Modeswitchcount, :) = Final_Matchnew;
    end
    else
    Final_Match = {'No Matches'};
    commonmodes_Final(1,1) = 0;
```

```
end

xlswrite([data_directory data_folder '\' 'Mode_Results_' filename
'.xlsx'], Final_Match, 1 , 'H2');
xlswrite([data_directory data_folder '\' 'Mode_Results_' filename
'.xlsx'], commonmodes_Final(:,1)-1, 1, 'G2')%-1 because Angles in table
begin at 0
%Determine maximum amplitude experienced within the chamber
%This is based upon the amplitude detected at P1 and
%The first determined node angle
if commonmodes_Final >0
    Max_AR_Table = xlsread('Max AR Table.xlsx');
    %commonmodes_Final lists node angle, mode type
    CF_Node = commonmodes_Final(1,1); %Node angle
    CF_Mode = commonmodes_Final(1,2); %Mode type

    Max_AR=Max_AR_Table (CF_Node,CF_Mode) ;
    Max_Amp_Mode = Max_AR * Max_Amplitude(1);
%      Amp_Max(n);
    xlswrite([data_directory data_folder '\' 'Mode_Results_' filename
'.xlsx'], Max_Amp_Mode, 1 , 'B11');
    xlswrite([data_directory data_folder '\' 'Mode_Results_' filename
'.xlsx'], {'Max Amplitude for Mode (P/Pchamber, %)'}, 1 , 'A11');
end
```

Test Case Generation Code

```
%Create plots and data for different test cases
syms nu z
% clear all
% close all
% clc
z=0:.01:10;
for nu = 0:6
b(nu+1,:)= besselj (nu,z);
x(nu+1,:)=-besselj(nu+1,z)+nu./z.*besselj(nu,z); %Bessel function first
derivative
bk(nu+1,:) = bessely(nu,z);
end
nu =0;
f=@(z)-besselj(nu+1,z)+nu./z.*besselj(nu,z);
k01 = fzero(f,4);
k02 = fzero(f,7);
k03 = fzero(f,10);
nu=1;
f=@(z)-besselj(nu+1,z)+nu./z.*besselj(nu,z);
k10 = fzero(f,1.5);
k11 = fzero(f,5);
k12 = fzero(f,7);
nu=2;
f=@(z)-besselj(nu+1,z)+nu./z.*besselj(nu,z);
k20 = fzero(f,3);
k21 = fzero(f,6);
k22 = fzero(f,9);
nu=3;
f=@(z)-besselj(nu+1,z)+nu./z.*besselj(nu,z);
k30 = fzero(f,3);
```

```
k31 = fzero(f,7);
nu=4;
f=@(z)-besselj(nu+1,z)+nu./z.*besselj(nu,z);
k40 = fzero(f,4);
k41 = fzero(f,8);
nu=5;
f=@(z)-besselj(nu+1,z)+nu./z.*besselj(nu,z);
k50 = fzero(f,5);
nu=6;
f=@(z)-besselj(nu+1,z)+nu./z.*besselj(nu,z);
k60 = fzero(f,6);
K(1)= k10;
K(2)= k20;
K(3)= k30;
K(4)= k40;
K(5)= k50;
K(6)= k60;
K(7)= k01;
K(8)= k02;
K(9)= k03;
K(10)= k11;
K(11)= k21;
K(12)= k31;
K(13)= k41;
K(14)= k12;
K(15)= k22;
%Enter the mode number and the graph and y1,y2,y3 pressure data is
generated
fignum = 6;
%  for n = 1:15
if n <=6
    mode = n;
elseif n  >=7 && n <= 9
    mode = 0;
elseif n == 10 || n == 14
        mode = 1;
elseif n == 11 || n == 15
    mode = 2;
elseif n == 12
    mode = 3;
elseif n == 13
mode = 4;
end
%f = frequency
switch n
    case 1
        Mode_Name = '1-T Mode';
        f = 3250;
    case 2
        Mode_Name  = '2-T Mode';
        f = 3250;
    case 3
        Mode_Name  = '3-T Mode';
        f = 3250;
    case 4
        Mode_Name  = '4-T Mode';
        f = 3500;
```

```
    case 5
        Mode_Name  = '5-T Mode';
        f = 4500;
    case 6
        Mode_Name  = '6-T Mode';
        f = 5500;
    case 7
        Mode_Name  = '1-R';
        f = 2500;
    case 8
        Mode_Name  = '2-R';
        f = 5000;
    case 9
        Mode_Name  = '3-R';
        f = 7000;
    case 10
        Mode_Name  = '1-R,1-T Mode';
        f = 3500;
    case 11
        Mode_Name  = '1-R,2-T Mode';
        f = 4500;
    case 12
        Mode_Name  = '1-R,3-T Mode';
        f = 5500;
    case 13
        Mode_Name  = '1-R,4-T Mode';
        f = 6000;
    case 14
        Mode_Name  = '2-R,1-T Mode';
        f = 5500;
    case 15
        Mode_Name  = '2-R,2-T Mode';
        f = 6500;
    otherwise
        Mode_Name  = {'No Match'};
end
t=0:1/60000:.010;           %For 20 cycles at 2000 hz
t= t' ;
r_chamber = 0.10555 ;       %Radius of the chamber
A = 1 ;                    %Amplitude
r_count = 1;
for r = 0:.001:r_chamber
    for phase = 1:361   %rotate the pressure transducers 360 degrees
around the chamber
        Theta(r_count,phase) = (0 + phase-1)/360*2*pi;
        Radius(r_count, phase) = r;
        jmn = besselj(mode, (K(n)/r_chamber*r));
        y(:,phase)=1/2*A*jmn*cos(-f*2*pi*t- mode*Theta(r_count,phase)
)+1/2*A*jmn*cos(f*2*pi*t-mode*Theta(r_count,phase));

    %Find Max, Min
    max1(r_count,phase) = max (y(:,phase));
    min1(r_count,phase) = min (y(:,phase));
    end
r_count = r_count+1;
end
%Find Amp
```

```
amp = (max1-min1)/(14.7*2);
figure (fignum)
plot (1:361, amp)
fignum = fignum +1;
figure (fignum)
fignum = fignum +1;
[X,Y,Z] = pol2cart(Theta,Radius,amp);
[Xcyl,Ycyl,Zcyl] = cylinder(r_chamber);
Zcyl = Zcyl * max(max(amp));
surf(Xcyl,Ycyl,Zcyl,'facecolor', 'w', 'FaceAlpha', .1);
 hold on
surf (X,Y,Z, 'EdgeColor','white','LineStyle', 'none')
colormap jet
colorbar ('location', 'EastOutside')
xlabel('Distance (meters)')
ylabel('Distance (meters)')
zlabel('Pressure (nondimensionalized)')
% axis([ -.15 .15 -.15 .15 -inf inf])
title(sprintf('Pressure Distribution within a Cylinder for a %s',
Mode_Name))
% saveas (figure (7),['C:\Users\Joel\Desktop\Acoustics\Mode Plots' '\'
Mode_Name '.jpg'])
R_Chamber_Amp = amp(106,:);
if n <7 || n>9
[rowmin colmin ] =ind2sub (size(R_Chamber_Amp),find (R_Chamber_Amp ==
min(R_Chamber_Amp)));
[rowmax colmax ] =ind2sub (size(R_Chamber_Amp),find (R_Chamber_Amp ==
max(R_Chamber_Amp)));
elseif n >=7 && n <= 9
    colmin = 1;
    colmax = 1;
end
%%
%the variable "col" represents the angular location of the first node
line
%Node angle offset from pressure transducer
offset = -10;
Node_Loc = colmin-1;
P1_Loc = (colmin-1) + offset;
P2_Loc = P1_Loc + 90;
if P2_Loc > 360
    P2_Loc = P2_Loc -360;
end
P3_Loc = P1_Loc + 225;
if P3_Loc > 360
    P3_Loc = P3_Loc -360;
end
%Transducer locations in radians.
P1_Loc_Rads = P1_Loc /360*2*pi;
P2_Loc_Rads = P2_Loc /360*2*pi;
P3_Loc_Rads = P3_Loc /360*2*pi;
% %Test Data
t=0:1/60000:(1-1/60000);
y1=1/2*jmn*cos(-f*2*pi*t- mode*P1_Loc_Rads) + 1/2*jmn*cos(f*2*pi*t-
mode*P1_Loc_Rads);
y2=1/2*jmn*cos(-f*2*pi*t- mode*P2_Loc_Rads) + 1/2*jmn*cos(f*2*pi*t-
mode*P2_Loc_Rads);
```

```
y3=1/2*jmn*cos(-f*2*pi*t- mode*P3_Loc_Rads) + 1/2*jmn*cos(f*2*pi*t-
mode*P3_Loc_Rads);
y4 = .0001 *cos (2*pi*2000*t);
Pressures = [y1', y2', y3', y4'] ;
% %Find the Amplitudes Ratios between any point and the max value
(peak)
colmax = colmax(1);
% %start colmin as Loc = 0
Amp_Max(n) = R_Chamber_Amp (colmax);
Adjusted_Loc = 1;
for Loc = colmin:colmin + 360;
    if Loc >361
        Loc = Loc -360;
    end
Amp_Loc = R_Chamber_Amp(Loc);
AR_Max(Adjusted_Loc,n) = Amp_Max(n)/Amp_Loc;
Adjusted_Loc = Adjusted_Loc +1;
end
verify(n) = R_Chamber_Amp(81) *AR_Max(11,n)
end
```

APPENDIX E

Acoustic mode analysis results for test data

Table E.1 Acoustic Mode Analysis Results for Byrd SP1.

Pressure Transducer	P1	P2	P3	P4	Node Angle	Matches Freq, AR and Phase
Skewness	0.226925	0.021380	-0.014182	-0.022838	-1	No Matches
Kurtosis	4.711748	2.970155	2.377889	2.921212		
Standard Deviation (P/Pchamber)	0.001788	0.003530	0.001936	0.003518		
Average Pressure (P/Pchamber)	-0.017847	0.002046	0.000297	0.003759		
Max Amplitude from FFT (P/Pchamber)	0.000243	0.000351	0.000357	0.000482		
Dominant Frequency from FFT(Hz)	2205.5	2205.5	2205.5	2205.5		
	P1/P2	P2/P3	P1/P3			
Amp Ratios from FFT	0.6922	0.9819	0.6797			
Phase Diff (degrees)	103.3818	98.3590	5.0227			

Table E.2 Acoustic Mode Analysis Results for Byrd SP2.

Pressure Transducer	P1	P2	P3	P4	Node Angle	Matches Freq, AR and Phase
Skewness	0.146943	0.038273	0.014052	-0.04018	70	2-T Mode
Kurtosis	4.490324	2.747182	2.120487	2.683479	71	2-T Mode
Standard Deviation (P/Pchamber)	0.001867	0.003793	0.002553	0.004212	72	2-T Mode
Average Pressure (P/Pchamber)	-0.01792	0.002085	0.00039	0.003774	73	2-T Mode
Max Amplitude from FFT (P/Pchamber)	0.000248	0.000257	0.00034	0.000441	74	2-T Mode
Dominant Frequency from FFT(Hz)	2194.5	2194.5	2194.5	2194.5	160	2-T Mode
	P1/P2	P2/P3	P1/P3		161	2-T Mode
Amp Ratios from FFT	0.962986	0.756382	0.728385		162	2-T Mode
Phase Diff (degrees)	140.9318	163.2821	22.3503		163	2-T Mode
Max Amplitude for Mode (P/Pchamber)	0.000386				164	2-T Mode
					250	2-T Mode
					251	2-T Mode
					252	2-T Mode
					253	2-T Mode
					254	2-T Mode
					340	2-T Mode
					341	2-T Mode
					342	2-T Mode
					343	2-T Mode
					344	2-T Mode

Table E.3 Acoustic Mode Analysis Results for Byrd SP3.

Pressure Transducer	P1	P2	P3	P4	Node Angle	Matches Freq, AR and Phase
Skewness	0.077398	0.044741	0.012043	-0.02087	-1	No Matches
Kurtosis	3.177847	2.704503	1.920527	2.544652		
Standard Deviation (P/Pchamber)	0.002473	0.008858	0.004168	0.00761		
Average Pressure (P/Pchamber)	-0.01796	0.002052	0.000274	0.003755		
Max Amplitude from FFT (P/Pchamber)	0.000259	0.00104	0.000679	0.000848		
Dominant Frequency from FFT(Hz)	1743.5	1743.5	1743.5	2167		
	P1/P2	P2/P3	P1/P3			
Amp Ratios from FFT	0.248809	1.530193	0.380725			
Phase Diff (degrees)	77.7233	153.0076	75.2842			

Table E.4 Acoustic Mode Analysis Results for Byrd SP4.

Pressure Transducer	P1	P2	P3	P4	Node Angle	Matches Freq, AR and Phase
Skewness	0.125906	0.056317	0.069131	0.03534	-1	No Matches
Kurtosis	2.770932	2.1561	1.836021	2.363734		
Standard Deviation (P/Pchamber)	0.003353	0.016119	0.006554	0.009841		
Average Pressure (P/Pchamber)	-0.01794	0.001879	0.001711	0.003849		
Max Amplitude from FFT (P/Pchamber)	0.000474	0.003113	0.001359	0.001548		
Dominant Frequency from FFT(Hz)	2145	2145	2145	2145		
	P1/P2	P2/P3	P1/P3			
Amp Ratios from FFT	0.152182	2.290385	0.348556			
Phase Diff (degrees)	97.3392	248.8448	151.5056			

Table E.5 Acoustic Mode Analysis Results for Byrd SP5.

Pressure Transducer	P1	P2	P3	P4	Node Angle	Matches Freq, AR and Phase
Skewness	-0.02547	0.14083	0.114211	0.126165	-1	No Matches
Kurtosis	3.403973	2.291101	2.57347	2.437867		
Standard Deviation (P/Pchamber)	0.003505	0.023559	0.004473	0.014957		
Average Pressure (P/Pchamber)	-0.02297	0.001848	1.93E-05	0.003656		
Max Amplitude from FFT (P/Pchamber)	0.000252	0.002599	0.000426	0.002061		
Dominant Frequency from FFT(Hz)	1739.375	1739.375	1739.375	1739.375		
	P1/P2	P2/P3	P1/P3			
Amp Ratios from FFT	0.097035	6.099241	0.591838			
Phase Diff (degrees)	27.07544	129.2149	156.2903			

Table E.6 Acoustic Mode Analysis Results for Byrd SP6.

Pressure Transducer	P1	P2	P3	P4	Node Angle	Matches Freq, AR and Phase
Skewness	0.18899	0.102078	0.156274	0.17718	-1	No Matches
Kurtosis	3.10653	2.171438	2.046959	2.455386		
Standard Deviation (P/Pchamber)	0.004764	0.027812	0.007804	0.018608		
Average Pressure (P/Pchamber)	-0.0229	0.002009	0.000555	0.003777		
Max Amplitude from FFT (P/Pchamber)	0.000434	0.003229	0.000962	0.002172		
Dominant Frequency from FFT(Hz)	2139.5	2139.5	2139.5	1749		
	P1/P2	P2/P3	P1/P3			
Amp Ratios from FFT	0.134255	3.356971	0.450689			
Phase Diff (degrees)	0.626681	162.0985	162.7252			

Table E.7 Acoustic Mode Analysis Results for Byrd SP7.

Pressure Transducer	P1	P2	P3	P4	Node Angle	Matches Freq, AR and Phase
Skewness	-0.2181	0.195838	0.193778	0.236314	-1	No Matches
Kurtosis	2.546617	2.291784	2.190444	2.269388		
Standard Deviation (P/Pchamber)	0.005401	0.026507	0.006984	0.023218		
Average Pressure (P/Pchamber)	-0.02194	0.002112	0.00212	0.003771		
Max Amplitude from FFT (P/Pchamber)	0.000998	0.003582	0.001139	0.004194		
Dominant Frequency from FFT(Hz)	2123	2123	2123	2398		
	P1/P2	P2/P3	P1/P3			
Amp Ratios from FFT	0.278621	3.144731	0.876189			
Phase Diff (degrees)	52.65868	77.31691	24.65824			

Table E.8 Acoustic Mode Analysis Results for Byrd SP8.

Pressure Transducer	P1	P2	P3	P4	Node Angle	Matches Freq, AR and Phase
Skewness	-0.22195	0.220017	0.282511	0.255621	-1	No Matches
Kurtosis	3.669973	2.133171	2.352686	2.390138		
Standard Deviation (P/Pchamber)	0.004595	0.032923	0.00722	0.021536		
Average Pressure (P/Pchamber)	-0.02295	0.001739	-0.0034	0.003905		
Max Amplitude from FFT (P/Pchamber)	0.000322	0.005452	0.00108	0.001734		
Dominant Frequency from FFT(Hz)	2117.5	2117.5	2117.5	1771		
	P1/P2	P2/P3	P1/P3			
Amp Ratios from FFT	0.059041	5.048162	0.298048			
Phase Diff (degrees)	40.10662	140.5994	100.4928			

Table E.9 Acoustic Mode Analysis Results for Byrd SP9.

Pressure Transducer	P1	P2	P3	P4	Node Angle	Matches Freq, AR and Phase
Skewness	-0.17197	0.278889	0.336174	0.450192	-1	No Matches
Kurtosis	2.364052	2.402961	2.681071	2.977533		
Standard Deviation (P/Pchamber)	0.00573	0.027121	0.007136	0.022834		
Average Pressure (P/Pchamber)	-0.02445	0.001728	0.002633	0.004102		
Max Amplitude from FFT (P/Pchamber)	0.000627	0.003591	0.00083	0.002362		
Dominant Frequency from FFT(Hz)	2970	2970	2970	2970		
	P1/P2	P2/P3	P1/P3			
Amp Ratios from FFT	0.174682	4.327471	0.75593			
Phase Diff (degrees)	145.1269	215.81	70.68303			

Table E.10 Acoustic Mode Analysis Results for Byrd SP10.

Pressure Transducer	P1	P2	P3	P4	Node Angle	Matches Freq, AR and Phase
Skewness	-0.14479	0.299178	0.316777	0.098114	-1	No Matches
Kurtosis	2.307369	2.116257	2.429079	1.996805		
Standard Deviation (P/Pchamber)	0.00423	0.032933	0.006836	0.015533		
Average Pressure (P/Pchamber)	-0.01617	0.00225	-0.00145	0.003799		
Max Amplitude from FFT (P/Pchamber)	0.000342	0.002661	0.000541	0.001219		
Dominant Frequency from FFT(Hz)	2101	2101	2101	3030.5		
	P1/P2	P2/P3	P1/P3			
Amp Ratios from FFT	0.128713	4.921068	0.633408			
Phase Diff (degrees)	1.545357	167.7579	166.2126			

Table E.11 Acoustic Mode Analysis Results for Byrd SP11.

Pressure Transducer	P1	P2	P3	P4	Node Angle	Matches Freq, AR and Phase
Skewness	-0.04566	0.423211	0.540709	0.580258	-1	No Matches
Kurtosis	2.249504	2.416151	2.485732	3.465497		
Standard Deviation (P/Pchamber)	0.007908	0.032703	0.014142	0.026719		
Average Pressure (P/Pchamber)	-0.02193	-0.00184	-0.00329	0.003011		
Max Amplitude from FFT (P/Pchamber)	0.000608	0.003858	0.001291	0.002341		
Dominant Frequency from FFT(Hz)	3063.5	3063.5	3063.5	2447.5		
	P1/P2	P2/P3	P1/P3			
Amp Ratios from FFT	0.157513	2.98799	0.470646			
Phase Diff (degrees)	20.15169	28.65397	8.502279			

Table E.12 Acoustic Mode Analysis Results for Byrd SP12.

Pressure Transducer	P1	P2	P3	P4	Node Angle	Matches Freq, AR and Phase
Skewness	-0.20701	0.576231	0.68758	0.32916	-1	No Matches
Kurtosis	2.771374	3.483654	4.497613	3.174871		
Standard Deviation (P/Pchamber)	0.007802	0.028869	0.015709	0.029252		
Average Pressure (P/Pchamber)	-0.02057	0.003605	0.006108	0.005455		
Max Amplitude from FFT (P/Pchamber)	0.000591	0.001433	0.00088	0.002032		
Dominant Frequency from FFT(Hz)	3095.714	3095.714	3095.714	2506.429		
	P1/P2	P2/P3	P1/P3			
Amp Ratios from FFT	0.412561	1.628507	0.671859			
Phase Diff (degrees)	39.23504	19.18525	20.04979			

Table E.13 Acoustic Mode Analysis Results for Byrd SP13.

Pressure Transducer	P1	P2	P3	P4	Node Angle	Matches Freq, AR and Phase
Skewness	0.044016	0.556847	0.62866	0.000834	174	1-T Mode
Kurtosis	2.417216	3.114589	2.460785	2.676316	175	1-T Mode
Standard Deviation (P/Pchamber)	0.005847	0.027726	0.016969	0.011686	176	1-T Mode
Average Pressure (P/Pchamber)	-0.02054	0.000664	-3.1E-05	0.004441	177	1-T Mode
Max Amplitude from FFT (P/Pchamber)	0.000599	0.003547	0.001918	0.000897	354	1-T Mode
Dominant Frequency from FFT(Hz)	3069	3069	3069	2189	355	1-T Mode
	P1/P2	P2/P3	P1/P3		356	1-T Mode
Amp Ratios from FFT	0.168906	1.849183	0.312339		357	1-T Mode
Phase Diff (degrees)	53.15789	176.9125	123.7546		174	1-R/1-T Mode
Max Amplitude for Mode (P/Pchamber)	0.005731				175	1-R/1-T Mode
					176	1-R/1-T Mode
					177	1-R/1-T Mode
					354	1-R/1-T Mode
					355	1-R/1-T Mode
					356	1-R/1-T Mode
					357	1-R/1-T Mode

Table E.14 Acoustic Mode Analysis Results for SP11- 9/13/2011.

Pressure Transducer	P1	P2	P3	P4	Radial Mode Matches
Skewness	-0.00327	-0.01705	-0.01361	-0.06187	1-R Mode
Kurtosis	2.711198	2.683581	2.65964	1.854957	
Standard Deviation (P/Pchamber)	0.001676	0.00191	0.001799	0.00135	
Average Pressure (P/Pchamber)	0.000656	0.002105	-0.00668	-0.00023	
Max Amplitude from FFT (P/Pchamber)	0.000745	0.000714	0.000683	0.000165	
Dominant Frequency from FFT(Hz)	2235	2235	2235	2235	
	P1/P2	P2/P3	P1/P3		
Amp Ratios from FFT	1.043495	1.04634	1.09185		
Phase Diff (degrees)	0.066773	9.727849	9.794622		
Max Amplitude for Mode (P/Pchamber)	0.000745				

Table E.15 Acoustic Mode Analysis Results for SP11- 9/14/2011.

Pressure Transducer	P1	P2	P3	P4	Node Angle	Matches Freq, AR and Phase
Skewness	-0.02145	-0.02764	-0.02477	-0.01129	-1	No Matches
Kurtosis	2.322423	2.599907	2.53486	3.106473		
Standard Deviation (P/Pchamber)	0.00133	0.0014	0.001184	0.004362		
Average Pressure (P/Pchamber)	0.000852	0.002176	-0.00659	0.001606		
Max Amplitude from FFT (P/Pchamber)	0.000215	0.000294	0.00025	0.001384		
Dominant Frequency from FFT(Hz)	2559	2559	2559	2559		
	P1/P2	P2/P3	P1/P3			
Amp Ratios from FFT	0.732323	1.173252	0.859199			
Phase Diff (degrees)	7.924322	7.380783	15.3051			

Table E.16 Acoustic Mode Analysis Results for SP11- 9/19/2011.

Pressure Transducer	P1	P2	P3	P4	Node Angle	Matches Freq, AR and Phase
Skewness	-0.00411	-0.00306	-0.00955	-0.01294	62	2-T Mode
Kurtosis	2.885827	2.821604	2.945855	2.930195	63	2-T Mode
Standard Deviation (P/Pchamber)	0.002383	0.00185	0.002089	0.013488	64	2-T Mode
Average Pressure (P/Pchamber)	0.000469	0.00212	-0.00675	-0.00124	65	2-T Mode
Max Amplitude from FFT (P/Pchamber)	0.000739	0.000502	0.000449	0.004308	152	2-T Mode
Dominant Frequency from FFT(Hz)	2302	2302	2302	2302	153	2-T Mode
	P1/P2	P2/P3	P1/P3		154	2-T Mode
Amp Ratios from FFT	1.470756	1.118019	1.644333		155	2-T Mode
Phase Diff (degrees)	191.3776	161.5279	29.84972		242	2-T Mode
Max Amplitude for Mode (P/Pchamber)	0.000891				243	2-T Mode
					244	2-T Mode
					245	2-T Mode
					332	2-T Mode
					333	2-T Mode
					334	2-T Mode
					335	2-T Mode

Table E.17 Acoustic Mode Analysis Results for SP11- 9/21/2011.

Pressure Transducer	P1	P2	P3	P4	Node Angle	Matches Freq, AR and Phase
Skewness	-0.01154	-0.0232	-0.01473	0.006901	-1	No Matches
Kurtosis	2.820864	3.006037	2.86598	3.112047		
Standard Deviation (P/Pchamber)	0.002082	0.002071	0.00165	0.014059		
Average Pressure (P/Pchamber)	0.000657	0.002176	-0.00666	-0.00031		
Max Amplitude from FFT (P/Pchamber)	0.000509	0.000541	0.000436	0.004967		
Dominant Frequency from FFT(Hz)	2978	2978	2978	2361		
	P1/P2	P2/P3	P1/P3			
Amp Ratios from FFT	0.939745	1.240999	1.166222			
Phase Diff (degrees)	97.39215	98.23435	195.6265			

Table E.18 Acoustic Mode Analysis Results for SP12- 9/13/2011.

Pressure Transducer	P1	P2	P3	P4	Radial Mode Matches
Skewness	7.84E-05	-0.02501	-0.01428	-0.0602	1-R Mode
Kurtosis	2.819329	2.627759	2.590949	1.857858	
Standard Deviation (P/Pchamber)	0.001412	0.001712	0.001605	0.001353	
Average Pressure (P/Pchamber)	0.000652	0.002103	-0.00667	-0.00015	
Max Amplitude from FFT (P/Pchamber)	0.000617	0.000593	0.000553	0.000157	
Dominant Frequency from FFT(Hz)	2264	2264	2264	2264	
	P1/P2	P2/P3	P1/P3		
Amp Ratios from FFT	1.040738	1.071678	1.115337		
Phase Diff (degrees)	4.333657	6.989363	11.32302		
Max Amplitude for Mode (P/Pchamber)	0.000617				

Table E.19 Acoustic Mode Analysis Results for SP12- 9/14/2011.

Pressure Transducer	P1	P2	P3	P4	Radial Mode Matches
Skewness	-0.00527	-0.01221	-0.01463	-0.00248	1-R Mode
Kurtosis	2.746732	2.788109	2.760628	2.789547	
Standard Deviation (P/Pchamber)	0.002154	0.002062	0.001882	0.009224	
Average Pressure (P/Pchamber)	0.000658	0.002101	-0.00668	0.000759	
Max Amplitude from FFT (P/Pchamber)	0.000914	0.000892	0.000812	0.004597	
Dominant Frequency from FFT(Hz)	2255	2255	2255	2255	
	P1/P2	P2/P3	P1/P3		
Amp Ratios from FFT	1.024743	1.0987	1.125885		
Phase Diff (degrees)	5.687134	4.252639	9.939772		
Max Amplitude for Mode (P/Pchamber)	0.000914				

Table E.20 Acoustic Mode Analysis Results for SP12- 9/19/2011.

Pressure Transducer	P1	P2	P3	P4	Node Angle	Matches Freq, AR and Phase
Skewness	-0.00507	-0.02206	-0.00211	-0.01601	-1	No Matches
Kurtosis	2.885767	2.779362	2.987786	3.054228		
Standard Deviation (P/Pchamber)	0.002175	0.001792	0.0022	0.012408		
Average Pressure (P/Pchamber)	0.000456	0.002127	-0.00674	-0.00533		
Max Amplitude from FFT (P/Pchamber)	0.000524	0.000263	0.000486	0.003237		
Dominant Frequency from FFT(Hz)	2348	2348	2348	2348		
	P1/P2	P2/P3	P1/P3			
Amp Ratios from FFT	1.989684	0.542223	1.078853			
Phase Diff (degrees)	148.3681	164.0136	15.64555			

Table E.21 Acoustic Mode Analysis Results for SP12- 9/21/2011.

Pressure Transducer	P1	P2	P3	P4	Node Angle	Matches Freq, AR and Phase
Skewness	-0.0053	-0.00601	-0.0173	0.009612	-1	No Matches
Kurtosis	2.807893	2.904931	2.75288	2.904738		
Standard Deviation (P/Pchamber)	0.002195	0.002064	0.001672	0.014782		
Average Pressure (P/Pchamber)	0.000376	0.00186	-0.00675	-0.01702		
Max Amplitude from FFT (P/Pchamber)	0.000536	0.000478	0.000403	0.005041		
Dominant Frequency from FFT(Hz)	2374	2374	2374	2374		
	P1/P2	P2/P3	P1/P3			
Amp Ratios from FFT	1.120391	1.186184	1.328991			
Phase Diff (degrees)	33.65208	23.92628	9.725801			

Table E.22 Acoustic Mode Analysis Results for SP19- 9/14/2011.

Pressure Transducer	P1	P2	P3	P4	Radial Mode Matches
Skewness	-0.007	-0.0073	-0.00801	-0.00757	1-R Mode
Kurtosis	2.871032	2.916336	2.895854	2.97163	
Standard Deviation (P/Pchamber)	0.002676	0.002526	0.002331	0.011414	
Average Pressure (P/Pchamber)	0.000662	0.002097	-0.00665	-7.1E-05	
Max Amplitude from FFT (P/Pchamber)	0.000949	0.000848	0.000809	0.004161	
Dominant Frequency from FFT(Hz)	2249	2249	2249	2247	
	P1/P2	P2/P3	P1/P3		
Amp Ratios from FFT	1.119195	1.048828	1.173844		
Phase Diff (degrees)	5.72094	4.533788	10.25473		
Max Amplitude for Mode (P/Pchamber)	0.000949				

Table E.23 Acoustic Mode Analysis Results for SP19- 9/19/2011.

Pressure Transducer	P1	P2	P3	P4	Node Angle	Matches Freq, AR and Phase
Skewness	0.003383	-0.00111	-0.00517	0.020076	67	2-T Mode
Kurtosis	2.987335	2.936619	2.981313	3.012143	68	2-T Mode
Standard Deviation (P/Pchamber)	0.002997	0.00232	0.003082	0.017056	69	2-T Mode
Average Pressure (P/Pchamber)	0.000504	0.002323	-0.00656	0.00593	157	2-T Mode
Max Amplitude from FFT (P/Pchamber)	0.000911	0.000756	0.000835	0.00479	158	2-T Mode
Dominant Frequency from FFT(Hz)	2368	2368	2368	2368	159	2-T Mode
	P1/P2	P2/P3	P1/P3		247	2-T Mode
Amp Ratios from FFT	1.204593	0.905045	1.09021		248	2-T Mode
Phase Diff (degrees)	197.1376	177.5767	19.56081		249	2-T Mode
Max Amplitude for Mode (P/Pchamber)	0.001266				337	2-T Mode
					338	2-T Mode
					339	2-T Mode

Table E.24 Acoustic Mode Analysis Results for SP19- 9/21/2011.

Pressure Transducer	P1	P2	P3	P4	Node Angle	Matches Freq, AR and Phase
Skewness	-0.00709	-0.01061	0.012986	-0.02125	-1	No Matches
Kurtosis	2.88053	2.989985	2.939913	3.003562		
Standard Deviation (P/Pchamber)	0.002339	0.002066	0.001925	0.017124		
Average Pressure (P/Pchamber)	0.000246	0.00181	-0.00683	-0.02384		
Max Amplitude from FFT (P/Pchamber)	0.000534	0.000414	0.000562	0.005319		
Dominant Frequency from FFT(Hz)	1738	1738	1738	2398		
	P1/P2	P2/P3	P1/P3			
Amp Ratios from FFT	1.289955	0.737329	0.951122			
Phase Diff (degrees)	184.6321	9.72799	174.9041			

Table E.25 Acoustic Mode Analysis Results for SP20- 9/14/2011.

Pressure Transducer	P1	P2	P3	P4	Radial Mode Matches
Skewness	-0.01337	-0.04272	-0.0217	0.01043	1-R Mode
Kurtosis	2.424747	2.563386	2.560292	3.006879	
Standard Deviation (P/Pchamber)	0.001386	0.001366	0.001212	0.004406	
Average Pressure (P/Pchamber)	0.000513	0.002084	-0.00674	-0.00146	
Max Amplitude from FFT (P/Pchamber)	0.000179	0.000175	0.00019	0.000976	
Dominant Frequency from FFT(Hz)	2569	2569	2569	2569	
	P1/P2	P2/P3	P1/P3		
Amp Ratios from FFT	1.0214	0.921445	0.941163		
Phase Diff (degrees)	1.558631	10.72084	9.162212		
Max Amplitude for Mode (P/Pchamber)	0.000179				

Table E.26 Acoustic Mode Analysis Results for SP20- 9/21/2011.

Pressure Transducer	P1	P2	P3	P4	Node Angle	Matches Freq, AR and Phase
Skewness	0.007839	-0.00486	0.006245	-0.02279	-1	No Matches
Kurtosis	2.834087	2.761184	3.023274	2.886242		
Standard Deviation (P/Pchamber)	0.00221	0.001764	0.002243	0.012913		
Average Pressure (P/Pchamber)	0.000466	0.002223	-0.00667	0.001033		
Max Amplitude from FFT (P/Pchamber)	0.000478	0.000316	0.000471	0.003094		
Dominant Frequency from FFT(Hz)	2378	2378	2378	2378		
	P1/P2	P2/P3	P1/P3			
Amp Ratios from FFT	1.51554	0.669683	1.014931			
Phase Diff (degrees)	136.3522	139.098	2.745778			

Table E.27 Acoustic Mode Analysis Results for SP20- 9/21/2011.

Pressure Transducer	P1	P2	P3	P4	Node Angle	Matches Freq, AR and Phase
Skewness	-0.00555	-0.00653	-0.00204	0.015593	-1	No Matches
Kurtosis	2.759621	3.003044	2.801218	2.922546		
Standard Deviation (P/Pchamber)	0.002035	0.001971	0.001609	0.013572		
Average Pressure (P/Pchamber)	0.000843	0.002292	-0.00661	0.009637		
Max Amplitude from FFT (P/Pchamber)	0.000403	0.000503	0.000534	0.003418		
Dominant Frequency from FFT(Hz)	1749	1749	1749	2394		
	P1/P2	P2/P3	P1/P3			
Amp Ratios from FFT	0.801213	0.941708	0.754509			
Phase Diff (degrees)	172.408	12.35958	184.7676			

Table E.28 Acoustic Mode Analysis Results for SP22- 9/13/2011.

Pressure Transducer	P1	P2	P3	P4	Radial Mode Matches
Skewness	-0.00185	-0.03202	-0.01897	-0.0628	1-R Mode
Kurtosis	2.917014	2.633656	2.586137	1.944493	
Standard Deviation (P/Pchamber)	0.001311	0.001687	0.001552	0.001378	
Average Pressure (P/Pchamber)	0.000625	0.002109	-0.00669	-0.00021	
Max Amplitude from FFT (P/Pchamber)	0.000415	0.000443	0.000407	0.000176	
Dominant Frequency from FFT(Hz)	2261	2261	2261	2261	
	P1/P2	P2/P3	P1/P3		
Amp Ratios from FFT	0.936895	1.089658	1.020895		
Phase Diff (degrees)	5.374112	7.143138	12.51725		
Max Amplitude for Mode (P/Pchamber)	0.000415				

Table E.29 Acoustic Mode Analysis Results for SP22- 9/14/2011.

Pressure Transducer	P1	P2	P3	P4	Radial Mode Matches
Skewness	-0.00645	-0.01451	-0.01531	-0.00272	1-R Mode
Kurtosis	2.743424	2.82288	2.784137	3.114314	
Standard Deviation (P/Pchamber)	0.00174	0.001705	0.00154	0.004691	
Average Pressure (P/Pchamber)	-0.00018	0.001977	-0.00696	-0.00593	
Max Amplitude from FFT (P/Pchamber)	0.000424	0.000427	0.000416	0.001272	
Dominant Frequency from FFT(Hz)	2406	2406	2406	2406	
	P1/P2	P2/P3	P1/P3		
Amp Ratios from FFT	0.993928	1.024686	1.018464		
Phase Diff (degrees)	0.187793	9.246438	9.058645		
Max Amplitude for Mode (P/Pchamber)	0.000424				

Table E.30 Acoustic Mode Analysis Results for SP22- 9/19/2011.

Pressure Transducer	P1	P2	P3	P4	Node Angle	Matches Freq, AR and Phase
Skewness	-0.00337	-0.00828	0.010905	0.006912	-1	No Matches
Kurtosis	2.807611	2.832218	2.890852	2.941295		
Standard Deviation (P/Pchamber)	0.002295	0.001854	0.002284	0.013292		
Average Pressure (P/Pchamber)	0.000597	0.002142	-0.00669	-0.0009		
Max Amplitude from FFT (P/Pchamber)	0.000686	0.000372	0.000701	0.004201		
Dominant Frequency from FFT(Hz)	1694	1694	1694	2307		
	P1/P2	P2/P3	P1/P3			
Amp Ratios from FFT	1.841022	0.531648	0.978776			
Phase Diff (degrees)	167.8887	151.4311	16.45761			

Table E.31 Acoustic Mode Analysis Results for SP22- 9/22/2011.

Pressure Transducer	P1	P2	P3	P4	Node Angle	Matches Freq, AR and Phase
Skewness	-0.00306	-0.01543	0.013607	-0.00127	-1	No Matches
Kurtosis	2.831382	2.861397	2.955878	2.831058		
Standard Deviation (P/Pchamber)	0.002287	0.002099	0.001684	0.017345		
Average Pressure (P/Pchamber)	0.000556	0.002157	-0.0067	-0.00168		
Max Amplitude from FFT (P/Pchamber)	0.000716	0.000548	0.000358	0.007795		
Dominant Frequency from FFT(Hz)	2338	2338	2338	2338		
	P1/P2	P2/P3	P1/P3			
Amp Ratios from FFT	1.307404	1.531248	2.001959			
Phase Diff (degrees)	42.8618	49.97081	7.109003			

Table E.32 Acoustic Mode Analysis Results for SP27- 9/14/2011.

Pressure Transducer	P1	P2	P3	P4	Radial Mode Matches
Skewness	-0.01088	-0.02285	-0.01239	-0.00529	1-R Mode
Kurtosis	2.988312	2.921452	3.309343	3.294812	
Standard Deviation (P/Pchamber)	0.001638	0.001652	0.00155	0.00545	
Average Pressure (P/Pchamber)	0.000594	0.002072	-0.00671	-0.00151	
Max Amplitude from FFT (P/Pchamber)	0.000264	0.000272	0.000272	0.001289	
Dominant Frequency from FFT(Hz)	2455	2455	2455	2455	
	P1/P2	P2/P3	P1/P3		
Amp Ratios from FFT	0.971232	1.00159	0.972776		
Phase Diff (degrees)	2.912491	5.962252	3.049762		
Max Amplitude for Mode (P/Pchamber)	0.000264				

Table E.33 Acoustic Mode Analysis Results for SP27- 9/19/2011.

Pressure Transducer	P1	P2	P3	P4	Node Angle	Matches Freq, AR and Phase
Skewness	0.247874	0.103841	0.070411	0.088129	-1	No Matches
Kurtosis	3.139213	2.874687	2.918908	3.156482		
Standard Deviation (P/Pchamber)	0.002494	0.00194	0.00235	0.012727		
Average Pressure (P/Pchamber)	-0.00145	0.000824	-0.00795	-0.00639		
Max Amplitude from FFT (P/Pchamber)	0.00061	0.000267	0.000643	0.003775		
Dominant Frequency from FFT(Hz)	1721	1721	1721	2355		
	P1/P2	P2/P3	P1/P3			
Amp Ratios from FFT	2.285684	0.415138	0.948874			
Phase Diff (degrees)	195.4402	224.9253	29.48518			

Table E.34 Acoustic Mode Analysis Results for SP27- 9/21/2011.

Pressure Transducer	P1	P2	P3	P4	Node Angle	Matches Freq, AR and Phase
Skewness	-0.0053	-0.00281	-0.00349	-0.00967	-1	No Matches
Kurtosis	2.879198	2.8546	2.883128	3.019963		
Standard Deviation (P/Pchamber)	0.00214	0.002074	0.001655	0.015518		
Average Pressure (P/Pchamber)	0.000611	0.002178	-0.00667	-0.0019		
Max Amplitude from FFT (P/Pchamber)	0.00056	0.000621	0.000491	0.005827		
Dominant Frequency from FFT(Hz)	2981	2981	2981	2357		
	P1/P2	P2/P3	P1/P3			
Amp Ratios from FFT	0.90223	1.26453	1.140897			
Phase Diff (degrees)	179.9848	263.7517	83.76685			

Table E.35 Acoustic Mode Analysis Results for SP28- 9/14/2011.

Pressure Transducer	P1	P2	P3	P4	Radial Mode Matches
Skewness	-0.00629	-0.01092	-0.01026	-0.00223	1-R Mode
Kurtosis	3.005812	3.070168	3.02107	3.004225	
Standard Deviation (P/Pchamber)	0.002159	0.002086	0.001908	0.008577	
Average Pressure (P/Pchamber)	0.000583	0.002116	-0.00672	7.68E-05	
Max Amplitude from FFT (P/Pchamber)	0.000664	0.00065	0.000604	0.003134	
Dominant Frequency from FFT(Hz)	2290	2290	2290	2290	
	P1/P2	P2/P3	P1/P3		
Amp Ratios from FFT	1.022704	1.075614	1.100034		
Phase Diff (degrees)	8.274623	3.711686	11.98631		
Max Amplitude for Mode (P/Pchamber)	0.000664				

Table E.36 Acoustic Mode Analysis Results for SP28- 9/19/2011.

Pressure Transducer	P1	P2	P3	P4	Node Angle	Matches Freq, AR and Phase
Skewness	-0.01012	-0.0179	0.005832	-0.02227	70	2-T Mode
Kurtosis	2.871828	2.876206	3.035062	3.129341	71	2-T Mode
Standard Deviation (P/Pchamber)	0.002177	0.00185	0.002363	0.013236	72	2-T Mode
Average Pressure (P/Pchamber)	0.000661	0.002188	-0.00663	-0.00011	73	2-T Mode
Max Amplitude (P/Pchamber)	0.000432	0.000319	0.000588	0.00302	74	2-T Mode
Dominant Frequency FFT (Hz)	1730	1730	1730	2380	75	2-T Mode
	P1/P2	P2/P3	P1/P3		76	2-T Mode
Amp Ratios from FFT	1.354202	0.54227	0.734342		77	2-T Mode
Phase Diff (degrees)	193.0718	220.9821	27.91028		78	2-T Mode
Max Amplitude (P/Pchamber)	0.000672				79	2-T Mode
					160	2-T Mode
					161	2-T Mode
					162	2-T Mode
					163	2-T Mode
					164	2-T Mode
					165	2-T Mode
					166	2-T Mode
					167	2-T Mode
					168	2-T Mode
					169	2-T Mode
					250	2-T Mode
					251	2-T Mode
					252	2-T Mode
					253	2-T Mode
					254	2-T Mode
					255	2-T Mode
					256	2-T Mode
					257	2-T Mode
					258	2-T Mode
					259	2-T Mode
					340	2-T Mode
					341	2-T Mode
					342	2-T Mode
					343	2-T Mode
					344	2-T Mode
					345	2-T Mode
					346	2-T Mode
					347	2-T Mode
					348	2-T Mode
					349	2-T Mode

Table E.37 Acoustic Mode Analysis Results for SP28- 9/21/2011.

Pressure Transducer	P1	P2	P3	P4	Node Angle	Matches Freq, AR and Phase
Skewness	-0.00492	-0.00637	-0.00653	-0.00383	16	2-T Mode
Kurtosis	2.982359	2.92117	2.85785	3.232444	17	2-T Mode
Standard Deviation (P/Pchamber)	0.002182	0.001941	0.001908	0.015634	18	2-T Mode
Average Pressure (P/Pchamber)	0.000655	0.002106	-0.0067	-0.00186	19	2-T Mode
Max Amplitude from FFT (P/Pchamber)	0.000402	0.000389	0.000516	0.004143	20	2-T Mode
Dominant Frequency from FFT(Hz)	1728	1728	1728	2382	21	2-T Mode
	P1/P2	P2/P3	P1/P3		106	2-T Mode
Amp Ratios from FFT	1.033872	0.753138	0.778649		107	2-T Mode
Phase Diff (degrees)	176.6312	8.555222	185.1864		108	2-T Mode
Max Amplitude for Mode (P/Pchamber)	0.000758				109	2-T Mode
					110	2-T Mode
					111	2-T Mode
					196	2-T Mode
					197	2-T Mode
					198	2-T Mode
					199	2-T Mode
					200	2-T Mode
					201	2-T Mode
					286	2-T Mode
					287	2-T Mode
					288	2-T Mode
					289	2-T Mode
					290	2-T Mode
					291	2-T Mode

Table E.38 Acoustic Mode Analysis Results for SP30- 9/14/2011.

Pressure Transducer	P1	P2	P3	P4	Radial Mode Matches
Skewness	0.00148	-0.00956	-0.00238	0.002931	1-R Mode
Kurtosis	2.829887	2.887956	2.851513	2.860575	
Standard Deviation (P/Pchamber)	0.002164	0.002154	0.002	0.009878	
Average Pressure (P/Pchamber)	0.000289	0.001974	-0.00681	-0.00238	
Max Amplitude from FFT (P/Pchamber)	0.000795	0.000807	0.00077	0.004194	
Dominant Frequency from FFT(Hz)	2289	2289	2289	2289	
	P1/P2	P2/P3	P1/P3		
Amp Ratios from FFT	0.984581	1.048814	1.032642		
Phase Diff (degrees)	6.326669	3.991126	10.3178		
Max Amplitude for Mode (P/Pchamber)	0.000807				

Table E.39 Acoustic Mode Analysis Results for SP30- 9/19/2011.

Pressure Transducer	P1	P2	P3	P4	Angle	Matches	Angle	Matches
Skewness	-0.01072	-0.01112	0.003225	-0.01343	70	2-T Mode	256	2-T Mode
Kurtosis	2.808591	2.819122	2.980393	2.945447	71	2-T Mode	257	2-T Mode
Standard Deviation (P/Pchamber)	0.002092	0.001796	0.002233	0.012081	72	2-T Mode	258	2-T Mode
Average Pressure (P/Pchamber)	0.000646	0.002177	-0.00667	-0.00062	73	2-T Mode	259	2-T Mode
Max Amplitude FFT (P/Pchamber)	0.000413	0.000325	0.000598	0.002645	74	2-T Mode	260	2-T Mode
Dominant Frequency from FFT(Hz)	1726	1726	1726	2371	75	2-T Mode	340	2-T Mode
	P1/P2	P2/P3	P1/P3		76	2-T Mode	341	2-T Mode
Amp Ratios from FFT	1.2678	0.5445	0.6903		77	2-T Mode	342	2-T Mode
Phase Diff (degrees)	174.2074	143.1062	31.1012		78	2-T Mode	343	2-T Mode
Max Amplitude (P/Pchamber)	0.000642				79	2-T Mode	344	2-T Mode
					80	2-T Mode	345	2-T Mode
					160	2-T Mode	346	2-T Mode
					161	2-T Mode	347	2-T Mode
					162	2-T Mode	348	2-T Mode
					163	2-T Mode	349	2-T Mode
					164	2-T Mode	350	2-T Mode
					165	2-T Mode		
					166	2-T Mode		
					167	2-T Mode		
					168	2-T Mode		
					169	2-T Mode		
					170	2-T Mode		
					250	2-T Mode		
					251	2-T Mode		
					252	2-T Mode		
					253	2-T Mode		
					254	2-T Mode		
					255	2-T Mode		

Table E.40 Acoustic Mode Analysis Results for SP30- 9/21/2011.

Pressure Transducer	P1	P2	P3	P4	Radial Mode Matches
Skewness	-0.00045	-0.02407	-0.00404	0.016742	1-R Mode
Kurtosis	2.87851	2.861414	2.852787	2.914467	
Standard Deviation (P/Pchamber)	0.002187	0.001976	0.001614	0.014926	
Average Pressure (P/Pchamber)	0.000513	0.001957	-0.00672	-0.0114	
Max Amplitude from FFT (P/Pchamber)	0.000465	0.000433	0.000456	0.004372	
Dominant Frequency from FFT(Hz)	2374	2374	2374	2381	
	P1/P2	P2/P3	P1/P3		
Amp Ratios from FFT	1.074922	0.949528	1.020669		
Phase Diff (degrees)	37.37329	37.7591	0.385806		
Max Amplitude for Mode (P/Pchamber)	0.000465				

Table E.41 Acoustic Mode Analysis Results for SP31- 9/14/2011.

Pressure Transducer	P1	P2	P3	P4	Radial Mode Matches
Skewness	-0.01443	-0.02158	-0.016	-0.02314	1-R Mode
Kurtosis	2.620046	2.775481	2.742055	3.213255	
Standard Deviation (P/Pchamber)	0.001559	0.001695	0.001407	0.005376	
Average Pressure (P/Pchamber)	0.000667	0.002069	-0.00662	-0.00062	
Max Amplitude from FFT (P/Pchamber)	0.000272	0.000306	0.000265	0.001204	
Dominant Frequency from FFT(Hz)	2466	2466	2466	2498	
	P1/P2	P2/P3	P1/P3		
Amp Ratios from FFT	0.889422	1.152049	1.024658		
Phase Diff (degrees)	0.171946	12.55677	12.72872		
Max Amplitude for Mode (P/Pchamber)	0.000272				

Table E.42 Acoustic Mode Analysis Results for SP31- 9/19/2011.

Pressure Transducer	P1	P2	P3	P4	Node Angle	Matches Freq, AR and Phase
Skewness	-0.0082	-0.01819	-0.00625	-0.01613	-1	No Matches
Kurtosis	2.840082	2.842989	2.802032	2.970234		
Standard Deviation (P/Pchamber)	0.002284	0.001899	0.002193	0.013115		
Average Pressure (P/Pchamber)	0.000791	0.002173	-0.00664	0.000174		
Max Amplitude from FFT (P/Pchamber)	0.000547	0.00035	0.000558	0.003378		
Dominant Frequency from FFT(Hz)	1701	1701	1701	2343		
	P1/P2	P2/P3	P1/P3			
Amp Ratios from FFT	1.560124	0.627569	0.979086			
Phase Diff (degrees)	165.0306	144.3767	20.65389			

Table E.43 Acoustic Mode Analysis Results for SP31- 9/21/2011.

Pressure Transducer	P1	P2	P3	P4	Node Angle	Matches Freq, AR and Phase
Skewness	-0.01278	-0.00888	-0.01092	0.001209	-1	No Matches
Kurtosis	2.847767	2.85322	2.788045	2.943116		
Standard Deviation (P/Pchamber)	0.002154	0.002039	0.001605	0.015367		
Average Pressure (P/Pchamber)	0.000796	0.002306	-0.00662	0.005732		
Max Amplitude from FFT (P/Pchamber)	0.000514	0.00055	0.000392	0.005103		
Dominant Frequency from FFT(Hz)	3002	3002	3002	2373		
	P1/P2	P2/P3	P1/P3			
Amp Ratios from FFT	0.933348	1.403927	1.310353			
Phase Diff (degrees)	244.1322	117.8274	126.3048			

Table E.44 Acoustic Mode Analysis Results for SP32- 9/14/2011.

Pressure Transducer	P1	P2	P3	P4	Radial Mode Matches
Skewness	-0.00783	-0.01448	-0.00861	-0.00229	1-R Mode
Kurtosis	2.918862	2.945822	2.929945	2.97219	
Standard Deviation (P/Pchamber)	0.001982	0.001913	0.001707	0.00784	
Average Pressure (P/Pchamber)	0.000736	0.002078	-0.00665	-0.00069	
Max Amplitude from FFT (P/Pchamber)	0.000475	0.000454	0.000415	0.002389	
Dominant Frequency from FFT(Hz)	2282	2282	2282	2301	
	P1/P2	P2/P3	P1/P3		
Amp Ratios from FFT	1.047813	1.093216	1.145485		
Phase Diff (degrees)	8.051342	4.117405	12.16875		
Max Amplitude for Mode (P/Pchamber)	0.000475				

Table E.45 Acoustic Mode Analysis Results for SP32- 9/19/2011.

Pressure Transducer	P1	P2	P3	P4	Node Angle	Matches Freq, AR and Phase
Skewness	-0.00024	-0.01319	-0.00654	-0.00217	70	2-T Mode
Kurtosis	2.714557	2.879803	2.935156	2.996141	71	2-T Mode
Standard Deviation (P/Pchamber)	0.001842	0.001856	0.002484	0.016216	72	2-T Mode
Average Pressure (P/Pchamber)	0.000657	0.002133	-0.00677	-0.00269	73	2-T Mode
Max Amplitude FFT (P/Pchamber)	0.000356	0.000481	0.00064	0.003949	74	2-T Mode
Dominant Frequency FFT(Hz)	1708	1708	1708	2339	75	2-T Mode
	P1/P2	P2/P3	P1/P3		76	2-T Mode
Amp Ratios from FFT	0.740286	0.750999	0.555954		77	2-T Mode
Phase Diff (degrees)	195.4169	170.0156	25.40128		78	2-T Mode
Max Amplitude (P/Pchamber)	0.000553				79	2-T Mode
					160	2-T Mode
					161	2-T Mode
					162	2-T Mode
					163	2-T Mode
					164	2-T Mode
					165	2-T Mode
					166	2-T Mode
					167	2-T Mode
					168	2-T Mode
					169	2-T Mode
					250	2-T Mode
					251	2-T Mode
					252	2-T Mode
					253	2-T Mode
					254	2-T Mode
					255	2-T Mode
					256	2-T Mode
					257	2-T Mode
					258	2-T Mode
					259	2-T Mode
					340	2-T Mode
					341	2-T Mode
					342	2-T Mode
					343	2-T Mode
					344	2-T Mode
					345	2-T Mode
					346	2-T Mode
					347	2-T Mode
					348	2-T Mode
					349	2-T Mode

Table E.46 Acoustic Mode Analysis Results for SP32- 9/19/2011.

Pressure Transducer	P1	P2	P3	P4	Node Angle	Matches Freq, AR and Phase
Skewness	0.000996	-0.01126	-0.01714	0.019943	17	2-T Mode
Kurtosis	2.846382	2.817441	2.777872	3.064475	18	2-T Mode
Standard Deviation (P/Pchamber)	0.002217	0.001923	0.001669	0.016128	19	2-T Mode
Average Pressure (P/Pchamber)	0.000933	0.002382	-0.00659	0.015268	20	2-T Mode
Max Amplitude from FFT (P/Pchamber)	0.000437	0.000416	0.000518	0.004382	21	2-T Mode
Dominant Frequency from FFT(Hz)	1733	1733	1733	2367	107	2-T Mode
	P1/P2	P2/P3	P1/P3		108	2-T Mode
Amp Ratios from FFT	1.050626	0.802041	0.842645		109	2-T Mode
Phase Diff (degrees)	172.2806	9.411134	181.6917		110	2-T Mode
Max Amplitude for Mode (P/Pchamber)	0.000781				111	2-T Mode
					197	2-T Mode
					198	2-T Mode
					199	2-T Mode
					200	2-T Mode
					201	2-T Mode
					287	2-T Mode
					288	2-T Mode
					289	2-T Mode
					290	2-T Mode
					291	2-T Mode

WORKS CITED

[1] Sutton, George Paul, and Oscar Biblarz. Rocket Propulsion Elements. Hoboken, N.J: Wiley, 2010.

[2] Oefelein, Joseph C., and Vigor Yang. "Comprehensive Review of Liquid-Propellant Combustion Instabilities in F-1 Engines." *Journal of Propulsion and Power* 9.5 (1993).

[3] Yang, Vigor, and William E. Anderson. *Liquid Rocket Engine Combustion Instability*. Washington, DC: American Institute of Aeronautics and Astronautics, 1995.

[4] Penland, Dane. *F-1 Rocket Engine at the Steven F. Udvar-Hazy Center*. National Air and Space Museum. Web. 23 Apr. 2012. <http://www.nasm.si.edu/imageDetail.cfm?imageID=1979>.

[5] "NASA's New Ares Rocket Engine Passes Review." *Space Tourism, Space Transport and Space Exploration News*. Web. 26 Jan. 2012. <http://www.space-travel.com/reports/NASA_New_Ares_Rocket_Engine_Passes_Review_999.html>.

[6] Harrje, David T., and Frederick H. Reardon. *Liquid Propellant Rocket Combustion Instability.* Washington: Scientific and Technical Information Office, National Aeronautics and Space Administration, U.S. Govt. Print., 1972. NASA SP 194.

[7] Fisher, Mark F., James R. Hulka, Konstantin P. Denisov, Alexander A. Shibanov, and Anatoly F. Agarkov. "Scaling Techniques for Design, Development, and Test." By Carol E. Dexter. U.S Government. 553-99.

[8] Hulka, James R. "Scaling of Performance in Liquid Propellant Rocket Engine Combustion Devices." 44th AIAA/ASME/SAE/ASEE Joint Propulsion Conference & Exhibit (2008). AIAA 2008-5113.

[9] Huynh, Huy Huu. *Mode Assessment of Single-Element Shear Coaxial Injector*. Thesis. University of Alabama in Huntsville, 2009. Huntsville, AL.

[10] Byrd, Robert, Jr E. *Laboratory-Scale Injector Instability Mode Assessment*. Thesis. University of Alabama in Huntsville, 2008. Huntsville, AL.

[11] Sweeney, Brian A. Scaling a Single Element Combustor to Replicate Combustion Instability Modes of a Liquid Rocket Engine. Thesis. University of Alabama in Huntsville, 2010. Huntsville, AL.

[12] Cavitt, Ryan, and Dr. Robert Frederick. "Experimental Methodology for Measuring Combustion and Injection-Coupled Responses." AIAA-2006-4527. Proc. of 42nd AIAA/ASME/SAE/ASEE Joint Propulsion Conference and Exhibit, Sacremento, CA. Huntsville, AL: UAH Propulsion Research Center, 2006.

[13] Cavitt, Ryan, and Dr. Robert Frederick. "Laboratory Scale Survey of Pentad Injector Stability Characteristics." Journal of Propulsion and Power 24.No. 3 (2008): 534-40.

[14] Cavitt, Ryan, and Dr. Robert Frederick. "On The Laboratory Scale Survey of Pentad Injector."AIAA-2007-5587. Proc. of 43rd AIAA/ASME/SAE/ASEE Joint

Propulsion Conference and Exhibit, Cincinnati, OH. Huntsville, AL: UAH Propulsion Research Center, 2007.

[15] Cavitt, Ryan C. *Experimental Methodology for Measuring Combustion and Injector Coupled Responses*. Thesis. University of Alabama in Huntsville, 2007. Huntsville, AL.

[16] Byrd, Robert, Jr. E., and Robert, Jr. A. Frederick. "Instability Characteristics of a Gaseous-Oxygen/Methane Pentad Injector." *Journal of Propulsion and Power* 26.4 (2010): 689-95.

[17] Ikard, Robert Lashawn. *Experimental Injector Element Stability Characterization and Combustion Imaging*. Thesis. University of Alabama in Huntsville, 2009. Huntsville, AL.

[18] Brooks, John Whitlock. *Evaluating Combustion Instability in a Sub-Scale Combustion Experiment with Three Scaling Parameters*. Thesis. University of Alabama in Huntsville, 2010. Huntsville, AL.

[19] Richman, Benjamin M. *On The Method of Combustion Instability Mode Determination in a Cylindrical Chamber and Usage with Experimental Data*. Thesis. University of Alabama in Huntsville, 2011. Huntsville, AL.

[20] Lee, Kwang-Jin, Seonghyeon Seo, Joo-Young Song, Yeoung-Min Han, Hwan-Seok Choi, and Woo-Seok Seol. "Combustion Stability Assessment of Double Swirl Coaxial Injectors Using Simulant Propellants." *American Institute of Aeronautics and Astronautics, Korea Aerospace Research Institute, Daejeon, Korea, 305-333*.

[21] Conrad, T., A. Bibik, D. Shcherbik, E. Lubarsky, and B.T. Zinn. "Control of the Stability Margin in a Liquid Fueled Combustor using a “Smart” Fuel Injector." Proc. of 42nd AIAA/ASME/SAE/ASEE Joint Propulsion Conference & Exhibit, Sacremento, CA. Atlanta, GA: Aerospace Combustion Laboratory, School of Mechanical and Aerospace Engineering, Georgia Institute of Technology, 2006.

[22] Farassat, F., and M.K. Myers. "A Study of Wave Propagation in a Duct and Mode Radiation." *AIAA 96-1677*. Proc. of 2nd AIAA/CEAS Aeroacoustics Conference, State College, PA.

[23] *Analogies and Differences Between Sound Propagation in Circular Duct and Light Propagation in Optical Fiber*. Rep. Denmark: Engineering College of Odense, 2002.

[24] Kinsler, Lawrwnce E., Austin R. Frey, Alan B. Coppens, and James V. Sanders. Fundamentals of Acoustics. John Wiley & Sons. Inc.: USA, 2000. Print.

[25] MacDonough, Robert N., and Anthony D. Whalen. *Detection of Signals in Noise*. San Diego, Academic, 1995.

[26] Coleman, Hugh W., and W. Glenn. Steele. Experimentation, Validation, and Uncertainty Analysis for Engineers. Third ed. Hoboken, NJ: John Wiley & Sons, 2009. Print.

[27] "1.3.5.11. Measures of Skewness and Kurtosis." Information Technology Laboratory Homepage. Web. 14 Feb. 2012. <http://www.itl.nist.gov/div898/handbook/eda/section3/eda35b.htm>.

[28] "Signal Analysis." Signal Analysis. Gphysics.net. Web. 18 Feb. 2012. <http://www.gphysics.net/signal-analysis.html>.